THE UNIVERSITY OF CHICAGO

INVESTIGATION AND CHARACTERIZATION OF RNA MODIFICATIONS

A DISSERTATION SUBMITTED TO

THE FACULTY OF THE DIVISION OF THE PHYSICAL SCIENCES

IN CANDIDACY FOR THE DEGREE OF

DOCTOR OF PHILOSOPHY

DEPARTMENT OF CHEMISTRY

BY

WEN ZHANG

CHICAGO, ILLINOIS

JUNE 2021

Table of Content

List of Figures

List of Tables

Abbreviations

Ψ	Pseudouridine
MS	Mass Spectrometry
HPLC-MS	High-Performance Liquid Chromatography-Mass Spectrometry
m^1A	N^1-Methyladenosine
m^5C	5-Methylcytosine
m^3C	3-Methylcytidine
m^6A	N^6-Methyladenosine
Q	Queuosine
PUS	Pseudouridine Synthase
CD	Circular Dichroism
ncRNA	Non-Coding RNA
CMC	N-Cyclohexyl-N'-(2-Morpholinoethyl)Carbodiimide
RT	Reverse Transcription
RBS-seq	RNA Bisulfite Sequencing
galQ	Galactosyl-Q
manQ	Mannosyl-Q
TGT	tRNA Guanine Transglycosylase
QTRT1	Queuine tRNA-Ribosyltransferase 1
QTRTD1	Queuine-tRNA Ribosyltransferase Domain Containing 1
DLAT	Dalton's Lymphoma Ascites Transplanted
APB	3-(Acrylamido)phenylboronic Acid

HPLC-MS/MS	HPLC-Coupled Triple QuadrupoleMass Spectrometry
DM	Demethylase
CLAP	CMC-RT and Ligation Assisted PCR Analysis of Ψ
AMV	Avian Myoblastoma Virus
m^1G	N^1-Methylguanosine
$m^2{}_2G$	N^2,N^2-Dimethylguanosine
m^3U	N^3-Methyluridine
Pen-Strep	Penicillin-Streptomycin
PNK	Polynucleotide Kinase
LC/MS	Liquid Chromatography/Mass Spectrometry
HRP	Horseradish Peroxidase
ECL	Enhanced Chemiluminescence
acp^3U	N^3-(3-Amino-3-Carboxypropyl)-Uridine
MSR-seq	MultiplexSmallRNA Sequencing
tRF	tRNA Fragments
CHO	Capture Hairpin Oligonucleotide
TdT	Terminal Transferase Product
CHX	Cycloheximide
TE	Translational efficiency

Acknowledgements

I have had a very pleasant and rewarding experience finishing my Ph.D. studies in the Pan Lab at the Univerisity of Chicago. First and foremost, I want to thank my wonderful advisor, Dr. Tao Pan for his unwavering support in my research and thesis preparation. He has provided a lot of help to my research and my life during my doctoral studies. I want to thank him for constantly helping me design the experiments and optimize the protocols, giving me numerous good advice and ideas over the years. This has helped me significantly during my research transition from polymer chemistry to molecular biology. I appreciate his understanding of theatypicalwork schedule I oftentimes adoptso that I can take care of my son, especially during the past year. I also feel very grateful to Dr. Pan for allowing me to stay on in his lab to finish my research projects as part of my post-doctoral studies.It is a great pleasure and privilege to do my post-doc in the Pan Lab. I would like to thank Dr. Chuan He for being my pro forma advisor andbeing part of my thesis committee. The annual talks with him helped me a lot with my research. I would like to thank Dr. Joseph A. Piccirilli for his help in my 6^{th} year review and thesis defense.

I would like to thank the current and previous members of the Pan Lab: Dr. Qing Dai, Dr. Yuru Wang, Dr. Chris Katanski, Chris Watkins, Adam Wylder, Sihao Huang, Marcus Foo, Noah Peña, Mateusz Halucha, Dr. Xiaoyun Wang, Dr. Matthew Eckwahl, Dr. Katherine Zhou, Dr. Molly Evans, Ruyi Xu, and Żaneta Matuszek. I want to thank their help in research and life. In many ways, they have helped me with my research. They alsomake the lab a pleasant and invigorating place for doing research. I feel happy and relaxed when working with them. I would

like tothank the people in our neighboring labs, Dr. Phoebe Rice's and Dr. Jingyi Fei's labs. Their equipment and lab supply materials help me a lot during experimental emergencies. I also want to thank the people in Dr. He'slab for their advice on experiment design and equipmentoperation. I also want to thank the lab supporting staff for their help with the autoclave and labware cleaning.

I would like to express my gratitude to the admistrative staff in both the Department of Chemistry and the Department of Biochemistry and Molecular Biology. I want to thank Dr. Melinda Moore and Dr. Vera Dragisich for their advice and support in academic issues. Their consistently helpful responses to all my inquiries make things go smoothly during my Ph.D. study. I also want to thank Ms. Holly McGuinness for her help in visa application.

Finally, I want to thank my family, my parents, my parents-in-law, my wife and my son for their understanding and support during my study. I want to thank my wife for making a home and harbor for our family. I feel grateful to her for giving up her Ph.D. studies at the University of Chicago in order to take care of our son. Her looking after our son allows me to focus more on my research work. I also want to thank my son for being such a good boy.

Summary

My thesis focuses on the investigation and characterization of RNA modifications. RNA is post-transcriptionally modified on the nucleoside bases and/or on the ribose-phosphate backbone. RNA modifications are conserved from prokaryotes to eukaryotes. Each modification has its own functions in vivo. Efficient and quantitative detection methods are necessary for the elucidation of the functions of specific RNA modifications. Some methods are useful for the detection of a specific modification, while other methods can detect multiple RNA modifications simultaneously. In the chapters 2 and 3 of my thesis, I describe the methods that I developed for the sensitive and quantitative detection of pseudouridine (Ψ) and glycosylated queuosine (Q). Chapter 4 is about the usage of small RNA sequencing methods (MSR-seq) for the investigation of tRNA modification response under stress conditions.

Chapter 2 describes the development of a sensitive and quantitative method called "CLAP" for Ψ detection. This PCR-based method takes advantages of the CMC reaction with Ψ which leaves a stop signature during reverse transcription. This method is useful for sensitive quantification of the modification fraction of target Ψ sites in low abundant long non-coding RNAs and mRNAs. CLAP has the potential of being adapted for the studies of other RNA modifications.

Chapter 3 describes an acid denaturing gel based Northern blot method for the quantitative detection of glycosylated Q modifications. This method combines the acid denaturing gel and Northern blot. Non-radioactive Northern blot probes are used for detection of Q-modified tRNAs.

The acid denaturing gel based Northern blot is useful for measuring the glycosylated Q modification levels in tRNAs. By combining the acid denaturing gel based Northern blot and 3-(Acrylamido)phenylboronic acid (APB) gel based Northern blot, we investigated the Q modification and glycosylation kinetics in tRNAs in three human cell lines, HEK293T, HeLa, and MCF7.

Chapter 4 describes a study of using small RNA sequencing method to study tRNA abundance and modification response under different stress conditions including heat shock, H_2O_2, and $NaAsO_2$. We identified new stress responses by m^3C modifications in tRNAs and a tRNA-based regulation of translational elongation, and a relationship between tRNA modification and tRNA fragment biogenesis.

In conclusion, efficient and simple detection methods are often required for studying the functional roles of RNA modifications. The development of quantitative methods of Ψand glycosylated Q will help the elucidation of the diverse functions of Ψ in different RNA species and uncover the mysterious functions of glycosylated Q modifications in tRNAs.

1. Introduction

1.1. RNA modifications and epi-transcriptome

RNA can be post-transcriptionally modified either on nucleoside bases or on ribose-phosphate backbone. Since the discovery of the first RNA modification, pseudouridine (Ψ), in the 1950s [3], around 170 different types of RNA modifications have been identified [4]. In analogy to epigenetics which studiesfunctionally relevant chemical changes in the genome, the investigation of functionally relevant chemical changes inthe transcriptome is called epitranscriptomics. A large amount ofresearch has been conducted on RNA modifications.Almost all RNA species, including rRNAs, tRNAs, mRNAs, snRNAs, snoRNAs, and ncRNAs, are post-transcriptionally modified. tRNAs and rRNAs are the most extensively modified RNA species. On average, there are ~13 modified nucleotidesin each tRNA molecule [5]. The human 80S ribosome contains 228 modification sites [6]. mRNAs are modified to a lesser extent. Investigation of the chemical properties of all RNA modifications reveals a diverse pool of modified bases including methyl adducts, acetyl adducts, structural isomers, and hyper-modified bases [4]. Methyl adduct such as m^6A, m^1A, m^7G, and m^3C is the most common modification type on RNA. Each RNA modification shows a unique distribution pattern among RNA species. For example, in eukaryotes m^6A is found in mRNAs, but not in tRNAs. Human rRNAs also harbor two m^6A sites. mRNA-containing m^6A shows differentiated distribution along 5'-UTR, coding sequence, and 3'-UTR. Another example is queuosine (Q) modification that is only found in a subset of tRNAs.The distribution of RNA modifications among RNA species or within an RNA molecule reflects the properties and functions of each modification. For instance, it is

expected that modifications that induce RT stops are unlikely to reside in coding sequence region of mRNAs. In addition, many modifications are also localized to functionally important regions of specific RNA species.

The discoveries of functions of RNA modifications are still emerging and each modification displays unique biological roles. RNA modifications affect the lifecycle of RNA from transcription to translation spanning co-transcriptional control, RNA biogenesis, RNA stability, and protein synthesis. The same RNA modification may show several distinct functions. For example, the most extensively studied m^6A modification in mRNA has been shown to modulate mRNA decay, mRNA stability, mRNA spicing, mRNA translation, and microRNA processing through various m^6A reader proteins [7]. Another abundant RNA modification, Ψ, has been found to modulate RNA structure, affect mRNA stability, regulate mRNA translation, and mediate pre-mRNA processing [8]. m^5C modifications in different RNA species such as tRNA, mRNA, and rRNA also show distinct functions including affecting tRNA charging, tRNA cleavage, decoding fidelity, mRNA nuclear export, mRNA translation and translation fidelity [9]. In conclusion, each RNA modification is unique and may show a distinct pattern of cellular functions. The biological functions of RNA modifications are also transcript-, location- and context-dependent. In addition, the investigation of the roles of RNA modifications in cancer progression and development uncovered diverse roles of RNA modifications in tumorigenesis [10].

In order to betterunderstand and elucidatethe functions of each RNA modification, reliable detection methods are crucial. Many methods have been developed for the detection of RNA

modification to date. The methods can be classified into different groups including mass spectrometry (MS) based methods (e.g. HPLC-MS), low-throughput methods (e.g. primer extension and gel based methods), and sequencing based high-throughput methods. MS based methods are useful for the initial detection and validation of a modification. In principle, MS based methods can detect any RNA modifications. However, the requirements of expensive instrumentation, high RNA input and lack of quantification information at each modified sites have limited its application. Low-throughput methods are useful for studying specific sites but are not ideal for transcriptome-wide identification of RNA modifications. High-throughput sequencing methods are useful for transcriptome-wide mapping of RNA modifications. Current high-throughput sequencing methods usually require reverse transcription and PCR amplification. The reverse transcription step provides a key tool to modulate the cDNA pool and pattern by RNA modifications. This modulation in turn enables the detection of RNA modifications through analyzing the distinct features of cDNA libraries induced by each modification. Some Watson-Crick face modifications such as N^1-methyladenosine (m^1A) cause a stop or mutation signature during RT. This feature can be directly used for m^1A detection by sequencing [11]. Some modification can generate a unique feature during RT after reaction with some chemicals or treatment with certain enzymes. For example, the reaction of Ψ with CMC, the reaction of 5-methylcytosine (m^5C) with bisulfite, and the reaction of 3-methylcytosine (m^3C) with hydrazine/aniline enables the detection of Ψ, m^5C, and m^3C, respectively [12-20]. Treatment of tRNA with demethylase enables the quantitative detection of multiple methylations in tRNAs at the same time [21, 22]. Another widely used RNA modification mapping technique involves

immunoprecipitation (IP) of the modification containing RNA by the corresponding antibody. For example, the m^6A-seq method utilized an N^6-methyladenosine (m^6A) specific antibody to enrich m^6A containing RNA for the detection of m^6A [23]. However, the IP based methods lose quantitation information and do not have single-base resolution.

Recent development of Nanopore sequencing provides a revolutionarily new method for sequencing long RNA directly without going through RT and PCR steps. The direct RNA sequencing by Nanopore enables the direct detection of RNA modifications [24-26]. Identification of modifications through Nanopore sequencing requires sophisticated data analysis and entails deep machine learning and enough data to train modification predictors for data analysis. In addition, current Nanopore sequencing of RNA generates about one million reads which is challenging for the detection of modifications in low abundant transcripts.

1.2. Pseudouridine modification: functions and detections

1.2.1. Biogenesis of pseudouridine

Ψ was discovered nearly 70 years ago [3].The biogenesis and biological functions of Ψ have been extensively studied after its initial discovery. Ψ is the most abundant modification in cellular RNAs. Ψ is present in tRNA, rRNA, snRNA, snoRNA, and mRNA. Ψ forms through the isomerization of uridine, a process catalyzed by pseudouridine synthase (PUS) (**Fig. 1.1A**). During uridine isomerization, the uracil base rotates 180 degrees around N3-C6 line to form the C5-C1' carbon-carbon bond in place of the N1-C1' nitrogen-carbon bond. There are 13 pseudouridine synthases discovered in mammals [27, 28]. Each PUS enzyme has a specific

subset of substrate RNA. For example, PUS1, PUS7, TRUB1, and DKC1 can all catalyze the formation of Ψ in mRNA. After exstensive characterization of the transcriptome-wide distribution of Ψ, Safra et al. discovered PUS7 and TRUB1 as the two main mammalian mRNA PUSs [29]. In addition to mRNA activity, PUS1 and TRUB1 also act on tRNA, while PUS7 and DKC1 act on rRNA. All the PUS enzymes can be classified into two types: snoRNP or RNA-dependent PUS and stand-alone or RNA-independent PUS. DKC1 is the only guide RNA-dependent PUS enzyme. DKC1 forms box H/ACARNP with GAR1, NOP10, NHP2, and H/ACA guide snoRNA [30]. The H/ACA snoRNA forms two hairpin structures connected by a single stranded RNA harboring the box H. Each hairpin structure binds with the 4 snoRNP proteins and guides the pseudouridylation at target sites. Standalone PUS enzymes catalyze the formation of Ψ at target sites by recognizing the consensus sequence or the secondary structure of the target RNA [31]. E. coli pseudouridine synthase 1 is responsible for the formation of Ψs at position 38, 39, and 40 of tRNA anticodon stemloop. It dimerizes to perform pseudouridylation activity. The crystal structure of the PUS1 dimer shows that the active site imposes some structural constraints for tRNA recognition and Ψ formation [32]. Just as E.coli PUS1 catalyzed pseudouridylation has these structural requirements, another study of pseudouridylation mechanisms by human PUS1 revealed that human PUS1 catalyzed Ψ formation in mRNA is also mRNA structure dependent [33].

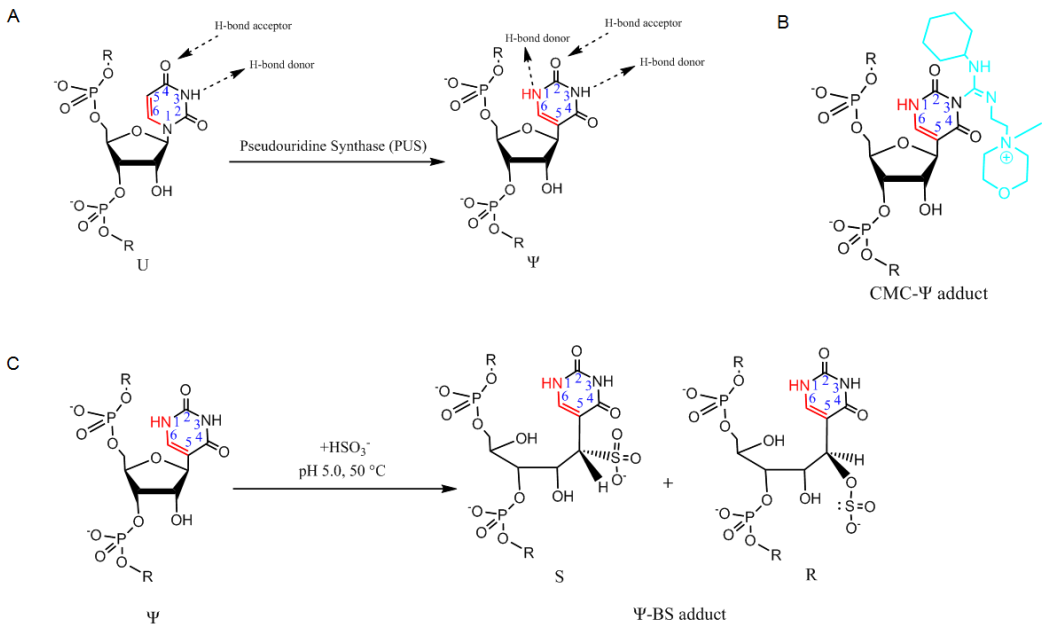

Fig. 1.1 Ψ and chemical reactions with Ψ. (A) Structure representation of pseudouridylation catalyzed by pseudouridine synthases. (B) Structure of CMC-Ψ adduct. The large CMC-adduct on the Watson-Crick face of Ψ causes a stop or mutation signature during RT. (C) Reaction between Ψ and bisulfite (HSO_3^-). The structures of the two products isomers are adapted from reference [34]. The Ψ-BS adducts will cause a deletion signature during RT.

Several PUS enzymes may modify the same Ψ site. The substrates of each PUS enzyme are related to its sub-cellular location [27]. For example, mammalian nuclear TRUB1, mitochondrial TRUB2, and cytoplasmic PUS10 can all catalyze the formation of Ψ55 in tRNAs. However, the pseudouridylation activity of these PUS enzymes is not redundant. A recent study found that TRUB1, PUS10, and TRUB2 produce conserved Ψ55 in different groups of tRNA in nucleus, cytoplasm, and mitochondria, respectively [34]. TRUB1 and PUS10 works in coordination for the TRUB1 catalyzed Ψ55 in T54Ψ55- and A54Ψ55- containing elongator tRNAs in nucleus and the PUS10 catalyzed Ψ54 and Ψ55 in Ψ54Ψ55-containing tRNAs and A54U55-containing $tRNA^{iMet}$ [34]. Pseudouridine synthases may have other functions in addition to

pseudouridylation activity. For example, TRUB1 can regulate the maturation of evolutionary conserved let-7 microRNA by enhancing the interaction between pri-let-7 and the microprocessor DGCR8 [35]. Besides being a crucial component in Box H/ACA snoRNP, DKC1 is also an essential partof the telomerase complex.

1.2.2. Functions of pseudouridine

Ψ has diverse functions in cells. We now know that Ψ modulates the fate of RNA at every step of RNA biogenesis. Ψ has a direct effect on RNA structure through the additional hydrogen bond donor and the more rotational freedom of the C5-C1' carbon-carbon bond (**Fig. 1.1A**). ^{1}H NMR, UV, and Circular Dichroism (CD) spectroscopy results suggested that Ψ can stabilize RNA stacking through the extra imino hydrogen [36]. The contribution of Ψ to RNA structure stability has been systematically studied under different sequence context and Ψ base pairs. Ψ can enhance stability relative to U when paired with A, G, U or C inside a double helix [37]. Ψs in different RNA species show various functions. Ψ deposition may confer different molecular properties to the modified RNAs and changes their fate or activity. Ψ is the most abundant RNA modification in snRNA. Ψs in snRNAs are important for enhancing snRNA interaction with pre-mRNA, maintaining favorable local RNA structure, and facilitating branch site recognition [38]. Ψ in nuclear non-coding RNA (ncRNA) affects nuclear transcription and pre-mRNA splicing. For example, Ψs in SRA and 7SK snRNA play an important role in maintaining normal transcription activity. Spliceosome ncRNA pseudouridylation is crucial for splicing. The functions of Ψs in U2 snRNA are investigated the most. Ψs are essential for U2 snRNP

biogenesis and pre-mRNA splicing [39]. Ψs on rRNA affect ribosome biogenesis and ribosomal function [30]. Profiling of complete RNA chemical modifications in the human 80S ribosome by mass spectrometry reveals 2 Ψ sites in 5.8S rRNA, 42 Ψ sites in 18S rRNA, and 60 Ψ sites in 28S rRNA [6]. Conserved Ψ sites often reside in functionally important regions of rRNA such as the peptidyl transferase center, the A-site finger, and the decoding center [6].

RPUSD4 is responsible for the formation of Ψ3069 in mammalian mitochondrial 16S rRNA [40] and Ψ39 in mitochondrial $tRNA^{Phe}$ [41]. Ψ3069 is essential for the stability of mt-16S rRNA. TRUB2 and RPUSD3 modify Ψ6294 in COXI and Ψ9904-9906 that are crucial for the efficient synthesis of the corresponding polypeptides without affecting the stability of the mRNA [40]. Depletion of RPUSD4 causes a reduction of Ψ levels in mt-16S rRNA and a decrease of the 16S rRNA, mitoribosome large subunit and monosome amounts. Furthermore, this leads to decreased synthesis of mt-DNA encoded polypeptides and impaired global mitochondrial translation [42]. At the codon level, Ψ affects decoding during translation. Pseudouridylation of the uridine of a stop codon (UAA, UAG, or UGA) enables the ribosome read-through at the modified stop codon by incorporating sense amino acids serine, threonine, tyrosine, or phenylalanine both in vitro and in vivo[43]. Recently, the same group also showed that Ψ-mediated ribosome stop codon read-through is sequence context-independent in S. cerevisiae [44]. Similarly, at the anticodon level, Ψ in the anticodon position of tRNA can also affect tRNA decoding efficiency. E. coli $tRNA^{Tyr}$s have two pseudouridines at positions 39 and 55. A recent study demonstrated the presence of Ψ at position 35 of $tRNA^{Tyr}$ anticodon loop and showed that RluF is the responsible PUS. Although no growth phenotype is observed, the translation of a synthetic luciferase reporter

gene containing several tyrosine codons is imparied in RluF deleted cells, indicating the importance of Ψ in tRNA decoding [45]. Loss of TruA and RluA catalyzed Ψ of tRNA anticodon stem loop leads to elevated mutation frequency in bacteria. The mechanism behind this phenotype remains unknown [46]. PUS6 modifies Ψs on both YEF3 mRNA and $tRNA^{Met}$. These sites are all read by methionine aminoacyl $tRNA^{Met}$ synthase leading to gene-specific or global translational response [47].

Functions of Ψ in mRNA have been investigated for in vitro transcribed mRNAs before Ψ is found in cellular mRNA. In vitro transcribed Ψ-containing mRNAs have significantly elevated translation levels compared to U-containnig mRNAs[48]. Anderson et al. showed that Ψ-containing mRNAs bind RNA-dependent protein kinase (PKR) less efficiently than U-containing mRNAs and this in turn inhibits PKR activation. Reduced PKR activation causes less phosphorylation of translation initiation factor 2-alpha (eIF-2a) and represses translation inhibition by p-eIF-2a [48]. The efficacy of Ψ-containing mRNAs for treating disease has been investigated. The results showed that Ψ-containing mRNA delivered systemically with liver-targeting lipid nanoparticles in vivo had no significant effect on protein expression in vivo, therapeutic improvements or mRNA immunogenicity compared to unmodified mRNA [49]. However, a recent study has found an opposite effect of Ψ on mRNA translation in vivo and in vitro. Incorporation of single Ψ into mRNA codon can perturb ribosome function, impede amino acid addition and hinder translation elongation [50]. Ψ affects the decoding speed of cognate tRNA and near-cognate tRNA, increases amino acid substitutions at Ψ-containing codons and promotes the low-level formation of multiple polypeptides from a single mRNA gene. These

results indicated a context-dependent function of Ψ on mRNA translation. Ψ in tRNA-derived mTOG fragments helped regulate and inhibited protein synthesis by targeting the translation initiation complex during embryonic stem cells developments [51]. Further N^1 methylation of Ψ (N^1mΨ) in mRNA has been shown to enhance translation by blocking the immune/eIF2 phosphorylation-dependent inhibition of translation and reduction of ribosome density on N^1mΨ containing mRNAs [52].

Functions of RNA modifications including Ψ have been widely studied in cancer cell biology. Considerable effort has been directed towards identifying candidate modifications as potential biomarkers of cancer development and progression. Although the functions of Ψ in cells and cancer are not fully understood, evidence has linked the elevated Ψ levels with the incidence and progression of male prostate cancer, implicating Ψ as a possible biomarker in prostate cancer progression [53]. Deregulation of the pseudouridylation process is associated with the progression of prostate cancer [54]. Many studies have shown that alterations in DKC1 expression or activity are significantly associated with cancer, however, the exact mechanism may be cell, tissue or DKC1 substrate dependent [55].

1.2.3. Detection methods of pseudouridine

Many methods have been developed for the identification of Ψ in different RNA species. In 1971, Ho and Gilham discovered a unique feature of the reaction between Ψ and N-cyclohexyl-N'-(2-morpholinoethyl)carbodiimide (CMC) [56]. Under urea denaturing conditions, CMC reacts with G, U, Ψ, and inosine residues in RNA to form N3-CMC and

N1-CMC adducts. All CMC adducts except N3-CMC adduct in Ψ are reversed by alkaline treatment (**Fig. 1.1B**). The CMC-Ψ adduct that survives introduces a bulky group to the Watson-Crick face of Ψ base which induces a stop or mutation signature during reverse transcription (RT). In 1993, Bakin and Ofengand developed a primer extension method based on the reaction of CMC with Ψ for the detection of Ψ[57]. In 2013, Liu et al. developed an RNase H cleavage and splint ligation based method called "SCARLET" for the detection of RNA modifications at single-base resolution. In principle, SCARLET can detect any RNA modification as long as the RNase H cleavage and splint ligation efficiency is not compromised by the modification. However, "SCARLET" requires a large amount of input RNA and ^{32}P labeling which limits its application in routine detection of Ψ. In 2014 and 2015, four transcriptome-wide sequencing approaches for Ψ detection were developed [12-15]. These four methods all took advantage of the reaction of Ψ with CMC and relied on the stop signature induced by the CMC-Ψ adduct during RT for the identification of candidate Ψ sites. Although very useful in identifying Ψ sites in the whole transcriptome, CMC-based high-throughput sequencing methods did not generate reliable Ψ profiles. Only one common Ψ site was detected by all 4 Ψ mapping methods after examining the Ψ profiles generated by each method [58]. Further investigation of CMC-based Ψ sequencing methods revealed context-dependent mutation and stop rates induced by the CMC-Ψ adduct [59]. A qPCR-based detection method for locus-specific Ψ identification has also been developed. It relied on the CMC-Ψ adduct induced mutation signature generated by RT read-through that will then lead to a distinct melting curve of cDNAs originating from the modified or unmodified RNA during qPCR [60]. However, the

quantitation information is not readily available for this qPCR-based method. A control pair of RNA transcripts with or without Ψ needs to be constructed for each site in order to obtain the modification fraction of the target Ψ site.

In addition to CMC-based detection methods, other chemical treatment based sequencing techniques have also been developed for the detection of Ψ. Khoddami et al. developed a bisulfite treatment based method called RNA bisulfite sequencing (RBS-seq) for transcriptome-wide mapping of m^5C, Ψ, and m^1A simultaneously at single-base resolution [61]. This method is semi-quantitative, but like the CMC-based sequencing method, the harsh chemical treatment conditions are prone to cause false positive signals. The chemical details of the reaction between bisulfite and Ψ were further investigated (**Fig. 1.1C**). The reaction mechanism provided more insights into the generation of deletion signature during reverse transcription and also the incomplete reaction between bisulfite and Ψ [62]. A novel transcriptome-wide and quantitative Ψ sequencing method relying on the specific protection of Ψ modified nucleotide from hydrazine/aniline (HydraPsiSeq) cleavage has also been developed [63]. However, this method is mainly useful for the study of Ψ in abundant rRNAs and tRNAs and requires normalization to unmodified RNA to get quantification information that is usually hard to obtain when the PUS enzymes for specific Ψ sites are unknown. These limitations hinder the application of HydraPsiSeq for investigating Ψs in low abundant mRNAs and lncRNAs [63]. The recently developed Nanopore sequencing that obviates the reverse transcription and PCR steps have also been used to detect RNA modifications directly [64]. However, identification of RNA modifications using Nanopore sequencing required advanced data analysis skills. Aside

from wet-lab based methods, several computational Ψ prediction methods based on deep machine learning have been developed [65-69]. The accuracy of different computaional Ψ predictors has also been studied and whether there is any sequence feature in Ψ prediction problem is unclear considering the undistinguishable improvement of performance for Ψ identification using sequence features [70]. An online web server which integrates the Ψ profiles from both wet-lab methods and computational methods for Ψ identification and functional annotation has also been built. The online server helps explore the mechanisms and functions of Ψ [71]. In conclusion, current Ψ detection methods are either costly or time-consuming and a simple, convenient locus-specific Ψ detection is needed.

1.3. Queuosine and glycosylated queuosine modifications

1.3.1. Biogenesis of queuosine and glycosylated queuosine in prokaryotes and eukaryotes

Queuosine is a hypermodified ribonucleotide thatwas first discovered in the E. coli $tRNA^{Tyr}$ in 1968 [10]. Subsequent studies soon identified Q at the wobble position in four types of tRNAs with $G_{34}U_{35}N_{36}$ anticodon that read codons encoding amino acids Tyr, His, Asn, and Asp [72]. Soon after the discovery of Q modification in the 4 types of tRNAs, the structure of Q was elucidated (**Fig. 1.2A**) [73]. In mammals, Q in $tRNA^{Tyr}$ and $tRNA^{Asp}$ are further glycosylated at the cis-diol group with galactose and mannose by unknown enzymes to generate galactosyl-Q (galQ) and mannosyl-Q (manQ), respectively (**Fig. 1.2A, 1.2B**) [74-76]. Q is synthesized de novo from GTP in prokaryotes via a series of 8 reactions catalyzed by a few enzymes whose expression levels are regulated by the preQ1 riboswitch [72, 77]. Mechanistic study of

prokaryotic Q biosynthesis found that the ribosyl moiety of AdoMet is the precursor of the cyclopentenediol moiety of Q [78]. The structural basis for preQ1 riboswitch controlled Q synthesis is investigated. A report found that preQ1 riboswitch in Bacillus subtillis shows preQ1 induced pseudoknot structure providing insights into the interaction between preQ1 and preQ1 riboswitch for translational control [77]. Q biosynthesis is essential for symbiotic S. meliloti-induced cytoskeletal modifications on HeLa cells [79].

Eukaryotes lack the cellular machinery for de novo synthesis of Q. Instead, eukaryotes have to salvage the Q precursor, queuine from dietary source or gut microbiota for the synthesis of Q-containing tRNAs [80]. The enzyme responsible for replacing guanine at the anticodon wobble positionof tRNA with the salvaged queuine is tRNA guanine transglycosylase (TGT). Mechanistic study proposed a sequential bi–bi mechanism triggered by queuine base binding for the eukaryotic TGT-catalyzed incorporation of queuine into tRNAs [81]. The TGT enzyme in eukaryotes is a heterodimer consisting of two subunits, Queuine tRNA-ribosyltransferase 1 (QTRT1) and queuine-tRNA ribosyltransferase domain containing 1 (QTRTD1 or QTRT2) [72]. QTRT1/QTRTD1 complex is located on the outer membrane of mitochondria [82]. Investigation of the TGT activity of HeLa cells cultured in either aerobic (21% O_2) or hypoxic conditions (7% O_2) identifies protein kinase C as an upstream modulator of HeLa QTRT1/QTRTD1 complex [83]. Activated protein kinase C restored the activity of QTRT1/QTRTD1 in serum factor depleted medium under hypoxic conditions. Structural analysis of prokaryotic TGTs and eukaryotic TGTs revealed that replacement of Cys158 and Val233 (Z. mobilis TGT numbering)) in bacterial TGT by valine and glycine, respectively, in eukaryotic TGT is responsible for the

substrate specificity of prokaryotic TGTs and eukaryotic TGTs [84]. Investigation of structural properties of Z. mobilis TGT identified queuine as an inhibitor of prokaryotic TGT [85]. In addition to the TGT enzyme, Q salvation pathway involves the membrane Q precursor transporter proteins and a possible queuosine hydrolase enzyme. Comparative genomic analysis identified DUF2419 protein family as a candidate queuine salvage enzyme that may have ribonucleoside hydrolase activity [86]. The queuosine hydrolase activity of DUF2419 from human, maize, S. thermophilus, and S. pombe has been validated by LC-MS/MS [86]. A recent study identified Quek in C. difficile as the bacterial queuosine hydrolase in queuine salvage pathway [87]. The relationship between Quek and DUF2419 is unknown. In addition to Quek, the novel queuine membrane transporter component QrtT and queuine lyase were also discovered in C. difficile [87]. However, the Q salvation proteins in humans remain elusive.

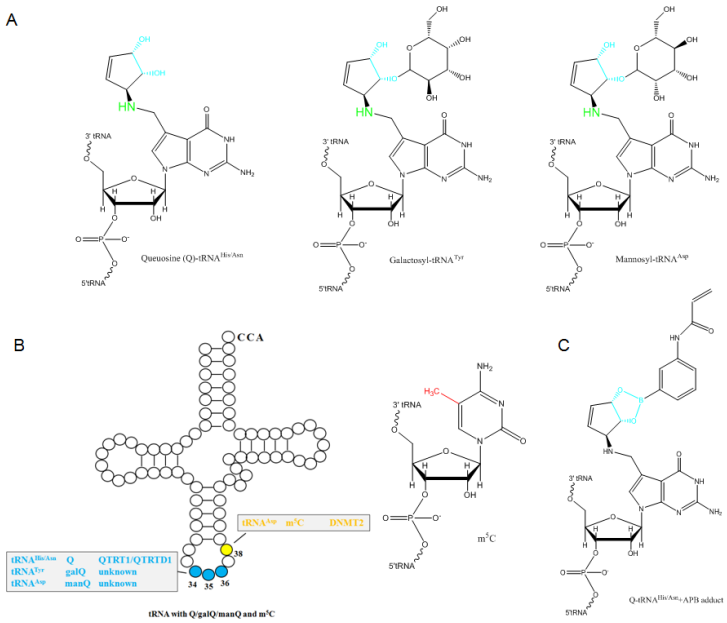

Fig. 1.2 Structures of Q and glycosylated Q and APB-Q adduct. (A) Structures of Q in $tRNA^{His/Asn}$, galQ in $tRNA^{Tyr}$, and manQ in $tRNA^{Asp}$. (B) Q, galQ, and manQ in $tRNA^{Tyr/His/Asn/Asp}$ and Q dependent m^5C38 in $tRNA^{Asp}$ and structure of m^5C. The enzymes responsible for the modification (if known) are also indicated. (C) APB-Q adduct of $tRNA^{His/Asn}$. The interaction between Q and APB through the cis-diol group slows the migration of Q modified $tRNA^{His/Asn}$ in APB gels.

1.3.2. Functions of queuosine

The cellular functions of Q have been continuously investigated since its discovery. Q displays a wide range of biological functions including translation, codon usage, cell proliferation, and cancer progression and development. Q modification affects the decoding properties and stability of its direct target tRNAs (Tyr, His, Asn, and Asp). Q modification regulates protein synthesis through tRNA decoding. Q-modified $tRNA^{Asp}$ shows higher reaction velocity and higher reaction rate compared to unmodified $tRNA^{Asp}$ [88]. Q modification affects codon preferences of substrate tRNAs in vivo during the elongation step of protein synthesis. In Drosophila, $tRNA^{His}$ with GUG anticodon decodes histidine codon CAC more efficiently than

codon CAU. However, Q modification at the wobble position of $tRNA^{His}$ eliminates these preferences [89]. In addition to codon usage, Q modification shows genome-wide translational control. In S. pombe, ribosome profiling indicates that the protein synthesis speed of C-ending codons (Asp and His) is enhanced by queuosine modification while the protein synthesis speed of U ending codons (Asn and Tyr) is reduced [90]. Furthermore, the misreading of the C-ending glycine codon GGC caused by the second codon position mismatch is supressed upon queuine incorporation while misreading of the U-ending glycine codon caused by the wobble position mismatch GGU remains unaffected [90].

Q modification in tRNAs promotes DNMT2-dependent m^5C38 methylation in tRNAs (**Fig. 1.2B**). The two modifications together affect protein translation. Q modification also shows diverse effects on codon mistranslation [91]. For example, Q modification of tRNAs promotes DNMT2-dependent m^5C38 methylation in the same substrate tRNAs such as $tRNA^{Asp}$ [92, 93]. This finding suggests a micronutrient-dependent regulation pathway of tRNA modifications. The queuine stimulated DNMT2-dependent methylation events are conserved in mice [90]. Q and Q stimulated DNMT2-mediated methylation of $tRNA^{Asp}$ regulate protein synthesis speed at Q-decoded cognate codon and near-cognate codons [92]. Queuine depletion causes translation disorder and protein folding defects which consequently triggers endoplasmic reticulum stress and activation of the unfolded protein response in human cell lines and germ-free mice [92]. A recent study reveals the dual role of queuine in enhancing oxidative resistance and inhibiting parasite virulence in Entamoeba histolytica [94]. Incorporation of queuine into $tRNA^{Asp}$ also induces the m^5C38 modification in $tRNA^{Asp}$. Q modification suppresses oxidative stress and

maintains translation by promoting expression of oxidative response proteins such as heat shock protein 70 (Hsp70), antioxidant enzymes, and enzymes involved in DNA repair. Queuine also reduced E. histolytica virulence by decreasing the expression of virulence related genes such as cysteine proteases, cytoskeletal proteins, and small GTPases [94].

Queuine availability induces variation in codon profiles of mRNA. Chiari et al. discovered a species-specific Q modification profile across different development stages of Drosophila [95]. Zaborske et al. showed a transcriptome-wide codon usage reprogramming modulated by Q modification levels in different developmental stages of fruit flies [96]. In addition to the decoding and translational properties of tRNAs, Q also affects the stability of substrate tRNAs. Wang et al. showed that Q modification affects tRNA fragment pool by protecting Q-modified tRNAs from ribonuclease cleavage [97].

Marks and Farkas investigated the effects of queuine on germ-free mice fed with tyrosine and queuine depleted diets [98]. Germ-free mice fed with tyrosine depleted diets developed ocular neurological and other abnormalities that led to death within two weeks. However, queuine supplement (0.1 μM) to the tyrosine-deficient diet prevents germ-free mice from developing fatal abnormalities [98]. The mechanism of the inhibition effect of queuine on tyrosine depletion induced lethal symptoms is further investigated. In queuine deficient human HepG2 cells and QTRT1 knockout mice, the tyrosine production from phenylalanine is reduced due to elevated oxidation of the phenylalanine hydroxylase cofactor, tetrahydrobiopterin [99]. Zhang et al. showed that QTRT1 enzyme and queuosine modification in tRNA regulate cell proliferation, tight junction formation, and microbiome recruitment to WT or QTRT1-KO MCF7

cells induced tumors planted on immune-deficient “nude” mice [100]. Queuine depletion promotes proton leak from mitochondrial membrane resulting in down regulation of ATP synthesis and decrease of cellular ATP levels without affecting the activity of individual mitochondrial complex [101]. Queuine has cell-type specific effects on cell proliferation. Queuine inhibits cell proliferation of U87 and HepG2 cells as well as in DLAT cancerous mouse by promoting cell death. The apoptosis inhibitory protein Bcl2 is down-regulated upon queuine treatments, suggesting that queuine promotes cell death in these cells [102]. However, no observable cell proliferation differences were found in HeLa and HEK293T cell lines.

Various studies have indicated an association between Q deficiency and cancer development [103]. The effects of queuine on mice Dalton’s lymphoma ascites transplanted (DLAT) cancer were investigated by several studies. Pathak et al. discovered that queuine treatments led to a decrease of activity and level of lactate dehydrogenase A in DLA mice [104]. Another report showed that queuine treatments reduced the levels of tyrosine phosphoproteins that were up regulated in DLAT cancerous mouse liver [105]. Further investigation of queuine functions in DLAT cancer also showed that queuine treatments caused the down-regulation of elevated lactate dehydrogenase activity and the elevated levels of c-Myc and c-Fos in DLAT cancerous mouse [106]. These results suggested queuine as an inhibitor of anaerobic metabolism and cell proliferation in certain cancer. Administration of queuine to the DLAT cancerous mouse increased oxidative stress and tumorigenesis resistance by promoting the activities of antioxidant enzymes and consequently enhancing antioxidant defense system [107]. Besides, QTRT1 up-regulation was found in lung adenocarcinoma patients with poor prognosis [108].

1.3.3. Detection methods of queuosine

The structure of Q was soon elucidated by ^{1}H NMR, UV-Vis spectroscopy, and MS methods after its original discovery [73-75].These characterization methods are useful for the initial discovery and structure determination of Q and glycosylated Q. However, routine detection and quantification of Q using these methods is not ideal. HPLC-MS method has been successfully used to detect and quantify Q and glycosylated Q [109]. However, HPLC-MS methods require a large amount of input RNA and the modification fraction of Q and glycosylated Q is not readily obtained. In 1985, Igloi and Kossel discovered the method of using 3-(Acrylamido)phenylboronic acid (APB) in denaturing polyacrylamide gel to detect Q-modified tRNAs [110]. The working principle of APB gel based separation of Q-modified tRNAs from unmodified tRNAs is the interaction between APB and the cis-diol group on the Q base slowing the migration of Q-modified tRNAs (**Fig. 1.2C**). In 2014, Zaborske et al. developed APB Northern blot for the detection of Q-modified tRNAs by combining the APB denaturing gel method with Northern blot [96]. The APB Northern blot is very convenient and quantitative. The Q modification fraction can be directly obtained by quantifying the unmodified band and the shifted modified band. However, the cis-diol group on Q base is further glycosylated in human $tRNA^{Tyr}$ and $tRNA^{Asp}$, which diminishes the ability of APB Northern blot in detecting glycosylated Q-modified tRNAs (galQ-$tRNA^{Tyr}$ and manQ-$tRNA^{Asp}$). The lack of efficient detection methods of glycosylated Q is one possible reason why few molecular functions of Q glycosylation have been discovered.

1.4. 3-methylcytidine modification: functions and detections

1.4.1. Biogenesis of 3-methylcytidine

m^3C was first discovered in the total RNA extracted from S. cerevisiae [111]. Further studies validated the presence of m^3C in eukaryotic tRNAs (**Fig. 1.3A**) [22, 112]. m^3C sites in tRNAs are the most extensively studied sites. Positions 20, 32 and 47d of different subsets of tRNAs can be modified by m^3C. At isoacceptor level, Clark et al. identified nine m^3C32 sites in cytosolic $tRNA^{Arg}$, $tRNA^{Ser}$, and $tRNA^{Thr}$, two m^3C32 sites in mitochondrial $tRNA^{Ser}$ and $tRNA^{Thr}$, five m^3C47d sites in the variable loop region of $tRNA^{Leu}$ and $tRNA^{Ser}$, and one m^3C20 site in elongator $tRNA^{Met}$ using DM-tRNA-Seq in HEK293T cells (**Fig. 1.3B**) [22]. Two separate studies discovered TRM140 as the writer enzyme for the m^3C modification in $tRNA^{Ser}$ and $tRNA^{Thr}$ in S. cerevisiae and showed that TRM140 modulated m^3C modifications have an effect on translation [113, 114]. A follow-up mechanism study found two separate recognition elements in TRM140 and that TRM140 binding stimulates tRNA m^3C modification [115]. In contrast, in S. pombe two closely related TRM140 homologs, $TRM140^+$ and $TRM141^+$, are responsible for $tRNA^{Thr}$ and $tRNA^{Ser}$, respectively, indicating that multiple enzymes may act on the same m^3C sites [116]. In mammals, METTL2A/B and METTL6 are responsible for the formation of m^3C32 in cytosolic tRNAs and METTL2B is responsible for the formation of m^3C32 in mitochondrial tRNAs [112, 117]. However, the enzyme(s) that catalyze the formation of m^3C20 and m^3C47d are unknown. The presence of m^3C in rRNAs is controversial. In 1968, a study claimed the discovery of m^3C modification in HeLa 18S and 28S rRNA [118]. However, the m^3C sites

haven't been identified by either the LC-MS/MS technique [6] nor the high-throughput sequencing method [18]. Recently, a high-throughput sequencing method specifically for m^3C mapping detected the transcriptome-wide m^3C profile [18]. However, only 2 m^3C sites were found in addition to tRNA sites, one in RNVU1-7 snRNA and one in 5S rRNA. The m^3C site in 5S RNA is questionable and needs further validation due to the high mutatation rate at the target m^3C site. No m^3C sites in mRNA have been identified though the enzyme responsible for the m^3C sites in mRNA, METTL8, has been discovered and m^3C in mRNA have been validated by HPLC-coupled triple quadrupole mass spectrometry (HPLC-MS/MS) [117]. Xu et al. identified three m^3C "writer" enzymes, METTL2, METTLE6, and METTLE8, in mice and humans. METTL2 and METTL6 catalyze m^3C formation in a subset of tRNAs and METTL8 is only responsible for the formation of m^3C in mRNAs [117]. Later, ALKBH1 was identified as the eraser of m^3C in mammalian mRNA. Ma et al. found that ALKBH1 can demethylate m^3C in mRNA both in vitro and in vivo using HPLC-MS/MS [119].

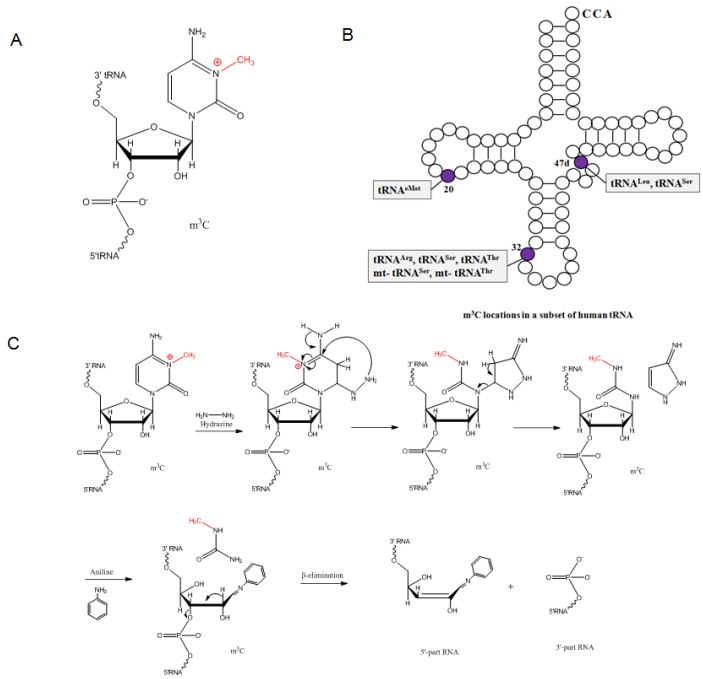

Fig. 1.3 Structures of m^3C and its location in tRNA. (A) Structure of m^3C. (B) m^3C location in subsets of tRNAs. (C) Mechanisms of hydrazine and aniline caused RNA cleavage at m^3C site. The RNA cleavage generates two RNA fragments, 3' part with intact Phosphate and 5' part RNA with broken 3' end.

1.4.2. Functions of 3-methylcytidine

The functions of m^3C are not fully understood. Based on current findings of m^3C, tRNAs harbor the most m^3C sites. Mao et al. showed that m^3C modification destabilized Watson-Crick base-pairing and induced a G to A mutation during RT by low fidelity RTs, such as HIV-1-RT, MMLV-RT, and MutiScribe-RT [120]. The m^3C writer, METTL8, is found to form a SUMOylated nuclear RNA-binding protein complex that induces R-loop and promotes tumorigenesis via m^3C modification in the nucleus [121]. A recent study of tRNA m^3C writer, METTL6, revealed a crucial role of METTL6 and m^3C modification of $tRNA^{Ser}$ in regulating mRNA translation, ribosome occupancy, and pluripotency of mouse embryonic stem cells and

tumor cell growth [122]. With the recent development of multiple m^3C detection methods, more insights into the biological functions of m^3C will be gained.

1.4.3. Detection methods of 3-methylcytidine

The original discovery and early studies of m^3C mainly used liquid chromatography to detect and characterize m^3C. m^3C modification bears a methyl group on position N3 of the Watson-Crick face (**Fig. 1.3A**) that causes a mutation or stop signature during RT, a feature that can be used for the detection of m^3C by primer extension or high-throughput sequencing methods. Three types of high-throughput mapping methods have been developed for the detection of m^3C. The first method is DM-tRNA-seq that was originally designed for tRNA sequencing using demethylase treatment [21]. AlkB demethylase (DM) and its mutants remove the methyl group on methylated bases such as m^3C and enable efficient RT read-through and reduce the mutation or stop signature at m^3C. By comparative analysis of ±DM treated samples, m^3C modification and fraction in tRNA can be deduced. However, other Watson-Crick face modifications such as m^1G, $m^{2,2}G$, and m^1A [22] also cause mutation or stop during RT, so DM-tRNA-seq is not specific for m^3C. The second method is AlkAniline-Seq that has been developed to detect m^7G and m^3C RNA modifications at single nucleotide resolution simultaneously [123]. This method relies on the alkaline and aniline induced cleavage at m^7G and m^3C sites. Similar to DM-tRNA-seq, AlkAniline-Seq is not specific for m^3C detection which limits its application to transcriptome-wide m^3C profiling. The third method is HAC-seq that can quantitatively map m^3C transcriptome-widely (**Fig. 1.3C**) [18]. This method employed optimized

hydrazine-aniline cleavage conditions for m^3C modification so as to only enable specific detection of m^3C. However, the background signal of HAC-seq is very high which makes it insensitive for detecting m^3C sites in low modification fractions and m^3C sites in low abundant mRNA.

1.5. Subjects of this thesis

My thesis focuses on the development of convenient low-throughput detection methods for routine detection of specific Ψ and Q modifications (Chapters 2 and 3). We also developed a solid-phase based library construction method for multiplexed high-throughput sequencing and RNA modification analysis. We have successfully applied the new sequencing method for the study of tRNA modifications including m^3C under various stress conditions (Chapter 4).

2. Sensitive and quantitative probing of pseudouridine modification in mRNA and long non-coding RNA

2.1. Abstract

Pseudouridine (Ψ) is the most abundant RNA modification in cellular RNA present in tRNA/rRNA/snRNAand also in mRNA and long non-coding RNA. Elucidation of Ψ function in mRNA/lncRNA requires mapping and quantitative assessment of its modification fraction at single-base resolution. The most widely used Ψ mapping method for mRNA/lncRNA relies on its reaction with N-Cyclohexyl-N′-(2-morpholinoethyl)carbodiimide (CMC), forming an adduct with the Ψ base in RNA that is detectable by reverse transcription (RT) stops. However, this method has not produced consistent Ψ maps in mRNAs; furthermore, available protocols do not lend confidence to the estimation of Ψ fraction at specificsites, which is a crucial parameter for investigating the biological relevance of mRNA modifications. Here we develop a quantitative RT-PCR based method that can detect and quantify the modification fraction of target Ψ sites in mRNA/lncRNA, termed CMC-RT and Ligation Assisted PCR analysis of Ψ modification (CLAP). The method still relies on RT stop at a CMC-Ψ site, but uses site-specific ligation and PCR to generate two distinct PCR products in the same sample, corresponding to the modified and unmodified site, that are visualized by gel electrophoresis. CLAP not only requires a small amount of cellular RNA to validate Ψ sites but also determines the Ψ fraction semi-quantitatively at target sites in mRNA/lncRNA. We determined the Ψ status of four mRNA sites and one lncRNA site whose modification fractions range from 30% to 84% in three human cell lines. Our method enables precise mapping and assessment of Ψ modification levels in low abundance

cellular RNAs.

2.2. Introduction

More than 170 types of RNA modifications have been identified in biology [124]. Pseudouridine (Ψ)was the first RNA modification discovered and is also the most abundant in cellular RNA [125].Ψ is the 5-ribosyl isomer of uridine (U) with a carbon-carbon (C5-C1′) bond in place of the nitrogen-carbon (N1-C1′) bond between the base and the sugar backbone. The C-C bond gives Ψ more rotational freedom and conformational flexibility [125, 126]. In addition, Ψ has an extra hydrogen bond donor at the N1 position. Ψ modification has been shown to rigidify RNA structure through hydrogen bonding to the ribosephosphate backbone and enhance RNA stacking. Ψ in rRNA and tRNA has been shown to fine-tune and stabilize the regional structure and help maintain their functions in mRNA decoding, ribosome assembly, processing, and translation [28, 31, 125, 126]. Ψ in snRNA has been shown to enhance spliceosomal RNA-pre-mRNA interaction to facilitate splicing regulation [127, 128]. A recent study unveile d arole for pseudouridylated tRNA fragments in translational control of stem cells [51].

Ψ has also been found in mRNA and long non-coding RNA (lncRNA) [12, 15, 129, 130]. Ψ is among the major mRNA modifications identified; its overall abundance as measured by mass spectrometry [12] is second only to N6-methyladenosine (m^6A). Additional Ψ modifications appear in the transcriptome under stress [129, 130], indicating that it is dynamic and plays multiple roles in the regulation of gene expression in a cell type- and cell state-dependent manner.

A well-defined function of Ψ in mRNA is to enable efficient stop codon readthrough [43].

To elucidate the biological function of Ψ in mRNA/lncRNA, it is crucial to validate the location of Ψ sites in low abundance RNA species. Like all mRNA/lncRNA modifications studied so far, the Ψ modification fraction at each mRNA site may also be highly variable and likely plays a role in regulating its function. At this time, all high-throughput sequencing methods rely on the reaction of N-cyclohexyl-N′-(2-morpholinoethyl)carbodiimide (CMC) with Ψ. CMC forms an adduct with Ψ residues in RNA after a series of chemical treatments. The CMC-Ψ adduct can be detected by primer extension methods that result in a reverse transcriptase (RT) stop [57] and/or occasional RT readthrough that leaves behind a mutation signature in the sequencing reads [59, 60]. The RT-stop method is the most commonly used approach. In either case, the multiple chemical handling steps generate higher than desired background in the sequencing reaction, so that mapping at the mRNA/lncRNA transcriptome level has not been consistent among different studies [28, 29]. Furthermore, transcriptome-wide mapping methods have not generated reliable information on the Ψ modification fraction at individual sites which is a biological variable in the response to cellular conditions.

Although candidate Ψ sites in abundant rRNA or snRNA can be validated by primer extension and denaturing gel analysis or thin-layer chromatography [131], validation of Ψ sites in low abundance mRNA/lncRNA has been challenging. In principle, a SCARLET-based method can be used to validate and quantify a target Ψ site in an mRNA [132], but this method requires radioactivity and requires a very large amount of input sample. Yi and colleagues developed a qPCR-based method for locus-specific detection of Ψ [60]. This method relies on induced

mutation/deletion in cDNA synthesis by the Superscript II RT; the resulting mutation/deletion PCR products generate distinct melting curves after RT-PCR. Although this method is radiolabel free and useful in identifying Ψ modification in mRNA, it cannot readily obtain quantitative information of Ψ fraction at individualsites.

Here we develop an RT-PCR- and gel electrophoresis-based method that validates and quantifies Ψ sites in mRNA/lncRNA at single-base resolution. Our method, termed CMC-RT and Ligation Assisted PCR analysis of Ψ modification (CLAP), still relies on the initial generation of the CMC-Ψ adduct at a target site and the RT stop it induces, but the RT stop product is selectively ligated to an oligonucleotide that subsequent PCR generates two different-sized products corresponding to the Ψ modified and unmodified target RNA in the same sample using a single set of PCR primers. This uniform amplification of cDNAs derived from Ψ modified and unmodified RNA produces quantitative information for individual Ψ sites. We first show that CLAP is quantitative in determining Ψ modification using an RNA standard and applying it to several rRNA Ψ sites. We then apply CLAP to 4 target mRNAs and 1 target lncRNAΨ site previously identified by high-throughput sequencing. We validate the presence of Ψ modification and obtain quantitative information about these mRNA/lncRNA sites in three human cell lines, thus demonstrating the utility of the method for quantitative investigations.

2.3. Results and discussion

2.3.1. Ψ in an RNA standard and rRNA

The unique feature of the CMC reaction with U-like and G-like residues has been known

since the 1970s and was first applied to identify Ψ in rRNA and tRNA in 1993 by primer extension [56, 57]. CMC can react with U, G, and Ψ residues to form N3-CMC and N1-CMC adducts. All except the N3-CMC-Ψ adducts are readily removed under alkaline conditions. In primer extension, the bulky N3-CMC group of Ψ stops the reverse transcriptase one nucleotide 3′ to the Ψ residue. This classical method has been adapted to map Ψ sites in the transcriptome at hundreds or even thousands of sites [12, 15, 129, 130]. The difficulty in using this method for low abundance mRNA transcripts is that sequencing reads that appear to be RT stops in the CMC-treated samples can be derived from multiple sources, which increases the noise for calling a Ψ site. Thus, quantitative assessment of Ψ fraction has not been reliable.

We developed a scheme to apply the CMC-based method for Ψ analysis, but with the goal of validating Ψ identification and at the same time quantifying the Ψ modification level at a target site (**Fig. 2.1A**). We reasoned that the RT stop product derived from a target CMC-treated Ψ site can be selectively amplified by ligating a DNA oligo guided by a complementary DNA splint to introduce the second PCR primer binding site. A crucial feature of our method is to make the second PCR primer binding site identical to a downstream region in the contiguous cDNA derived from the unmodified transcript encompassing the upstream RNA region to the target Ψ site so that a single set of PCR primers can be used to amplify both the RT-stopped and contiguous cDNA products simultaneously. Our design allows for the PCR products to have different lengths, a short one corresponding to the Ψ modified transcript and a ~30 base-pair longer product corresponding to the unmodified transcript. The application of a single set of PCR primers provides the uniformity needed to quantify both short and longPCR products in the same

reaction and in the same lane of a native gel. In contrast, conventional PCR methods involve two primer sets for RT-stop quantitation and use a subtractive strategy from two different PCR reactions, which increases a non-uniform bias in the PCR reaction [133]. Although multiplex PCR can also be used to detect different cDNA products, the need to use different PCR primer pairs may also impose a PCR amplification bias, and the ratio of the PCR products cannot be visualized in a single lane [134]. We termed our method CLAP which combines RT stops by CMC-Ψ, splint ligation, single-set primer PCR, and single lane visualization.

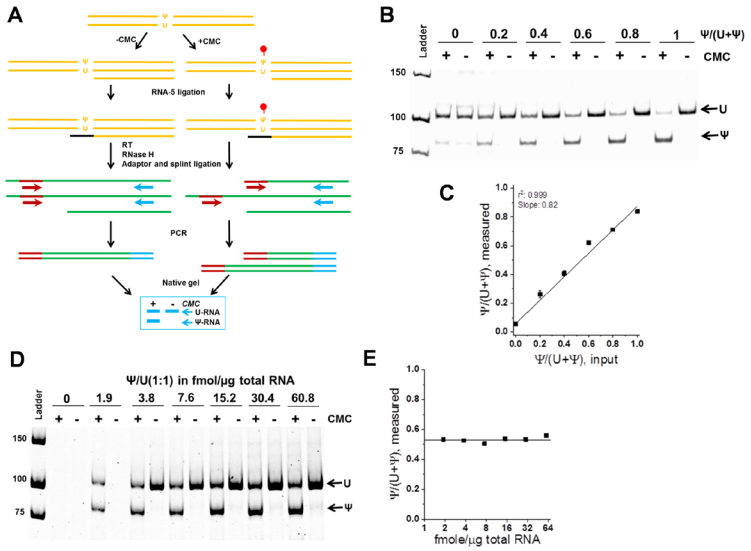

Fig 2.1: Schematics of the CLAP method and testing with U/Ψ-containing RNA standards. (A) Schematics. RNA-5 is a 5mer RNA oligo used to block the randomly cleaved RNA during the CMC treatment. RNA is shown as an orange line, RNA-5 as black line, cDNA as a green line, and the ligated primer binding site in Ψ +CMC as the red line at the end, with the same primer binding site in contiguous cDNA indicated as an embedded red line. PCR primers are represented by red and blue arrows. (B) Native PAGE showing two PCR bands derived from the U- and Ψ-containing RNA standard after the CLAP procedure. All samples contained 30 fmole of 100mer RNA standard at indicated Ψ fractionsspiked into 1 µg HEK293T total RNA. (C) Quantification of the result from panel B. The measured Ψ fraction is calculated by subtracting the fraction of the short product band in the -CMC lane from that of the +CMC lane. (D) Native PAGE showing the CLAP result of a 1:1 U/Ψ RNA standard mixture at different spike-in amounts added to 1 µg HEK293T total RNA. (E) Quantification of the result from panel D.

We first used a 100mer RNA standard to demonstrate the feasibility and the quantitative nature of the method (**Fig. 2.1B**). We mixed the fully Ψ-modified or unmodified 100mers at defined ratios and spiked the mixture into the HEK293T total RNA to mimic the subsequent analysis of mRNA transcripts. We started with an optimized CMC reaction with Ψ ([59], **Fig. 2.S1**) to obtain a nearly stoichiometric level of CMC-Ψ adduct.CMC procedures rely on harsh conditions and produce a higher than desired level of RNA fragmentation. The specific RNA

cleavage product 3′ to the target Ψ site would have produced the same RT product, thus increasing the background noise. To reduce this background, we first ligated a 5mer blocking RNA oligo to the free 5′ end of RNA cleavage products after the CMC treatment before carrying out the RT reaction (the RNA-5 ligation step in **Fig. 2.1A**). By optimizing the ligation conditions, we were able to reduce the non-Ψ derived, short PCR product by at least 4-fold (**Fig. 2.S2**). We performed RT reactions using the avian myoblastoma virus (AMV) reverse transcriptase, which is known to stop most frequently at Ψ-CMC adducts. In the CMC-treated sample, RT reaction would generate two cDNA products: a short one from the RT stop one nucleotide 3′ to the Ψ site and a long product from contiguous cDNA synthesis of the unmodified RNA. Guided by a complementary DNA oligo splint, we ligated the RT-stop cDNA product to a DNA oligonucleotide containing the identical forward PCR primer binding site >30 base pairs away from the Ψ site. Finally, we carried out PCR using just one set of forward and reverse primers to generate two PCR products corresponding to the Ψ-modified and unmodified RNA transcript. Analysis of the PCR products by native gel electrophoresis enabled the determination of Ψ modification fraction. Using ~30 fmole of the 100mer RNA standard (1 ng) spiked into one microgramof total RNA, we found that the CLAP method can quantitatively assess the input Ψ fraction (**Fig. 2.1B, 2.1C**). We also estimate from the calibration curve (**Fig. 2.1C**) that a Ψ site modified at ~5% level should be detectable using a 2-fold threshold above the background. To test the sensitivity of the CLAP method, we added a 1:1 mixture of Ψ/U-RNA standard to HEK293T total RNA at different concentrations. CLAP was able to precisely quantify the Ψ fractionat a ~1.9 fmol level in one microgram of total RNA (~60 pg/μg; **Fig. 2.1D, 2.1E**). Using

an estimate of total polyA+ RNA constituting ~3% of total RNA, this level corresponds to ~0.2% of total mRNA. In principle, CLAP should be able to analyze mRNA transcripts at even lower abundance upon increasing the PCR cycle number and additional optimization of PCR conditions.

To further validate the CLAP method, we examined three rRNA Ψ sites that can be independently tested by visualizing the CMC-Ψ derived RT stop products without amplification (**Fig. 2.2**). We chose one Ψ site (Ψ822) in 18S rRNA and two Ψ sites (Ψ3749 and Ψ4412) in 28S rRNA [6, 135]. Applying primer extension after CMC treatment, we found the Ψ levels to be 84% for 18S Ψ822, 74% for 28S Ψ3749, and 66% for 28S Ψ4412 (**Fig. 2.2A**). Applying the CLAP method, we determined the Ψ levels to be 83% for 18S Ψ822, 74% for 28S Ψ3749, and 71% for 28S Ψ4412 (**Fig. 2.2B**). This agreement between the primer extension and CLAP methods supports the feasibility of using CLAP for quantitative analysis of Ψ modifications. The modification fraction of the same three sites detected by mass spectrometry using TK6 rRNAwere all >99% [6]. This result suggests that the CLAP method is semi-quantitative to measure the absolute Ψ modification fraction and may underestimate the Ψ fraction by up to 1.4-fold, likely due to either incomplete CMC-Ψ adduct formation and/or a small amount of CMC-Ψ reversal in the CMC procedure.

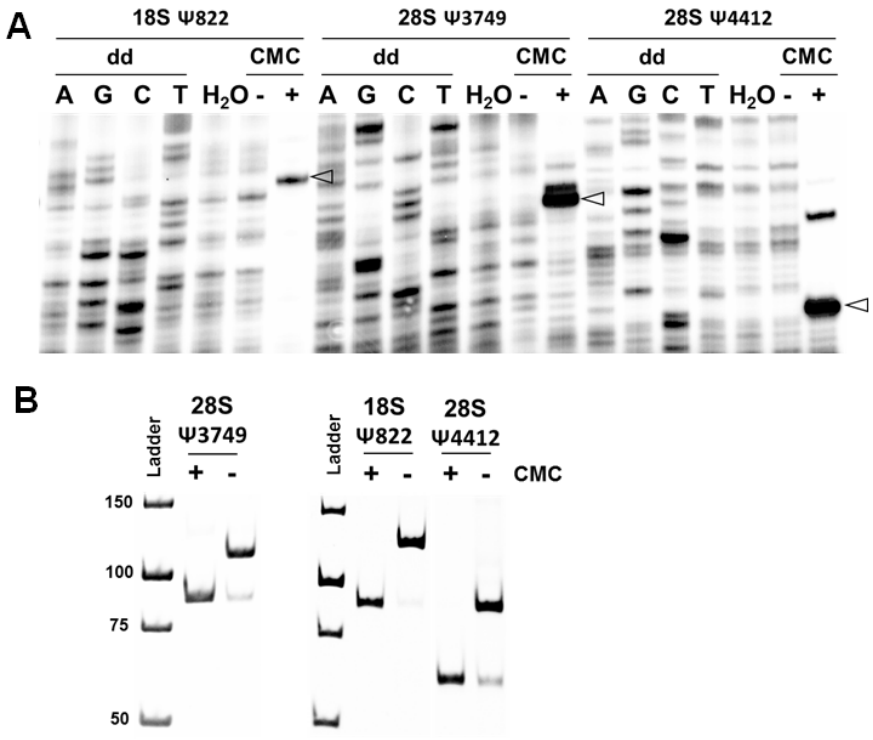

Fig 2.2: Quantification of Ψ levels in rRNA. (A) Primer extension of the 18S Ψ822, 28S Ψ3749, and 28S Ψ4412 sites. The RT stops are marked by a triangle. The estimated Ψ modification levels are 74% for Ψ3749, 84% for Ψ822, and 66% for Ψ4412. (B) CLAP result for the same three rRNA Ψ sites. The estimated Ψ modification levels are 74±3% for Ψ3749, 83±1% for Ψ822, and 71±1% for Ψ4412.

2.3.2. Ψ in mRNA and lncRNA

Next, we examined the Ψ status of two Ψ sites in the abundant eEF1A1 mRNA and one Ψ site in MALAT1 lncRNA. eEF1A1 is an isoform of the alpha subunit of the elongation factor-1 complex and playsan essential role in translation bydeliveringaminoacyl-tRNA to the ribosome. This mRNA hasbeen frequently used as a reference for qPCR studies [136, 137]. MALAT1 is a metastasis-promoting lncRNA and plays a role in alternative splicing, nuclear organization, epigenetic modulation of gene expression, synapse formation, and myogenesis [138]. Previous Ψ sequencing (CeU-seq, [12]) identified two Ψ sites in eEF1A1 (Ψ519 and Ψ875) and one Ψ site in

MALAT1 (Ψ5590).These sites have been validated by a qPCR-based Ψ detection method [60]. Applying the CLAP method, we determined the modification level of eEF1A1 Ψ519 at 31±2%, eEF1A1 Ψ875 at 56±3%, and MALAT1 Ψ5590 at 84±5% in HEK293T cells (**Fig. 2.3A**). The nearly complete pseudouridylation of the MALAT1 site is consistent with the high modification level (~75%) estimated by a qPCR-based method [60]. We also examined these Ψ sites in HeLa and MCF7 cell lines (**Fig. 2.3B**). eEF1A1 Ψ875 and MALAT1 Ψ5590 had similar Ψ modification levels in all three cell lines; in contrast,eEF1A1 Ψ875 levels ranged from 56±3% in HEK293T to 35±2% in MCF7.

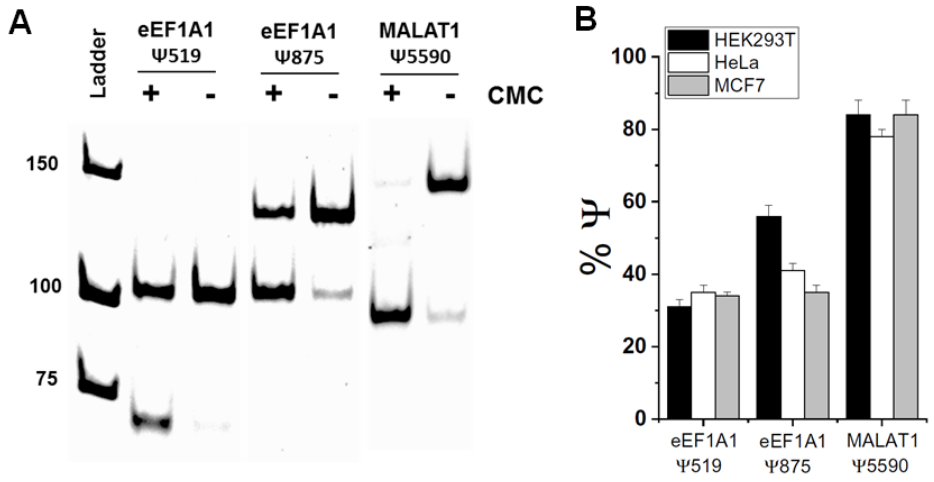

Fig 2.3: CLAP analysis of Ψ in high abundance mRNA and lncRNA transcripts. (A) CLAP examination of eEF1A1 Ψ519, eEF1A1 Ψ875, and MALAT1 Ψ5590 sites using 1 μg HEK293T total RNA. (B) Ψ modification levels in three cell lines, three biological replicates for each site.

To investigate the sensitivity of the CLAP method we chose two Ψ sites in low abundance mRNAs, hypoxanthine phosphoribosyltransferase 1 (HPRT1), and proteasome activator subunit 2 (PSME2) identified by CeU-seq [12, 60]. Both mRNAs are present at less than 1% the abundance of the eEF1A1 mRNA according to mRNA-seq analysis in HEK293T cells [139]. We

used 1 μg HEK293T total RNA to successfully measure the Ψ status of HPRT1 Ψ733 and PSME2 Ψ616. Applying the CLAP method, we determined that the modification level of HPRT1 Ψ733 was 51±1% and of PSME2 Ψ616 62±5% (**Fig. 2.4A**). To validate the accuracy and sensitivity of measuring Ψ status in low abundance mRNA in the context of total RNA by CLAP, we also used 50 ng polyA-selected RNA as input for the CLAP procedure (**Fig. 2.4B**). We found similar levels for HPRT1 Ψ733 (51% in total RNA and 46% in polyA-selected RNA) and a 1.4-fold higher level for PSME2 Ψ616 (62% in total RNA and 86% in polyA-selected RNA). Both sites showed similar modification levels among the three cell lines examined (**Fig. 2.4C**).

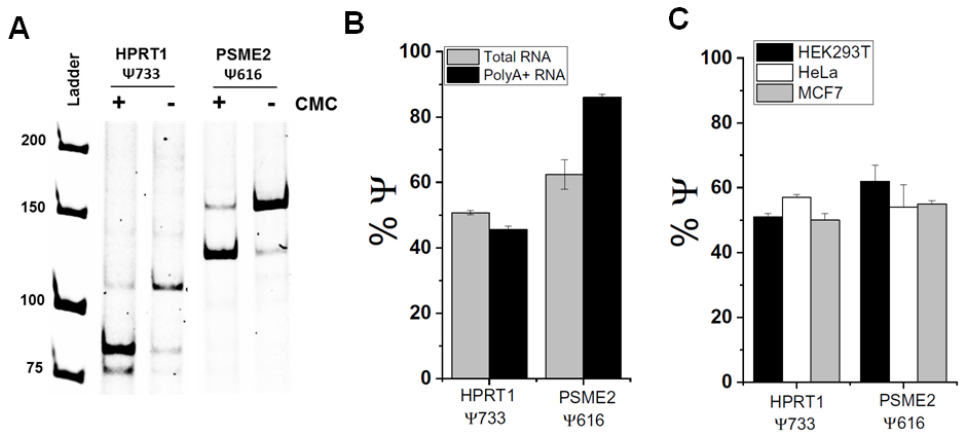

Fig 2.4: CLAP analysis of Ψ in low abundance mRNA transcripts. (A) CLAP results for HPRT1 Ψ733 and PSME2 Ψ616 using 1 μg of HEK293T total RNA as input. (B) CLAP quantitation of HPRT1 Ψ733 and PSME2 Ψ616 using HEK293T total RNA (1 μg input) or polyA+ RNA (50 ng input). (C) Ψ modification levels in three cell lines, three biological replicates for each site.

To assess the functional relevance of these 5 Ψ sites, we performed phylogenetic analysis among the vertebrate lineage (**Fig. 2.S3**) using Jalview [140]. The four mRNA Ψ-containing

regions are conserved across vertebrates, whereasthe Ψ5590-containing region is only present in the MALAT1 RNA from primates. All 4 mRNA sites are in the coding regions and part of a Val codon. The eEF1A1 Ψ519 site is in the third codon position (GUΨ); this uridine is sometimes changed to C, which still maintains the amino acid identity of the codon. eEF1A1 Ψ875, HPRT1 Ψ733, and PSME2 Ψ616 sites are in the second codon position (GΨU, GΨA); these uridines are unchanged in all vertebrates. The conserved Ψ modification in the second codon position may be useful for decoding these Val codons.

In summary, we developed a sensitive and quantitative RT-PCR method for site-specific analysis of Ψ modification. Our method can validate candidate Ψ sites in target mRNA and lncRNA using total RNA and directly visualize the modification levels. Since CLAP makes use of RT stops, in principle it can be applied to site-specific detection and quantitation of other RNA modifications that induce RT stops during cDNA synthesis. These include the Watson-Crick face RNA methylations of N^1-methyladenosine (m^1A), N^3-methylcytidine (m^3C), N^1-methylguanosine (m^1G), N^2,N^2-dimethylguanosine ($m^2{}_2G$), and N^3-methyluridine (m^3U). m^1A has already been shown to be present in mammalian mRNAs, but its modification levels at target sites have not been investigated [11, 141]. A potential limitation of the CLAP method is for closely spaced two or more Ψ sites in the same RNA, it can only accurately assess the 3' most Ψ site.

Among the mRNA/lncRNAtarget sites we analyze here, Ψ level ranges from 30% to 85%, which is compatible to the more abundant m^6A modification in mRNA/lncRNA. Quantitative measurement of the modification level is an important biological feature in the epitranscriptome

that has not received much attention. The quantitative nature of our CLAP method in the determination of Ψ status in low abundance mRNAs should enable the investigation of cell type- and cell state-dependent variations in Ψ levels.

2.4. Materials and Methods

2.4.1. Cell culture and RNA extraction

HEK293T, HeLa, and MCF7 cells were cultured under standard conditions. Briefly, HEK293T and HeLa cells were grown in Hyclone DMEM medium (GE Healthcare Life Sciences, SH30022.01) with 10% FBS and 1% Pen-Strep (Penicillin-Streptomycin) to 80% confluency. MCF7 cells were grown in EMEM medium (ATCC, 30-2003) with 10% FBS, 1% Pen-Strep, 0.01 mg/ml bovine insulin (Sigma-Aldrich, I0516), and 10 nM β-estradiol (Sigma-Aldrich, E2758) to 80% confluency. Total RNA was extracted using TRIzol reagent (ThermoFisher, 15596026) following the manufacturer's protocol. PolyA+ RNA was enriched using the PolyATtract mRNA Isolation System (Promega, Z5310) following the manufacturer's instructions.

2.4.2. In vitro transcription of U- or Ψ-containing control oligos

The 100-nt U- or Ψ-containing RNA standardwas in vitro transcribed using T7 RNA polymerase. In vitro transcription took place in 1× RNA polymerase buffer; 14 mM $MgCl_2$; 5 mM DTT; 4 mMeach ATP, GTP, CTP; 4 mM UTP or ΨTP (TriLink BioTechnologies, N-1019); 10 U/µl T7 RNA polymerase (NEB, M0251L); and 85 nM dsDNA template. The whole mixture was incubated at 37°C for 2.5 h. Then $1/10^{th}$ volumeof 3 M NaOAc/HOAc (pH 5.2) and 3x

volumeof 100% ethanol were added to the mixture to precipitate the RNA oligos. The precipitated RNA oligos were purified using 10% denaturing gels containing 7M urea.

The sequence of the RNA standard is as follows:

5′-GGGAGGCGAGAACACACCACAACGAAAACGAGCAAAACCCGG(Ψ/U)ACGCA ACACAAAAGCGAACAACGCGAAAAAGGACACCGAAGCGGAAGCAAAGACAAC-3′

2.4.3. CMC treatment of RNA

Total RNA or polyA+ RNA was CMC (N-cyclohexyl-N′-(2-morpholinoethyl)carbodiimide) labeled as previously described [59]. A major change in this work is the increased CMC reaction time (~16 hours) at lower temperature (30 °C) to ensure nearly complete conversion of Ψ to Ψ-CMC while minimizing RNA degradation. Briefly, 10µg total RNA or polyA+ RNA in 12 µl water was mixed with 24 µl of 1× TEU buffer consisting of 50 mM Tris-HCl (pH 8.3), 4 mM EDTA, 7 M urea, and 4 µl of 1M freshly prepared CMC in TEU buffer (+CMC) or just 4 µl TEU buffer (-CMC) for a final condition of 0.7× TEU buffer in 40 µl. The CMC reaction was carried out at 30°C for 16 h. To remove excess CMC, the following reagents were added to the reaction mixture: 160 µl of 50 mM KOAc (pH 7), 200 mM KCl; 3 µl of 5 µg/µl glycogen; and then 550 µl of ethanol. The mixture was incubated at –80°C for > 2h, then centrifuged at 15 krpm in a micro-centrifuge for 30 min. After removing the supernatant, the pellet was mixed with 500 µl of 75% ethanol and then kept at –80°C for at least 2h and centrifuged once more. The washing and precipitation steps were repeated one more time. To reverse the CMC-U/CMC-G adducts, the RNA pellet was mixed with 40 µl of 50 mM Na_2CO_3, 2 mM EDTA (pH 10.4), and incubated at 37°C for 6 h.The reaction mixture was then mixed with 160 µl of 50 mM KOAc (pH 7), 200 mM

KCl, followed by ethanol precipitation. The RNA recovery yield for this protocol was >65%.

2.4.4. RNA 5′ phosphorylation and RNA-5 blocking oligo ligation

To reduce the signal derived from RNA fragmentation during the CMC reaction, ±CMC-treated RNA in 6.5 µl H_2O was mixed with 0.5 µl RNase inhibitor (NEB, M0307L), 1 µl of 10× T4 PNK reaction buffer A, 1 µl of 1 mM ATP,1 µl of T4 Polynucleotide kinase (PNK), and then incubated at 37°C for 30 min.To ligate the RNA-5 oligo (/5AmMC6/rArCrCrCrA; Integrated DNA Technologies), 1 µl of 10×T4 RNA Ligase Reaction Buffer, 1 µl of 100 µM RNA-5 oligo, 1 µl of 1 mM ATP, 1 µl of RNase inhibitor, 3µl of DMSO, 2 µl of H_2O, and 1 µl of T4 RNA ligase I (NEB, M0437M) were added to this mixture and incubated at 16°C for 16h. The reaction was terminated upon the addition of 1.2 µl of 200 mM EDTA.

2.4.5. Reverse transcription and splint ligation

Reverse transcription was carried out using 3 µl of the above ligation mixture (~1 µg RNA) using AMV reverse transcriptase (NEB, M0277L) and target-specific primers. To anneal the primer,1 µl of 10× annealing buffer (250 mM Tris-HCl [pH 7.4], 480 mMKCl) and 1 µl of 0.5 µM target-specific RT primer were added, and the mixture was incubated at 93°C for 2min. To start the RT reaction, 5 µl of 2×AMV RT reaction mixture was added for a final condition of 0.6 U/µl AMV RT, 1× AMV RT buffer, and 0.5 mM of each dNTP. The RT reaction proceeded at 42°C for 1 h. After incubation at 85°C for 5 min to inactivate RT, 1 µl of 5 U/µl RNase H (NEB, M0297L) was added and the mixture incubated at 37°C for 20 min to digest the RNA. RNase H was inactivated by heating the mixture at 85°C for 5 min.

To anneal the adaptor, 1 µl of the adaptor/splint oligos mixture (1.5µM each) was added to

the above RT mixture, followed by incubation at 75°C for 3 min. To ligate the adaptor, 4 µl of 4× ligation mixture was added for a final concentration of 10 U/µl of T4 DNA ligase (NEB, M0202L), 1×T4 DNA ligase reaction buffer, and 12.5% DMSO. The ligation proceeded at 16°C for 16 h. DNA ligase was inactivated by heating the mixture at 65°C for 10 min.

2.4.6. PCR amplification and gel electrophoresis

To perform PCR, 2 µl of the above ligation mixture was mixed with various components for a final condition of 1× Q5 reaction buffer, 1× Q5 high GC enhancer, 200µM of each dNTP, 0.5 µM forward and reverse primers, and 0.02 U/µl Q5 high-fidelity DNA polymerase (NEB, M0491L); the final PCR reaction volume was 35 µl. PCR was done for high abundance eEF1A1 mRNA and MALAT1 RNA sites at 15 cycles and for low abundance PSME2 and HPRT1 sites 25-35 cycles.

Half of the PCR mixture (17.5 µl) was mixed with 3.5 µlof 6×TriTrack DNA Loading Dye (ThermoFisher, R1161). The entire mixture was loaded on a pre-run 10% non-denaturing gel containing 1× TBE, together with low range DNA ladder (ThermoFisher, SM1193). The gel was stained with SYBR gold nucleic acid gel stain (ThermoFisher, S11494) for 10 min. Product bands were visualized using the Bio-Rad ChemiDoc imaging system and the bands quantified using Image Lab.

2.4.7. CLAP Primer and oligonucleotide sequences

PseudoU_CtrlRT Primer: 5′-GTTGTCTTTGCTTCCGCTTCG-3′

PseudoU_Ctrl Adaptor: 5′-pCCATGGGTGTGTTCTCGCCTCCC-3′

PseudoU_Ctrl Splint: 5′-ACACCCATGGACGCAACACA/3SpC3/-3′

PseudoU_Ctrl Forward PCR Primer: 5′-GGGAGGCGAGAACACACC-3′

28S Ψ3749 RT Primer: 5′-TCGTTCATCCATTCATGCGC-3′

28S Ψ3749 Adaptor: 5′-pCCATGGCGCTTCATTGAATTTCTTCAC-3′

28S Ψ3749 Splint: 5′-AGCGCCATGGCTTAAGGTAG/3SpC3/-3′

28S Ψ3749 Forward PCR Primer: 5′-GTGAAGAAATTCAATGAAGCGC-3′

18S Ψ822 RT Primer: 5′-AACCGCGGTCCTATTCCATTATT-3′

18S Ψ822 Adaptor: 5′-pCCATGGACACTCAGCTAAGAGCATCG-3′

18S Ψ822 Splint: 5′-GTGTCCATGGTCAAAGCAGG/3SpC3/-3′

18S Ψ822 Forward PCR Primer: 5′- CGATGCTCTTAGCTGAGTGTC-3′

28S Ψ4412 RT Primer: 5′-TGCTTCACAATGATAGGAAGAGCC-3′

28S Ψ4412 Adaptor: 5′-pCCATGCCGCCACAAGCCAGTTAT-3′

28S Ψ4412 Splint: 5′-GGCGGCATGGCCTTCGATGT/3SpC3/-3′

28S Ψ4412 Forward PCR Primer:5′-ATAACTGGCTTGTGGCGG-3′

EEF1A1 Ψ519RT Primer: 5′-ATATCTCTTCTGGCTGTAGGGTG-3′

EEF1A1 Ψ519 Adaptor: 5′-pCCATGGCCAGAAGGGCATGCTCT-3′

EEF1A1 Ψ519 Splint: 5′-CTGGCCATGGAACAAAATGG/3SpC3/-3′

EEF1A1 Ψ519 Forward PCR Primer: 5′-AGAGCATGCCCTTCTGGC-3′

EEF1A1 Ψ875 RT Primer: 5′-TGCATTTCGACAGATTTTACTTCCG-3′

EEF1A1 Ψ875 Adaptor: 5′-pCCATGTACCACCAATTTTGTAGACATCCTG-3′

EEF1A1 Ψ875 Splint: 5′-TGGTACATGGTCTCAAACCC/3SpC3/-3′

EEF1A1 Ψ875 Forward PCR Primer: 5′-CAGGATGTCTACAAAATTGGTGGTA-3′

MALAT1 Ψ5590 RT Primer: 5′-TAAAGATGCAAATGCCTCTGAGTGA-3′

MALAT1 Ψ5590 Adaptor: 5′-pCCATGAGGAGAAAGTGCCATGGTTGATATT-3′

MALAT1 Ψ5590 Splint: 5′-CTCCTCATGGAGGACTTGTT/3SpC3/-3′

MALAT1 Ψ5590 Forward PCR Primer: 5′-AATATCAACCATGGCACTTTCTCCT-3′

HPRT1 Ψ733 RT Primer: 5′-GACACAAACATGATTCAAATCCCTG-3′

HPRT1 Ψ733 Adaptor: 5′-pCCATGAAAGTCTGGCTTATATCCAACACTT-3′

HPRT1 Ψ733 Splint: 5′-ACTTTCATGGAGGATATGCC/3SpC3/-3′

HPRT1 Ψ733 Forward PCR Primer: 5′-AAGTGTTGGATATAAGCCAGACTTT-3′

PSME2 Ψ616 RT Primer: 5′-TATGATAAAGCTCAGCATAGAAGGC-3′

PSME2 Ψ616 Adaptor:5′-pCCATGCGTTCTGAGAAGTACTTGGAAATGG -3′

PSME2 Ψ616 Splint:5′-GAACGCATGGAATGGATTAC/3SpC3/-3′

PSME2 Ψ616 Forward PCR Primer: 5′-CCATTTCCAAGTACTTCTCAGAACG-3′

3. Detection and quantification of glycosylated queuosine modified tRNAs by acid denaturing and APB gels

3.1. Abstract

Queuosine (Q) is a conserved tRNA modification in bacteria and eukaryotes. Eukaryotic Q-tRNA modification occurs through replacing the guanine base with the scavenged metabolite queuineat the wobble position of tRNAs with $\underline{G}_{34}U_{35}N_{36}$ anticodon (Tyr, His, Asn, Asp) by the QTRT1/QTRT2 heterodimeric enzyme encoded in the genome. In humans, Q-modification in $tRNA^{Tyr}$and $tRNA^{Asp}$ are further glycosylated with galactose and mannose, respectively. Although galactosyl-Q (galQ) and mannosyl-Q (manQ) can be measured by LC/MS approaches, the difficulty of detecting and quantifying these modifications with low sample inputs has hindered their biological investigations. Here we describe a simple acid denaturing gel and non-radioactive Northern blot method to detect and quantify the fraction of galQ/manQ-modified tRNA using just microgram amounts of total RNA. Our method relies on the secondary amine group of galQ/manQ becoming positively charged to slow their migration in acid denaturing gels commonly used for tRNA charging studies. We apply this method to determine the Q and galQ/manQ modification kinetics in three human cells lines. For Q-modification, $tRNA^{Asp}$ is modified the fastest, followed by $tRNA^{His}$, $tRNA^{Tyr}$ and $tRNA^{Asn}$. Compared to Q-modification, glycosylation occurs at a much slower rate for $tRNA^{Asp}$, but at a similar rate for $tRNA^{Tyr}$. Our method enables easy access to study the function of these enigmatic tRNA modifications.

3.2. Introduction

tRNA is the most extensively modified RNA in cells. On average, a eukaryotic tRNA

contains ~13 modifications [142]; among these, queuosine (Q) stands out as it is the only known eukaryotic tRNA modification that requires a metabolite from bacteria. First discovered in 1960s, Q-modification occurs in tRNA families of amino acids Tyr, His, Asn, Asp. These tRNAs have $G_{34}U_{35}N_{36}$ anticodons, and G_{34}-to-Q modification occurs exclusively at the wobble anticodon position. tRNA Q-modification in bacteria is synthesized de novo through a biogenesis pathway containing 8 steps. Eukaryotes cannot synthesize Q, rather, they depend on scavenging the metabolite queuine from diets or gut microbiome catabolism [143], followed by the G_{34}-to-Q incorporation in the same 4 tRNA families bya multimeric enzyme encoded in the genome (e.g. QTRT1 and QTRT2 genes in humans).

The exploration of molecular functions of Q-modification has been on-going since its identification [72, 91, 144]. Its occurrence at the wobble anticodon position indicates that it plays a role in mRNA decoding. All Q-modified tRNAs read codons composed of NAC/NAU, so Q_{34} directly pairs with C or U in the third codon position. Indeed, tRNA Q-modification has been shown to affect differential decoding of C or U ending codons to influence translation efficiency or protein misfolding [89, 90, 92]. tRNA Q-modification may also affect translation fidelity to facilitate genome-wide reprogramming of codon usage in Drosophilids [96]. tRNA Q-modification can also improve the activity of the antioxidant enzymes and suppress oxidative stress [145]. In S. pombe, $tRNA^{Asp}$ Q-modification affects its 5-methyl-C modification in the anticodon loop, resulting in differential activity of $tRNA^{Asp}$ in translation speed, accuracy and aminoacylation [92, 146]. In human cells, tRNA Q-modification can protect cognate tRNA from ribonuclease cleavage and affects cellular tRNA fragment pools [97].

Intriguingly, Q-modified $tRNA^{Tyr}$ and $tRNA^{Asp}$ in many eukaryotes are further glycosylated with galactose and mannose to generate galactosyl-Q (galQ) and mannosyl-Q (manQ, [74, 76], **Fig. 3.1A**). To our knowledge, these are the only known tRNA modifications that contain glycoslyation, yet, the function of these glycosylations has remained elusive.

tRNA Q-modification is commonly measured using liquid chromatography/mass spectrometry (LC/MS) or a N-acryloyl-3-aminophenylboronic acid (APB) gel-based approach [5, 96, 109, 110]. Although LC/MS based method is powerful and can quantify Q, galactosyl-Q and mannosyl-Q modified tRNAs (Costa et al. 2004), it requires very large amounts of input RNA, making its application difficult for routine investigation on these tRNA modifications. The glycosylated $tRNA^{Tyr}$ and $tRNA^{Asp}$ can be isolated by lectin-Sepharose affinity chromatography [75], but this method does not measure modification fraction. The APB gel method requires only microgram amount of total RNA, and quantitation is straightforward using Northern blots. The principle of APB gel separation is the presence of the cis-diol group on Q-modification that slows the migration of Q-modified versus unmodified tRNA in the presence of APB. This cis-diol group, however, is further modified in the galQ/manQ of $tRNA^{Tyr}$ and $tRNA^{Asp}$, so that the migration of these two tRNAs are no longer distinguishable from unmodified tRNAs in standard APB gels.

Acid denaturing gels are widely used in tRNA charging studies [147]. The principle of separating charged versus uncharged tRNA at pH ~5 is the protonation of the α-amino group of the amino acid attached to the 3' end of a charged tRNA. Here, we found that the same acid denaturing gel can also separate Q- as well as galQ/manQ-modified tRNAs through the

protonation of the secondary amine group (**Fig. 3.1A**). After separation, both unmodified and galQ/manQ modified tRNAs can be quantified by Northern blots using ^{32}P-labeled as well as non-radioactive, biotinylated DNA probes with similar amounts of input RNA. Our approach therefore uncouples the detection of Q-modification and Q-glycosylation. Using this method, we studied the biological incorporation kinetics of Q- and galQ/manQ-modified tRNAs in three human cell lines. Among the four tRNAs, the rank order of Q-modification rates was $tRNA^{Asp}$, $tRNA^{His}$, $tRNA^{Tyr}$, and $tRNA^{Asn}$, whereas the glycosylation rates were similar for $tRNA^{Asp}$ and $tRNA^{Tyr}$.

3.3. Results and discussion

3.3.1. Separation of glycosylated Q-tRNAs by acid denaturing gels

The current approach of separating Q-modified and unmodified tRNA is based on application of standard denaturing gels supplemented with a boric acid derivative [96, 110]. This method relies on the cis-diol group in the five membered ring of the Q-base; it does not work for galQ/manQ modifications as the cis-diol is now attached to galactose or mannose. Both Q and galQ/manQ modifications still retain the secondary amine group connecting the modified nucleobase with the five membered ring (**Fig. 3.1A**). We reasoned that this amine group may become protonated under pH ~5 conditions used to separate aminoacylated from uncharged tRNAs [147]. We took advantage of the cell lines generated by us [97] that either contains no Q-modification at all (0Q) or 100% Q-modification (100Q) in all tRNAs. After deacylation to remove 3’ attached amino acids, samples were run on pH 4.8, acid denaturing gels, followed by

membrane transfer and Northern blot (**Fig. 3.1B**). We found that the acid denaturing gel can indeed separate galQ/manQ modified from unmodified tRNA^{Tyr} and tRNA^{Asp} using ^{32}P-labeled tRNA probes (**Fig. 3.1C**).

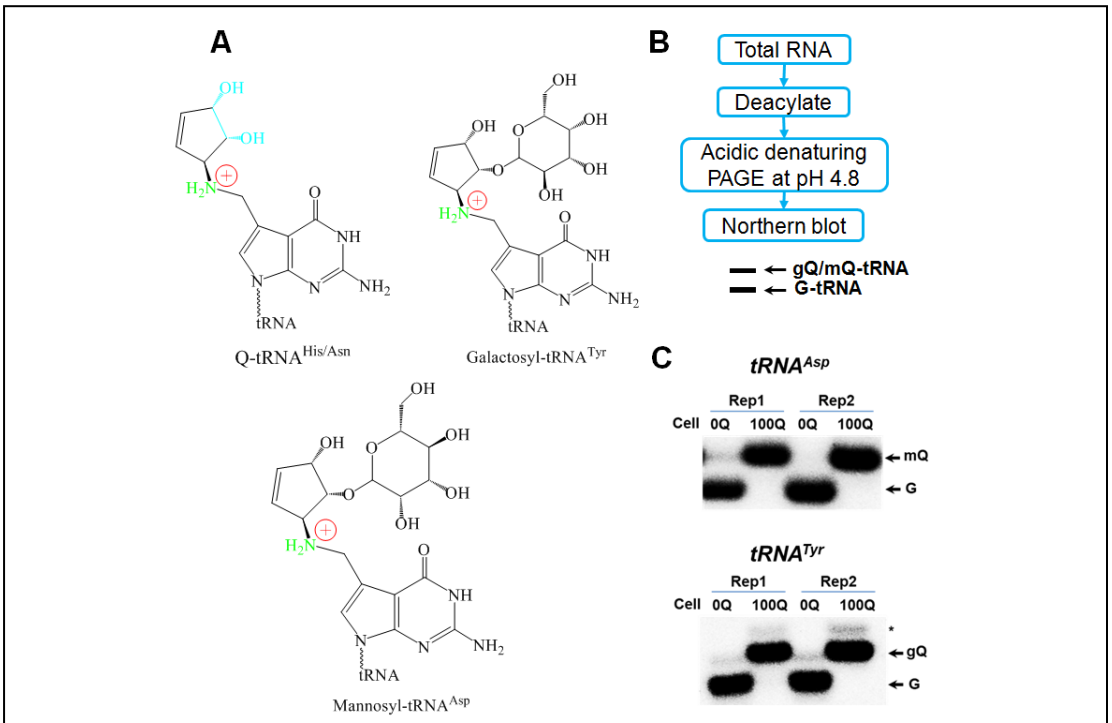

Fig 3.1: Queuosine and glycosylated queuosine modification and acid denaturing gel/Northern blot detection. (A) Structure of the protonated queuosine and glycosylated queuosine base. (B) Schematic of acid denaturing gel and Northern blot detection of Q- and glycosylated Q-modified tRNAs. Northern blots can be performed using either ^{32}P-labeled or 5' biotin-labeled tRNA probes. (C) Acid denaturing gel and Northern blot showing separation of glycosylated Q-modified tRNA^{Asp} (mQ: mannosyl-Q) and tRNA^{Tyr} (gQ: galactosyl-Q) from unmodified tRNA (G) using ^{32}P labeled probes. * indicates an unknown tRNA^{Tyr} species. 0Q: total RNA from cells without Q-modification; 100Q: total RNA from cells with full Q-modification. Total RNA was from HEK293T cells.

We examined the application of using biotinylated tRNA probes for sensitivity and convenience. After transferring the acid denaturing gel to the membrane, 5' biotinylated probe was hybridized and then directly detected by streptavidin conjugated horseradish peroxidase (HRP) and Enhanced chemiluminescence (ECL) reagents. We found that our biotin-detection

method worked for the glycosylated Q-modified $tRNA^{Tyr}$ and $tRNA^{Asp}$ as well as the Q-modified $tRNA^{His}$ and $tRNA^{Asn}$ (**Fig. 3.2A**) using a similar amount of total RNA input as ^{32}P-labeled tRNA detection. These results demonstrate the practicality of using biotinylated probes in tRNA Northern blots with good signal strength and low background.

A prediction of our method is that the acid denaturing gel based separation of Q, galQ/manQ and unmodified tRNA should be insensitive to periodate treatment. This is in contrast to APB gel based separation of Q and unmodified tRNA which is eliminated upon periodate oxidation of the cis-diol group on the Q-base [96]. Periodate, however, does not react with the secondary amine group in Q and galQ/manQ. Indeed, we found that the separation for $tRNA^{Tyr}$ and $tRNA^{Asp}$ was unaffected by periodate treatment (**Fig. 3.2B**). As a control, the same periodate reaction eliminated the separation of Q and unmodified tRNAs in the APB gels (**Fig. 3.S1**). Together, these results validate the utility of acid denaturing gels and biotin-probe Northern blots in the analysis of glycosylated Q-modified and also Q-modified tRNAs.

Our periodate and control experiment here used total RNA extracted from 0Q starter cells exposed to queuine after 1 and 24 hours. After 24 hours all tRNAs were modified (**Fig. 3.2B, 3.S1**). We noticed in the 1-hour time point sample in the APB gel (**Fig. 3.S1A**) that $tRNA^{Tyr}$ and $tRNA^{Asp}$ both showed a band sensitive to periodate treatment, suggesting that these were Q-modified tRNA intermediates before they became glycosylated.We took advantage of this result next to measure the tRNA Q-modification kinetics by combining acid denaturing gel and APB gel results.

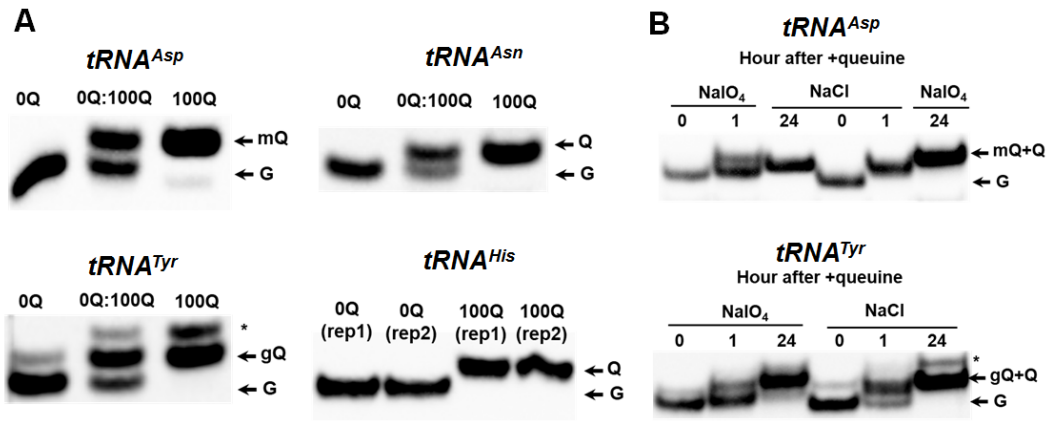

Fig 3.2: Analysis of Q and glycosylated Q-modified tRNAs using biotinylated tRNA probes. (A) Acid denaturing gels and Northern blot of individual, Q or glycosylated Q-modified tRNA. 0Q: total RNA from cells without Q-modification; 100Q: total RNA from cells with full Q-modification; 0Q:100Q: equal amount mixture of 0Q and 100Q total RNA. G: unmodified tRNA, Q: Q-modified tRNA, mQ: mannosyl-Q, gQ: galactosyl-Q. (B) Acid denaturing gels and Northern blot of $tRNA^{Asp}$ and $tRNA^{Tyr}$ with ($NaIO_4$) and without (NaCl) periodate treatment. 0: total RNA from 0Q cells; 1, 24: total RNA from cells 1 and 24 hours after the addition of queuine to 0Q cells.* indicates an unknown $tRNA^{Tyr}$ species. Total RNA was from MCF7 cells.

3.3.2. Q and galQ/manQtRNA modification dynamics in three cell lines

A biological application of our method is to measure the Q and glycosylation kinetics in cells to reveal the dynamic nature of these tRNA modifications. Queuine uptake dynamics of its cellular import from extracellular space into the cytosol has been studied previously. A biphasic queuine uptake mechanism was found in which a fast transporter component became saturated within 2-4 min and a slow transporter component equilibrated within 3-4 hours [72]. Administration of exogenous queuine to tRNA Q-modification depleted germ-free mouse showed faster queuine incorporation for $tRNA^{Asp}$ than for $tRNA^{His}$ [143].

We investigated the Q-modification kinetics in three human cell lines: HEK293T derived from embryonic kidney, HeLa from cervical cancer, and MCF7 from breast cancer. Our experiment started with the 0Q cells we generated as previously described [97]. At t = 0, queuine

was added at 1 μM or 10 nM directly to the medium. The high, 1 μM queuine likely results in the saturation of the transport and Q-modification kinetics, while the low, 10 nMqueuine approximates more of the physiological concentration of queuine in body fluids [148]. The Q-modification kinetics can include the cellular uptake of queuine and its enzymatic incorporation into the cognate tRNAs, both can be affected by the queuine concentrations in the medium.

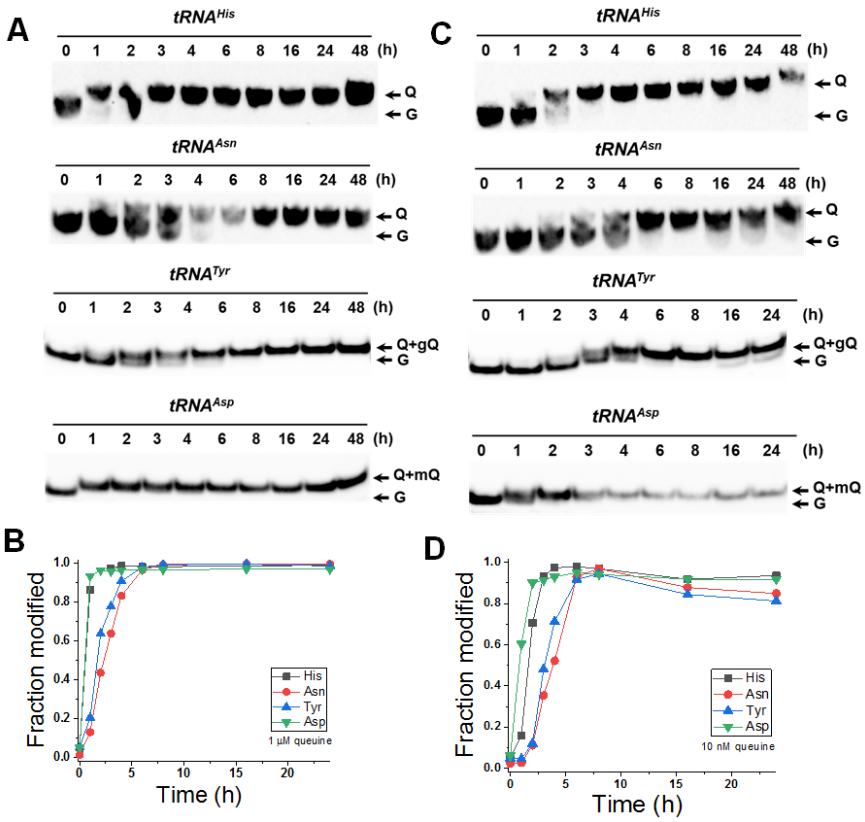

Fig 3.3: Q and glycosylated Q-modification kinetics ofHEK293T cells by APB and acid denaturing gels. (A)Time course of individual Q or glycosylated Q-modified tRNA. At t=0, 1 μM queuine was added to the medium of 0Q cells, total RNA was extracted after designated time points in hours. $tRNA^{His}$ and $tRNA^{Asn}$ are from APB gels, $tRNA^{Tyr}$ and $tRNA^{Asp}$ are from acid denaturing gels. G: unmodified tRNA, Q: Q-modified tRNA, mQ: mannosyl-Q, gQ: galactosyl-Q. (B) Quantitative modification fraction over time for individual tRNAs, from 1 μM queuine data. For $tRNA^{His}$ and $tRNA^{Asn}$, the modification fraction represents Q; for $tRNA^{Asp}$ and $tRNA^{Tyr}$, the modification fraction represents the sum of the Q and glycosylated Q modifications. (C), (D) Same as (A), (B) except at t=0, 10 nM queuine was added to the medium of 0Q cells.

In HEK293T cells, we found that the total tRNA modification measured by acid denaturing gels occurred at distinct rates for the 4 cognate tRNAs (**Fig. 3.3**). Our result is a combination of multiple steps in the modification pathway which includes a minimum of queuine uptake, a first enzymatic reaction for Q-modification of all 4 tRNAs, and a second enzymatic reaction for glycosylation of $tRNA^{Tyr}$ and $tRNA^{Asp}$, none of these steps could be readily measured independently. Instead of trying to fit our result using complex, multi-step equations, we chose to

use the simplest, one-exponential kinetics fitting of the modification fraction over time to obtain an approximate modification rate and a delay time which may be related to the time lag of queuine uptake. At both high and low queuine concentration, the rank order of modification rate was $tRNA^{Asp}$>$tRNA^{His}$>$tRNA^{Tyr}$ ~ $tRNA^{Asn}$, with $tRNA^{Asp}$ modified the fastest (**Table 3.1**). The rate difference between the fastest and the slowest tRNA was ~10-fold at high and ~4-fold at low queuine concentration. The delay time for individual tRNA ranged from too fast to be measured to ~0.5 h which also tracked with the rank order of the modification rates. We also quantified the Q-modified $tRNA^{Asp}$ and $tRNA^{Tyr}$ intermediates over time by APB gels (**Fig. 3.4**). This measurement allowed for an estimate of the glycosylation rates for both tRNAs (**Table 3.1**). Using the simplest exponential decay fit we found the glycosylation rates to be about the same at high and low queuine concentration for both $tRNA^{Asp}$ and $tRNA^{Tyr}$. Compared to the Q-modification rate, the glycosylation rate was more than ~3-fold slower for $tRNA^{Asp}$ but was about the same for $tRNA^{Tyr}$, thus explaining the appearance of the relatively high levels of Q-modified $tRNA^{Asp}$ intermediate.

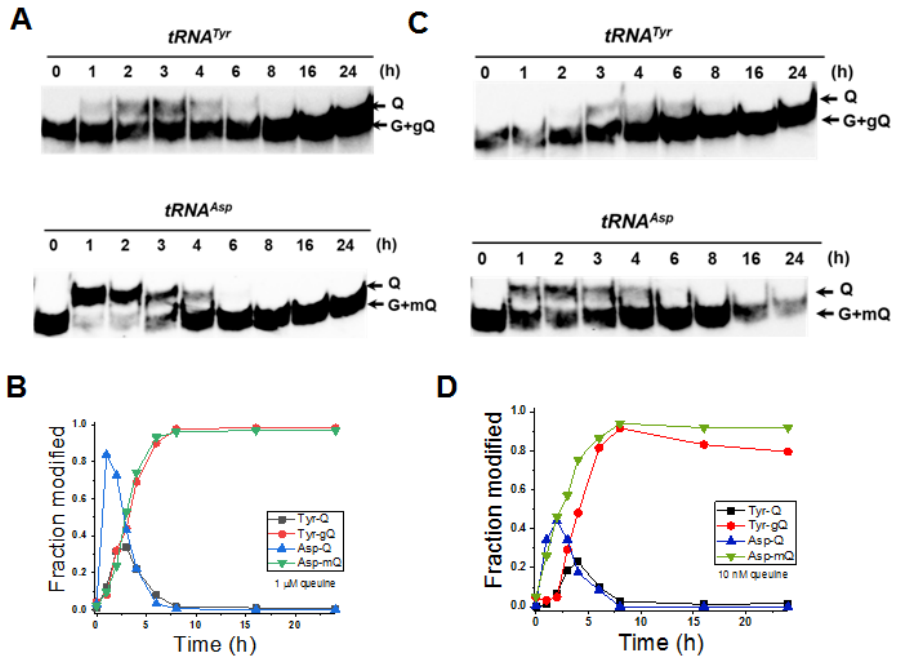

Fig 3.4: Q-modification kinetics of tRNAAsp and tRNATyrin HEK293T cells by APB gels. (A) At t=0, 1 μM queuine was added to the medium of 0Q cells, total RNA was extracted after designated time points in hours. G: unmodified tRNA, Q: Q-modified tRNA, mQ: mannosyl-Q, gQ: galactosyl-Q. The reversal to fast migration in later time points corresponds to gQ or mQ products as indicated by the acid denaturing gel results from Figure 3. (B) Quantitative modification fraction over time for individual tRNAs, from 1 μM queuine data. For comparison the total modification fraction from acid denaturing gel results in Figure 3 are also shown. (C), (D) Same as (A), (B) except at t=0, 10 nMqueuine was added to the medium of 0Q cells.

We also determined the Q-modification kinetics in HeLa and MCF7 cells using the same combination of acid denaturing gels and APB gels (**Table 3.1, Figs. 3.S2-3.S5**). In these cells, the rank order of $tRNA^{Asp}$>$tRNA^{His}$>$tRNA^{Tyr}$ ~ $tRNA^{Asn}$ was maintained, although the absolute rate constant was variable. The delay time was also of a similar magnitude as those in HEK293T cells. Still, even the lowest modification rate ($tRNA^{Asn}$) in all cases was ~0.25 h^{-1}, corresponding to a half-live of modification of ~3 hours. The glycosylation rates for HeLa and MCF7 were up to ~2.5 times faster than for HEK293T which may reflect the expression differences of the unknown glycosylase enzymes in these cells.

Table 1: Q and glycosylated Q modification rates in three human cell lines. Queuosine modification and glycosylation kinetics was done in HEK293T, HeLa, and MCF7 cells.

Queuine	**Asp**		**His**		**Tyr**		**Asn**	
HEK293T	Rate (h^{-1})[f]	Delay (h)	Rate (h^{-1})[f]	Delay (h)	Rate (h^{-1})	Delay (h)	Rate (h^{-1})	Delay (h)
1 μM	3.4±0.2[a] 0.41±0.02[b]	0	2.1±0.2[c]	0	0.46±0.07[d] 0.35±0.03[e]	0.03	0.35±0.05[c]	0.2
10 nM	1.1±0.1[a] 0.41±0.06[b]	0	0.59±0.14[c]	0.05	0.31±0.10[d] 0.35±0.03[e]	0.35	0.25±0.08[c]	0.5
HeLa								
1 μM	1.6±0.3[a] 0.43±0.07[b]	0	1.5±0.2[c]	0	0.65±0.09[d] 0.49±0.10[e]	0	0.51±0.16[c]	0.2
10 nM	0.86±0.16[a] 0.65±0.08[b]	0.07	0.55±0.19[c]	0.2	0.23±0.05[d] 0.61±0.02[e]	0.2	0.25±0.11[c]	0.6
MCF7								
1 μM	5.3±0.8[a] 0.87±0.08[b]	0	1.3±0.2[c]	0.04	0.86±0.19[d] 0.42±0.04[e]	0.04	0.59±0.09[c]	0.06
10 nM	1.2±0.1[a] 0.49±0.12[b]	0	0.50±0.10[c]	0.14	0.35±0.08[d] 0.91±0.08[e]	0.25	0.34±0.16[c]	0.25

a. G →Q+manQ.
b. Q →manQ.
c. G → Q.
d. G →Q+galQ.
e. Q →galQ
f. Errors are from curve fitting parameters.

3.3.3. Concluding remarks

In summary, we developed an acid denaturing gel methodfor the detection and quantitation of glycosylated Q-modified tRNAs. Our method takes advantage of the protonation of an amine group in the modified base; in principle it should also be applicable for other human tRNA modifications such as N^3-(3-amino-3-carboxypropyl)-uridine (acp^3U) [149]. Our acid denaturing gel method requires only microgram amounts of total RNA and setups in every laboratory. The acid denaturing gel method relies on the charge difference between unmodified and modified

tRNAs, so a limitation of the method is the difficulty of separating Q-modified from glycosylated Q-modified tRNAs. APB gel relies on the chemistry of the cis-diol and boric acid derivatives in the gel, so a limitation of the method is the difficulty of separating unmodified from glycosylated Q-modified tRNAs. By combining acid denaturing gel and the previously established APB gel for Q-modified tRNAs, our method allows for comprehensive analysis of Q and glycosylated Q-modifications in all human tRNAs.

Quantification of tRNA modification fractions is a crucial aspect of functional analysis of RNA modification. Our method is of interest specifically for the studies of glycosylated Q-modified tRNAs which had been difficult to perform due to the difficulties and limitations of existing approaches. Furthermore, the ease of Northern blots using biotinylated tRNA probes should enable more widespread applications of the acid denaturing gel and the APB gel methods described here. Future studies will include the identification of the glycosylation enzymes [150] and the functional analysis of these tRNA glycosylation modifications with yet-to-be assigned biological functions.

3.4. Materials and Methods

3.4.1. Generation of 0Q and 100Q cells

HEK293T, HeLa, and MCF7 cells were cultured with complete DMEM or EMEM medium under standard conditions. The 0Q and 100Q cells were obtained as previously described [97]. Briefly, MCF7 cells were grown in EMEM medium (ATCC, 30-2003) with dialyzed 10% FBS (ThermoFisher Scientific, 26400044), 0.01 mg/ml bovine insulin (Sigma-Aldrich, I0516), and 10

nM β-estradiol (Sigma- Aldrich, E2758) to 80% confluency and passaged. HEK293T and HeLa cells were grown in Hyclone DMEM medium (GE Healthcare Life Sciences, SH30022.01) with 10% dialyzed FBS to 80% confluency and passaged. Total RNAs were extracted using TRIzol (ThermoFisher, 15596026) by following the manufacturer's manual at each passage and Q-modification fraction of the $tRNA^{His/Asn}$ was determined using APB gel and northern blot. After ~10 passages, Q was depleted from these three cell lines (0Q cells). To get 100Q cells (100% Q-modified), 0Q cells were grown to 60-80% confluency and queuine was added to the medium to 1 μM final concentration. The cells were cultured for additional 24 hours to become fully Q-modified.

3.4.2. Acid denaturing gel electrophoresis and Northern blot

Three μg total RNA of each sample was added to a microcentrifuge tube in 4.5 μl H_2O. 0.5 μl 1M Tris-HCl (pH 9.0) was added to each tube and mixed. The tubes were incubated at 37 °C for 30 min to deacylate tRNAs. The tubes were briefly centrifuged and 5 μl 2× acidic RNA loading dye (8 M Urea, 0.1 M HOAc/NaOAc, pH 4.8, 0.05% Bromophenol blue, 0.05% Xylene cyanol) were added to each tube. All samples (10 μl each) were loaded to a 12% pre-run 0.4 mm thick acid denaturing PAGE gel (1× TBE, 0.1 M NaOAc/HOAc, pH 4.8). The gel was run at 16W for 8~9 hours in 4 °C cold room with acid TAE running buffer (1× TAE, 0.1 M NaOAc/HOAc, pH 4.8) until the xylene cyanol band was near the bottom. The gel area with the target RNA was cut and Hybond-XL membrane was put on top of the gel to take the gel out of the plate. The gel area with the target RNA was then transferred to Hybond-XL membrane (GE Healthcare, RPN303S) under vacuum using a gel dryer (Bio-Rad, 1651745) for 4 hours at 80 °C.

The gel was removed from the membrane by soaking the gel and membrane in distilled water. The membrane was UV-crosslinked two times (254 nm, 1200 mJ) and blocked for 30 minutes twice with hybridization buffer (20 mM phosphate, pH 7, 300 mM NaCl, 1% SDS). The membrane was incubated with 3 pmol/ml biotinylated tRNA probes for 16 hours at 60 °C in the UVP Hybridizer Oven (Analytik Jena, 95-0030-01). The membrane was washed for 30 mins twice with 50 ml washing buffer (20 mM phosphate, pH 7, 300 mM NaCl, 2 mM EDTA, and 0.1% SDS). The membrane was then incubated with streptavidin-HRP conjugate (Genscript, M00091) in 30 ml hybridization buffer (1:5000-1:10000 dilution) for 30 min at room temperature. The membrane was washed three times for 5 mins each in 25 ml washing buffer. The membrane was transferred to plastic wrap with RNA-side facing up. Peroxidase detection reagent 1 and 2 (Bio-Rad, 1705061) were mixed (0.1ml per $1cm^2$ membrane) and applied to the top of the membrane by pipetting. The membrane was incubated with the reagent mixture for 5 mins. The membrane was transferred to a new plastic wrap. The membrane was scanned using ChemiDoc imaging system (Bio-Rad) and the data was analyzed using ImageLab.

The oligonucleotide probe sequences were: $tRNA^{His}$: 5'-biotin-TGCCGTGACTCGGATTCGAACCGAGGTTGCTGCGGCCACAACGCAGAGTAC TAACCACTATACGATCACGGC; $tRNA^{Asn}$: 5'-biotin-CGTCCCTGGGTGGGCTCGAACCACCAACCTTTCGGTTAACAGCCGAACGCG CTAACCGATTGCGCCACAGAGAC; $tRNA^{Asp}$: 5'-biotin-CTCCCCGTCGGGGAATCGAACCCCGGTCTCCCGCGTGACAGGCGGGGATAC TCACCACTATACTAACGAGGA; $tRNA^{Tyr}$:

5’-biotin-TCCTTCGAGCCGGASTCGAACCAGCGACCTAAGGATCTACAGTCCTCCGCTC TACCARCTGAGCTATCGAAGG

3.4.3. APB gel electrophoresis

Three µg total RNA of each sample was deacylated with 5 µl 0.1M Tris-HCl (pH 9.0) at 37 °C for 30 mins. 5 µl 2× RNA loading dye (8 M Urea, 0.05% Bromophenol blue, 0.05% Xylene cyanol) were added to each tube after centrifugation. 10% denaturing PAGE gel with 0.5% (g/ml) Acrylamidophenylboronic acid (APB) was prepared and pre-run at 18W for 30 minutes in the 4 °C cold room using 1× TAE buffer. All samples were loaded onto the 10% denaturing PAGE gel with APB and the gel was run at 18W for ~2-3 hours until the xylene cyanol band was near the bottom. The gel was transferred and blotted as described above.

3.4.4. Periodate reaction

Six µg of HEK293T total RNA treated with 1µM queuine for 0, 1, and 24 hours were deacylated in 20 µl 0.1M Tris-HCl (pH 9.0) at 37 °C for 30 min. The RNA was concentrated using Zymo RNA clean and concentrator-5 kit (Zymo, R1016) and eluted in 6 µl sterile H_2O. The eluted RNA was split into two tubes (3 µl each). 5× periodate mix (250mM) was made by dissolving 27 mg sodium periodate in 417 µl H_2O and 83 µl of 3M sodium acetate (pH 4.8). 0.75 µl 5× periodate mix was added to each tube and the tubes were incubated at room temperature for 30 mins. The reaction was quenched with 0.75 µl of 1 M ribose for 5 min at room temperature. 4.5 µl 2x acidic RNA loading dye was added to each tube and all samples were loaded onto a 12% pre-run acid denaturing PAGE gel. The gel was transferred and blotted as described above.

3.4.5. Time course study

HEK293T, MCF7, and HeLa cells were cultured in 6-well plate as described above to 60-80% confluency. 1 mM or 10 μM queuine stock solution in water was added to the medium to get 1 μM or 10 nM final queuine concentration at t = 0. At designated time points, the medium was removed, and cells were washed by PBS twice. Total RNA was extracted immediately by adding 0.5 ml TRIzol reagent to each well and following the manufacturer's manual. The modification status of Q and glycosylated Q-modified tRNAs (His, Asn, Tyr, Asp) at different time points and different queuine concentrations were examined by APB or acid denaturing PAGE gel as described above.

Clearly, multiple processes are involved in installing Q and manQ/galQ modifications over time including at least the queuine uptake, Q-modification by the QTRT1 enzyme, and glycosylation by another, unknown enzyme. Instead of fitting the time courses using the consideration of all these parameters, we choose to use the simplest curve fitting equations with a simple goal to obtain plausible kinetic parameters.

The time courses for total Q and Q+manQ/galQ modification (**Fig. 3.3**) were fit to a single exponential growth: $y = A\left(1 - e^{-k(t-t0)}\right)$, where k is the rate constant of total tRNA modification, t0 is the delay time, A is the maximal modification fraction. For 1 μM and 10 nM queuine data, the fit coefficients for HEK293T ranged from r^2 = 0.964-0.999 and 0.886-0.991, for HeLa from r^2 = 0.898-0.976 and 0.839-0.955, and for MCF7 from r^2 = 0.930-0.995 and 0.950-0.984, respectively.

The time courses for Q-to-manQ/galQ (**Fig. 3.4**) starting with the time point with the highest fraction (B) of accumulated Q-modified tRNA were fit to a single exponential decay $y = B(e^{-kt})$, where k is the rate constant of Q-to-manQ/galQ conversion. For both 1 μM and 10 nM queuine data, the fit coefficients for HEK293T ranged from r^2 = 0.987-0.997, for HeLa from r^2 = 0.987-0.999, and for MCF7 from r^2 = 0.982-0.999.

4. A multiplex platform for small RNA sequencing elucidates multifaceted tRNA stress response and translational regulation

4.1. Abstract

Small RNAs include tRNA, snRNA, micro-RNA, tRNA fragments and others that constitute >90% of RNA copy numbers in a human cell and perform many essential functions. Popular small RNA-seq strategies limit the insights into coordinated small RNA response to cellular stress. Small RNA-seq also lacks multiplexing capabilities. Here, we report a multiplex small RNA-seq library preparation method (MSR-seq) to investigate cellular small RNA and mRNA response to heat shock, hydrogen peroxide, and arsenite stress. Comparing stress-induced changes of total cellular RNA to those on the polysome, we identify acoordinated tRNA response that involves polysome-specific tRNA abundance and synergistic N^3-methylcytosine (m^3C) tRNA modification. Combining tRNA and mRNA response to stress we reveal a new mechanism of stress-induced down-regulation in translational elongation. We also found that native tRNA molecules lacking several modifications are biased reservoirs for the biogenesis of tRNA fragments. Our results demonstrate the importance of simultaneous investigation of small RNAs and their modifications in response to varying biological conditions.

4.2. Introduction

High-throughput RNA sequencing has provided transformative insights into cellular homeostasis, dynamic response to stress and environmental change, and RNA modifications. However, significant challenges associated with characterization of small RNAs remain. Small RNAs are less than 200 nucleotides in length and include transfer RNAs (tRNA), microRNAs, small nucleolar RNAs, tRNA fragments and many others that play important roles in cellular pathways and physiology. Altogether, small RNAs constitute more than 90% of cellular RNAs in copy numbers; among these, tRNA is the most abundant [151]. The role of tRNA in translational regulation depends on the expression and aminoacylation (charging) levels of different tRNA species, as well as many modifications that fine tune tRNA activity [146, 152, 153]. Therefore, comprehensive and high-throughput characterization of tRNA is essential for a deeper understanding of the biological function of small RNAs.

Most commonly used RNA-seq methods are incompatible with comprehensive study of small RNAs. Many small RNA-seq techniques ligate adaptor oligonucleotides to the target RNAs, followed by cDNA synthesis. Products of incomplete reverse transcription, often induced by RNA modification or structure, are not amplified and not included in downstream analysis. tRNA is the RNA family most limited by these methods, due to rigid secondary structure and extensive modification. Several recent approaches have profoundly advanced our ability for efficient and quantitative tRNA sequencing [154-159]. A common drawback of these approaches involves size selection steps or sequence context requirements which limit the investigation of

RNAs to a certain size range or to specific families and uncouples the coordinated expression and response of small RNA families, e.g. tRNA with tRNA fragments. Finally, small RNA-seq procedures also lack the level of multiplexing enjoyed by mRNA sequencing [160]. Therefore, new small RNA-seq methods are still needed to better characterize tRNA properties, incorporate tRNA results with other small RNA families, and increase multiplexing capability.

Here, we describe multiplex small RNA sequencing (MSR-seq), a platform for RNA-seq library construction that provides multiplexing to greatly increase throughput. The key feature of MSR-seq is the design of a biotinylated oligonucleotide that is used for barcode adapter ligation, immobilization, on-bead reverse transcription, second adapter ligation, and PCR. This unification of multiple steps in RNA-seq library construction enables multiplexing of many samples in the same reaction which increases sample handling throughput and reduces sample input. Our method also allows for inclusion of enzymatic and chemical treatment of RNA on-bead, thus accommodating the investigation of RNA modifications. For biological application, we investigated the stress response of tRNA abundance, charging, and modification, as well as other small RNA families upon heat shock, exposure to hydrogen peroxide and to arsenite which are known to strongly affect translation [161-163]. Using MSR-seq measurements of tRNA in total RNA and in the polysome, we identified specific tRNA responses. Together with mRNA measurements, the tRNA response is consistent with stress- and tRNA-dependent translational downregulation during translational elongation. To demonstrate small RNA family coordination, we also found native tRNA molecules lacking several modifications as preferred or depleted reservoirs for tRNA fragment biogenesis. MSR-seq provides a new platform for small RNA-seq

with the emphasis on RNA components in translation and translational regulation and simultaneous analysis of multiple RNA families.

4.3. Results

4.3.1. MSR-seq enabled chemical treatment for RNA modification detection

We developed MSR-seq for sequencing small RNAs and sometime large RNAs (**Fig. 4.1**). The compatibility between MSR-seq and chemical treatment was evaluated. MSR-seq enabled chemical treatment of RNA on-bead useful for RNA modification studies or RNA structural mapping [164]. We used the well-established N-cyclohexyl-N′-β-(4-methylmorpholinium) ethylcarbodiimide (CMC) reaction for pseudouridine (Ψ) modification [165] to test the MSR-seq on-bead protocol for chemical treatments, since this reaction involved two steps under harsh conditions (**Fig. 4.S1A**). To map the Ψ sites in human rRNA, we fragmented total RNA, ligated the fragments to the CHO, then performed the CMC reaction on-bead. We assigned each rRNA position a stop and mutation fraction and observed good correlation between biological replicates (**Fig. 4.S1B**). We identified strong signals in the stop and/or mutation fractions in the CMC-treated sample at the 35 of 36 known Ψ sites [166] in the 18S rRNA (**Fig. 4.S1C**), validating the usefulness of our approach.

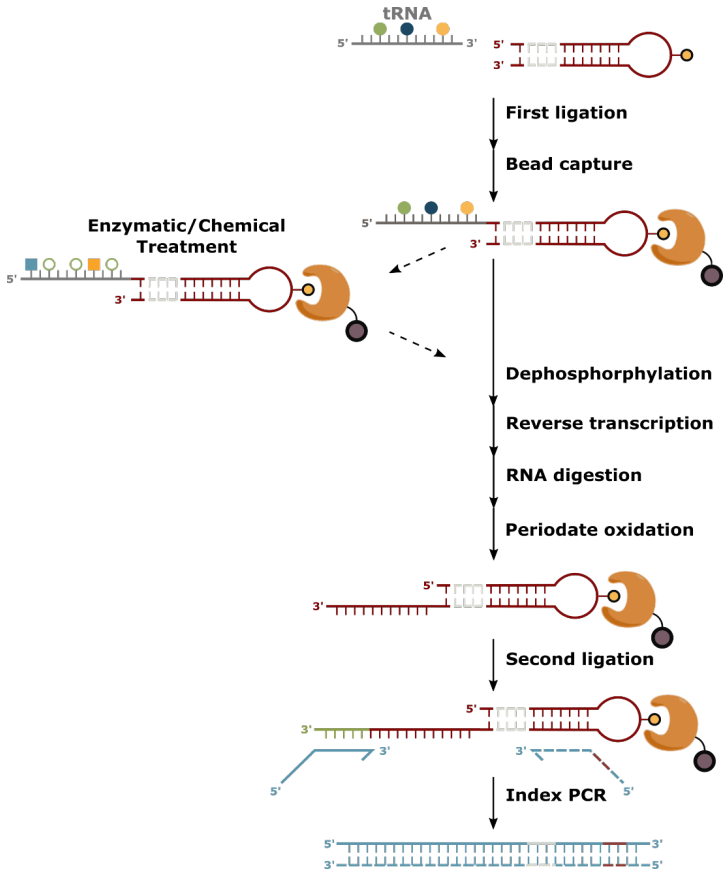

Fig 4.1: Schematic representation of multiplex small RNA-seq (MSR-seq). Immobilization of RNA on beads enables efficient sequencing of multiple RNA species from multiple samples.

4.3.2. Stress induces coordinated tRNA abundance and modification changes in total RNA

We applied MSR-seq to investigate stress response of tRNAs. To broaden the scope of our study, we subjected HEK293T cells to three commonly used, but different stress types: heat shock, hydrogen peroxide, and arsenite, plus the unstressed control. Using total RNA as input, we obtained on average 26 million reads mapped to the human genome among all samples (**Fig. 4.2A**). As expected, most reads were from nuclear-encoded tRNA, with the remaining from 5S and 5.8S rRNA, mitochondrial-encoded tRNA, spliceosomal RNA (snRNA), mRNA, and other RNA families.

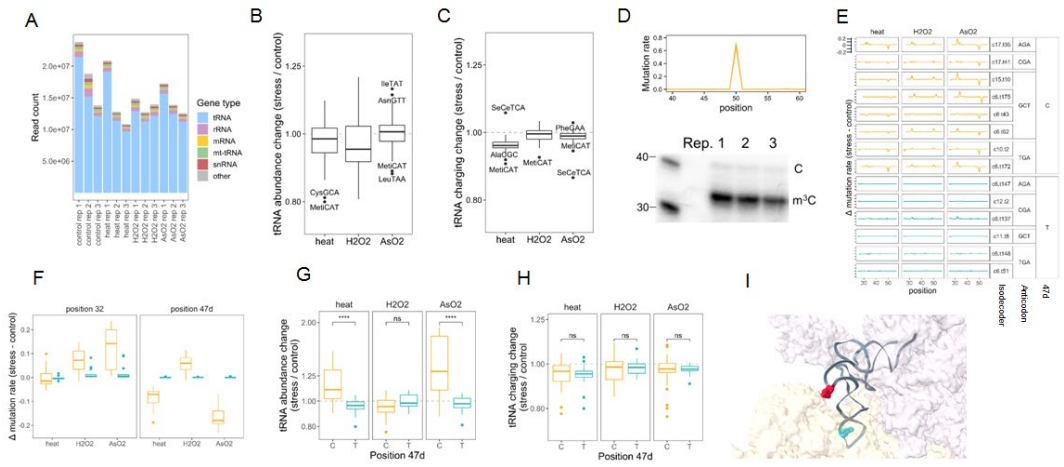

Fig 4.2: tRNA analysis in total RNA under stress. MSR-seq was performed in biological triplicates (n=3) for each condition: unstressed, 42°C/1h (heat), 0.6mM H_2O_2/2h (H_2O_2), 0.3mM $NaAsO_2$/2h (AsO_2). (A) Read coverage among RNA families. (B) Stress-induced tRNA abundance change at the isoacceptor level. Box and Whisker plots with 1.5 times interquartile range. (C) Stress-induced tRNA charging change at the isoacceptor level. (D) Top graph shows the mutation rate at the 50th nucleotide position in tRNA^{Ser}(GCT) at the isoacceptor level; this position corresponds to 47d in tRNA nomenclature. The three biological replicates are shown. Bottom gel image shows validation of sequencing mutation rates of m^{3}C47d in tRNA^{Ser}(GCT) by primer extension. (E) Stress-induced m^{3}C32 and m^{3}C47d change of tRNA^{Ser} isodecoders. C47d-tRNA^{Ser} isodecoders are in orange, T47d-tRNA^{Ser} in blue. Isodecoder designations are according to the hg19 genomic tRNA database [1], e.g. c17.t35 corresponds to chromosome 17, tRNA35. Shown are changes in mutation rate for each replicate, calculated as mutation rate minus the mean of control replicates. (F) tRNA^{Ser} m^{3}C32 and m^{3}C47d changes under stress. C47d-tRNA^{Ser} isodecoders in red and T47d-tRNA^{Ser} in blue. (G) Abundance change for C47d-tRNA^{Ser} isodecoders in red and T47d-tRNA^{Ser} in blue. ****: p<10^{-4}, *ns*: not significant. (H) Charging change for C47d-tRNA^{Ser} isodecoders in red and T47d-tRNA^{Ser} in blue. *ns*: not significant. (I) Location of m^{3}C32 in cyan and m^{3}C47d in red in the 3D structure of ribosome-bound tRNA^{Ser} (PDB 6Z6M from [2]). The 40S subunit is in light yellow, 60S subunit in light purple.

We extensively analyzed the nuclear-encoded tRNA results by comparing each stress condition with unstressed control. We analyzed tRNA abundance, charging, and modification at the isoacceptor level where reads mapped to all reference tRNA genes with the same anticodon were combined, and at the isodecoder level where reads mapped to each reference tRNA gene were kept separately. At the isoacceptor level, tRNA abundance changes were within 1.25-fold

(**Fig. 4.2B, Table 4.S1**), and tRNA charging level within 1.15-fold (**Fig. 4.2C, Table 4.S2**), indicating that tRNA abundance and charging in total cellular tRNA did not change widely under these stress conditions.

We searched for tRNA isodecoder modification responses under stress. We found that SSIV RT produced high mutation rates when reading through m^1A and m^3C under our new condition (**Fig. 4.S1D**). Using primer extension, we validated that the mutation rates of m^3C in MSR-seq could be used to quantify modification fractions (**Fig. 4.2D**). In human tRNAs, m^3C is present in the anticodon loop of $tRNA^{Arg}$(yCU)/$tRNA^{Ser}$/$tRNA^{Thr}$ (m^3C32 in tRNA nomenclature) and in the loop of the variable arm stem-loop of $tRNA^{Leu}$(CAG)/$tRNA^{Ser}$(m^3C47d) [22, 142]. The mutation rate of m^3C47d in $tRNA^{Ser}$, but not in $tRNA^{Leu}$(CAG) showed a marked decrease under heat and arsenite stress, and an increase under hydrogen peroxide stress (**Fig. 4.2E**).

Human $tRNA^{Ser}$ isodecoder genes have either C47d or T47d (**Fig. 4.S1E**). Unexpectedly, the m^3C32 for the C47d-$tRNA^{Ser}$ isodecoders generally showed an increase in the mutation rate, whereas the T47d isodecoders showed little change under the stress conditions (**Fig. 4.2E,F**). Furthermore, only C47d-$tRNA^{Ser}$ isodecoders showed an increase in abundance, but T47d-$tRNA^{Ser}$ isodecoders showed little change in heat and arsenite stress (**Fig. 4.2G**). On the other hand, there was no significant change in the charging levels of either sets of isodecoders under stress (**Fig. 4.2H**). m^3C introduces a positive charge at physiological pH. In the three-dimensional structure of $tRNA^{Ser}$ on the ribosome, m^3C47d and m^3C32 are on the same side of the tRNA. While m^3C32 is close to the tRNA-mRNA base pairs in the 40S, m^3C47d is at the 40S-60S interface [2] (**Fig. 4.2I**). These results suggest that m^3C47d and m^3C32

modifications respond synergistically under stress.

4.3.3. Stress induces coordinated tRNA abundance and modification changes in polysome

We performed MSR-seq of total RNA from polysome fractions to directly reveal tRNA involvement in translational regulation during stress. The polysome profile showed a significant decrease of global translation in all three stress conditions, with the largest decrease occurring under arsenite stress (**Fig. 4.3A**). We validated the known increase of eIF2α phosphorylation level for arsenite stress (**Fig. 4.S2A**). We obtained on average 4.8 million mapped reads among all samples (**Fig. 4.3B**). As expected for polysome samples, the rRNA and mRNA read portion was markedly increased, and tRNA portion decreased in the polysome compared to total RNA mapping.

The tRNA abundance change at the isoacceptor level on the polysome is the largest for the arsenite stress (**Fig. 4.3C, Table 4.S3**). Specifically, $tRNA^{Ile}$(AAT), $tRNA^{Ile}$(TAT) and $tRNA^{Lys}$(TTT) showed 3-4 fold increase (**Fig. 4.3D, 4.S2B**), while the bulk of the other tRNAs showed a slight overall decrease. We validated the increase of $tRNA^{Ile}$(AAT) under stress by Northern blot (**Fig. 4.3E**). In addition, C47d-$tRNA^{Ser}$ isodecoders showed an increase on the polysome compared to T47d-$tRNA^{Ser}$ in heat and arsenite stress (**Fig. 4.3F**), similar to the $tRNA^{Ser}$ isodecoder patterns observed in the total tRNA. The overall tRNA charging level on the polysome decreased slightly in heat and increased slightly in arsenite (**Fig. 4.3G, Table 4.S4**), and the charging levels for the bulk $tRNA^{Ser}$ isodecoders changed little (**Fig. 4.S2C**). The most striking result of polysome tRNA abundance and charging therefore was the dramatic increase of $tRNA^{Ile}$(AAT), $tRNA^{Ile}$(TAT), and $tRNA^{Lys}$(TTT) abundance in the arsenite stress. All three

tRNAs read A/T-rich codons, and may associate with ribosome stalling that contributes to the reduction of global translation (see below).

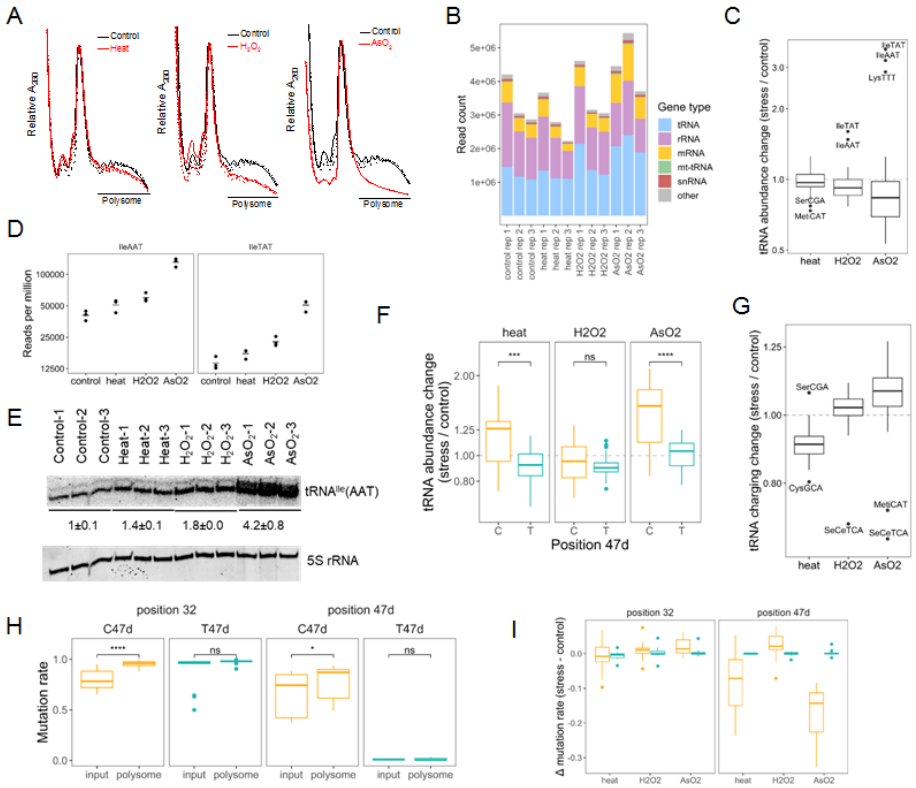

Fig 4.3: tRNA analysis of polysome under stress. MSR-seq was performed in biological triplicates (*n*=3) for each condition. (A) Polysome profile from sucrose density gradient. Unstressed control in black and stress in red. The three biological replicates are shown. The line "polysome" indicates the pooled fractions for MSR-seq. (B) Read coverage among RNA families. (C) Stress-induced tRNA abundance change on the polysome. Box and Whisker plots with 1.5 times interquartile range. (D) tRNA abundance change on the polysome for $tRNA^{Ile}$(AAT) and $tRNA^{Ile}$(TAT). (E) Validation of $tRNA^{Ile}$(AAT) change on polysome by Northern blot. 5S rRNA is the loading control. (F) Abundance change for C47d-$tRNA^{Ser}$ isodecoders in red and T47d-$tRNA^{Ser}$ in blue. ****: $p<10^{-4}$, ***: $p<10^{-3}$, *ns*: not significant. (G) Stress-induced tRNA charging change on the polysome. (H) Comparing mutation rate of position 32 and 47d of $tRNA^{Ser}$ isodecoders in the total RNA (input) and on polysome of the unstressed control. C47d-$tRNA^{Ser}$ isodecoders in red and T47d-$tRNA^{Ser}$ in blue. ****: $p<10^{-4}$, *: $p<0.05$, *ns*: not significant. (I) Stress-induced m^3C32 and m^3C47d change of $tRNA^{Ser}$ isodecoders. C47d-$tRNA^{Ser}$ isodecoders are in orange, T47d-$tRNA^{Ser}$ in blue.

We examined how $tRNA^{Ser}$ m^3C modifications were associated with the polysome. In

unstressed controls, polysome-associated $tRNA^{Ser}$ showed an increase of m^3C47d and m^3C32 levels on the polysome (**Fig. 4.3H, 4.S2D**). In heat and arsenite stress, m^3C47d was however markedly decreased on the polysome, whereas m^3C32 levels remained the same (**Fig. 4.3I, 4.S2E**). The $tRNA^{Ser}$ m^3C response to stress can be summarized in a model of coordinated response of m^3C47d and m^3C32 on the polysome. In unstressed cells, m^3C47d and m^3C32 levels are higher on the polysome than in the total tRNA, suggesting that m^3C modification enhances decoding in general. In the total RNA under arsenite and heat stress, the m^3C47d level decreases, possibly through the action of a cellular m^3C eraser [167, 168], whereas the m^3C32 level increases, possibly through the action of a cellular m^3C32 writer [117]. Under arsenite and heat stress, the m^3C47d level also decreases on the polysome, possibly in response to m^3C47d level decrease in total RNA. There is no change in m^3C32 levels on the polysome under stress, as m^3C32 in both C47d and T47d-$tRNA^{Ser}$ are already at nearly stoichiometric levels as indicated by their very high mutation rates in the total RNA (**Fig. 4.3H**).

4.3.4. Stress-induced change in translation efficiency is codon usage-dependent

To gain further insights on stress response, we sequenced polyA-selected mRNA using MSR-seq for the same total RNA and polysome profiling samples (**Fig. 4.S3A**). As expected, many mRNA transcripts changed expression under stress (**Fig. 4.S3B**). For example, heat stress increased the level of the hsp1a1 transcript by ~10-fold in total RNA, and ~30-fold in polysome-associated RNA (**Fig. 4.4A**); arsenite stress increased the eIF2α phosphorylation dependent translation of ATF4 transcript by ~3.5-fold (**Fig. 4.4B**). We found significant decrease in translation efficiency under each stress which was particularly pronounced in arsenite stress,

both globally (**Fig. 4.4c**) and for individual mRNA transcripts (**Fig. 4.S3C**). Gene ontology of the mRNA transcripts with highly increased or decreased translation efficiency showed most affected genes belonging to metabolic processes (**Fig. 4.4D**).

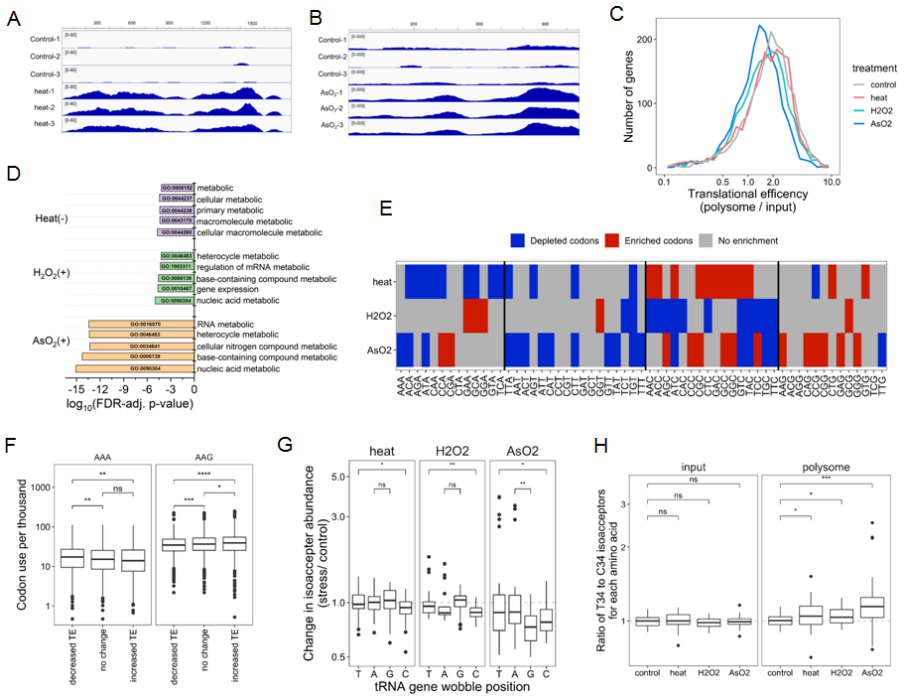

Fig 4.4: mRNA analysis of total RNA and on polysome under stress. mRNA-seq was performed in biological triplicates (n=3) for each condition. (A) IGV plot for the coding region of the HSP1A1 mRNA transcript, unstressed control (top) and heat stress (bottom). (B) IGV plot for the coding region of the ATF4 mRNA, unstressed control (top) and arsenite stress (bottom). (C) Histogram of translation efficiency (TE) among commonly detected mRNA genes in all conditions, in 30-gene increments. (D) Gene ontology analysis of biological processes. (+) Genes with highly increased translation efficiency, (-) Genes with highly decreased translation efficiency. (E) Heat map shows each codon enriched (red) or depleted (blue) in genes with increasing translation efficiency, sorted by the third codon position, A, T, C, G from left to right. Red: enriched in genes with stress-increased TE compared to stress-decreased TE (Wilcox-test p-value <0.05); blue: depleted in genes with stress-increased TE (Wilcox-test p-value <0.05). (F) Lysine AAA/AAG codon usage among genes with increased, decreased, or unchanged TE during arsenite stress. ****p<10^{-4}, ***p<10^{-3}, **p<0.01, *p<0.05, ns: not significant. (G) tRNA abundance change on the polysome for isoacceptors with different wobble anticodon nucleotide in the tRNA gene. **: p<0.01, *: p<0.05, *ns*: not significant. (H) tRNA abundance change of the ratios for T34 versus C34 wobble anticodon tRNA for each amino acid, total RNA input on the left, and on the polysome on the right.***: p<10^{-3}, *: p<0.05, *ns*: not significant.

We performed codon usage analysis to elucidate the translational response of mRNA to those of tRNA under stress [169, 170]. Comparing the sets of genes with stress-induced increase in TE to those with decreased TE, we found that during heat and arsenite stress, the A/T-ending codons were depleted, but the C/G-ending codons were enriched in the genes with highly increased translation efficiency (**Fig. 4.4E**). A specific example is shown for Lysine AAA and AAG codons (**Fig. 4.4F**). Human tRNA genes contain all four possible wobble anticodon nucleotides. T34 wobble tRNA prefers A-ending codons and C34 wobble tRNA reads only G-ending codons. Comparing the tRNA abundance change on the polysome under stress showed a preference of T34 over C34 tRNA in all cases (**Fig. 4.4G**). The T34 over C34 tRNA preference was further confirmed by comparing the abundance change of every T34 over C34 tRNA of the same amino acid on the polysome, and the absence of this preference in total RNA under stress (**Fig. 4.4H**). This tRNA preference was the opposite of the mRNA codon preference on the polysome (**Fig. 4.4E**). Abundance change of the A34 and G34 tRNAs was not significant on the polysome (**Fig. 4.4G**). However, human A34 in tRNA is modified to inosine, which, like G34, also reads both C-ending and T-ending codons.

The polysome mRNA and tRNA results can be explained by a tRNA-dependent down-regulation of translational elongation during stress. Even though mRNAs on the ribosome are enriched for C/G-ending codons, tRNAs on the ribosome are enriched for those that read A/T-ending codons. This is consistent with increased ribosome stalling at A/T-ending codons corresponding to slowed elongation exacerbated by stress. Potential ribosome stalling may be particularly pronounced at the Ile-AAT, Ile-ATA, and Lys-AAA codons under arsenite stress

which may explain the high level of on-polysome accumulation of $tRNA^{Ile}$ and $tRNA^{Lys}$(TTT) that read these codons.

4.3.5. tRNA modification affects tRNA fragment biogenesis

tRNA fragments (tRF) are a family of small RNAs that regulate many aspects of gene expression [171, 172]. tRF sequencing commonly uses size-selected RNAs of 20-60 nucleotides. Although this approach obtains a high coverage of tRF and other small RNAs, potential direct connections between tRF and full-length tRNA are diminished by sequencing them separately. To simultaneously analyze tRNA and tRF in MSR-seq, we used a simplistic approach by binning the 3' ends of all tRNA-aligned reads and assigning those with the 3' end up to the T loop (**Fig. 4.S4A**). We further binned the reads with the approximate 3' ends in the T stem-loop (50-60), variable loop and adjacent region (40-50), and anticodon stem-loop (30-40). Consistent with expectations, the amount of tRF mapped in this way was ~1% of the full-length tRNA (**Fig. 4.5A**). The total amount of tRF did not change much under our stress conditions which was consistent with literature using specific stress conditions and cell lines. For example, arsenite stress showed a high level of tRF only at ≥500 μM [173, 174] whereas our stress was at 300 μM. Most studies on arsenite stress were performed with HeLa cells, whereas we used HEK293T, which generated much lower levels of tRF at 500 μM arsenite [97]. We validated the tRF pattern by Northern blot (**Fig. 4.5B, 4.S4B**).

An important question in tRF biology is how specific tRNA modifications in the full-length tRNA affect tRF biogenesis. Reduction of modification levels by writer enzyme knock-down/knock-out has revealed that modifications such as m^5C, Q, and m^1G protect tRNA

from cleavage [124]. However, it is unclear whether naturally occurring tRNA lacking a specific modification enhances or hinders tRF biogenesis. We addressed this question by simultaneously comparing the mutation rates of the tRF and its cognate full-length tRNA of the same sequence. The m^3C47d level was much lower in tRF compared to their cognate full-length tRNA (**Fig. 4.5C, 4.S4C**), consistent with the C47d-hypomodified tRNA being preferred substrates for tRF biogenesis. Similarly, the m^1G37 level was lower for the tRFs compared to their cognate full-length $tRNA^{Leu}$(CAA) (**Fig. 4.5D, 4.S4D**). In contrast, the $m^2{}_2G$26 level was higher for tRFs compared to their cognate full-length $tRNA^{Trp}$ (**Fig. 4.5E, 4.S4E**). These results indicate that tRNA modifications can have both up and down effects on tRF biogenesis. Our results also show that tRNA modifications affect cleavage in the distal regions of tRNA, similar to those observed previously for m^5C48-50 and m^1G9 modifications [175, 176]. By directly comparing the modification levels of tRF and full-length tRNAs, MSR-seq provides a new avenue to investigate the mechanisms of tRF biogenesis.

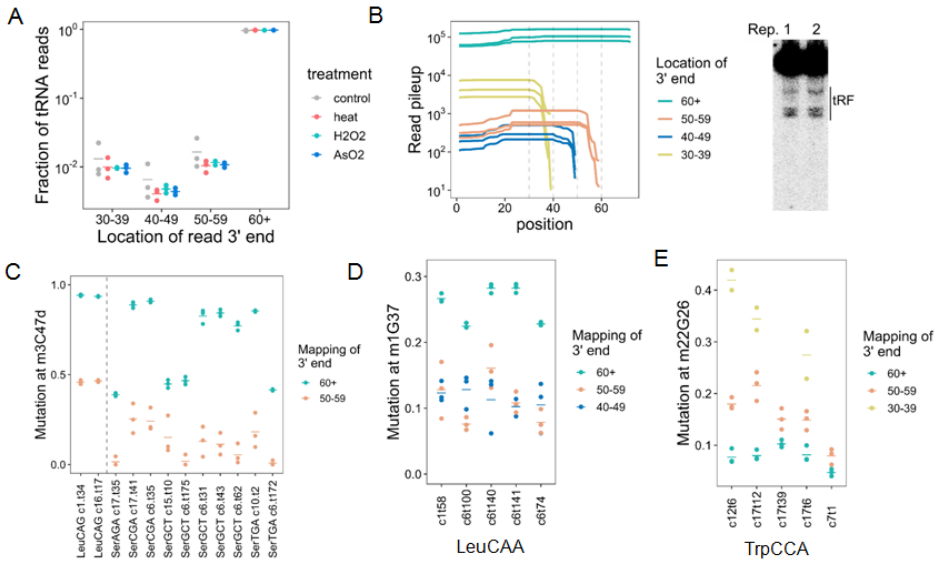

Fig 4.5: Analysis of tRNA fragment biogenesis and tRNA modification. MSR-seq was performed in biological triplicates (*n*=3) for each condition. (A) Total count of tRF relative to full-length tRNA in all 4 conditions. 60+ tRNA are considered full-length tRNAs; replicates shown as points, mean of replicates is shown as a bar. (B) Graph shows read pileup of the most abundant tRF^{Gly}(CCC) isodecoder showing the amount of tRFs with 3' ends in 30-39 (anticodon loop), 40-49 (variable loop), and 50-59 (T loop) in unstressed control samples. Gel shows Northern blot tRF^{Gly}(CCC) validation. (C) Comparing m^3C47d modification in tRF versus full-length cognate tRNA for $tRNA^{Leu}$(CAG) and $tRNA^{Ser}$ isodecoders in unstressed controls. (D) Comparing m^1G37 modification in tRF versus full-length cognate tRNA for $tRNA^{Leu}$(CAA) isodecoders in unstressed controls. (E) Comparing $m^2{}_2G26$ modification in tRF versus full-length cognate tRNA for $tRNA^{Trp}$ isodecoders in unstressed controls.

4.4. Discussion

Here we developed an RNA-seq method that enables multiplexed sequencing library preparation, on-bead enzymatic and chemical treatment, one-pot tRNA abundance, charging, and modification measurements, and simultaneous analysis of tRNA, tRNA fragment, and other small RNA families. We applied our method to human cell stress response and found new insights into translational regulation through tRNA response to stress, in microbiome, and in tRNA fragment biogenesis.

Advantages of carrying out sequencing library construction on solid support include rapid

exchange of buffers and reagents, thorough removal of contaminants, and elimination of size selection steps or adaptor/primer removal. The solid support platform also allows for on-bead treatment of RNA with chemicals and enzymes, which has become widely used in studies of RNA modifications [177-180]. We found that the streptavidin beads could withstand harsh chemical treatments such as the CMC reaction, which involves two steps at pH 8-10 and hours of incubation at 30-37°C. Chemical and enzymatic treatments are useful in profiling RNA modifications such as Ψ, m^5C, m^1A, or m^7G [141, 181] and for RNA structural mapping.

The key feature of our method is the design of the capture hairpin oligonucleotide (CHO). Our innovation is the inclusion of a 3'ribonucleotide and 3'phosphate which blocks the second ligation to the excess CHO upon periodate oxidation after the RT reaction so that only CHOs with cDNA product are amplified in the final PCR step. The presence of a substantial amount of the terminal transferase product (TdT) [182] in the RT reaction is the single issue that remains to be solved. We found that the amount of TdT was highly variable depending on the input sample and reaction conditions. Currently, we remove the TdT products by size selecting the final PCR products. Possible future solutions include screening other RTs, further optimization of reaction conditions, and finding new enzymes that can selectively remove the added deoxynucleotides.

Translational regulation in stress response has been extensively studied [183, 184], and our work here reveals new insights regarding tRNA abundance and modification. This was achieved by not only measuring the response of total tRNA, but also tRNA on the polysome under stress. Previous tRNA profiling from density gradients analyzed mostly the 80S peaks [185]. Our tRNA profiling includes the fractions of disomes and larger, thereby measuring tRNAs only in the

elongating ribosomes. Most previous stress response studies deal with regulation of global translation and translational initiation. By measuring tRNAs on elongating ribosomes, we were able to illuminate tRNA-based stress response in translational elongation.

For tRNA abundance, the most striking new result is the enrichment of tRNAs that decode A-ending codons over G-ending codons on the polysome under stress. At the same time, mRNAs from the same polysome samples show enrichment of C/G-ending over A/T-ending codons. Among the 3 tRNAs that are enriched at the highest level on the polysome, $tRNA^{Ile}$(AAT) reads ATT, $tRNA^{Ile}$(TAT) reads ATA, and $tRNA^{Lys}$(TTT) reads AAA codons. These results are consistent with increased ribosome stalling at A/T-ending codons under stress; furthermore, ATT, ATA, and AAA codons may be hotspots of such stalling under arsenite stress. Stress-induced, codon-dependent tRNA response in translational elongation may also be driven in part by the post-translational modification of the eEF2 protein [186].

For tRNA modification, we focused on m^3C, which can be studied by MSR-seq at high sensitivity. m^3C32 is present in the anticodon loop of $tRNA^{Ser}$, $tRNA^{Thr}$ and $tRNA^{Arg}$(yCT) and enhances translation [117]. m^3C47d is in the variable loop of $tRNA^{Ser}$ and $tRNA^{Leu}$(CAG), which is located at the 40S-60S interface in the 80S ribosome; however, its writer or function is not known [112]. Our most striking new result is the coordinated response of m^3C32 and m^3C47d under stress. There are two $tRNA^{Ser}$ groups that contain either the m^3C-modifiable C47d or T47d. Without stress, tRNAs with higher m^3C32 and m^3C47d levels are loaded on the polysome. Heat and arsenite stresses reduce the m^3C47d level in total RNA, possibly through the action of a tRNA eraser such as ALKBH3 [167]; this results in a corresponding reduction of m^3C47d level

in polysome-associated $tRNA^{Ser}$. However, the same stresses also increase m^3C32 levels in $tRNA^{Ser}$ to reach nearly stoichiometric levels in total RNA and in polysome. These results are consistent with both m^3C modifications working together to fine-tune decoding under stress.

We also revealed an underappreciated relationship of tRNA modification and tRNA fragment biogenesis in native tRNA. tRFs are involved in many aspects of gene expression, developmental biology, and human diseases. It is well known that tRNA modifications strongly influence tRF biogenesis, with a consensus that tRNA modification generally hinders tRF generation. We present two new insights here through simultaneous full-length tRNA and tRF analysis in the same data. First, certain tRFs have lower m^3C or m^1G levels compared to their cognate full-length tRNA, indicating that naturally occurring hypo-modified tRNAs can indeed be preferred reservoirs for tRF biogenesis. Second, tRFs can have higher $m^2{}_2G$ levels compared to their cognate tRNA, indicating that naturally occurring tRNA modifications can also hinder tRF biogenesis.

4.5. Methods

4.5.1. One-pot deacylation and β-elimination for tRNA charging

Up to 500 ng of total RNA in 7 µL was used for optional one-pot beta-elimination prior to library construction. To start, 1 µL of 90 mM sodium acetate buffer, pH 4.8 was added to 7 µL input RNA. Next, 1 µL of freshly prepared 150 mM sodium periodate solution was added for a reaction condition of 16 mM $NaIO_4$, 10 mM NaOAc pH 4.8. Periodate oxidation proceeded for 30 min at room temperature. Oxidation was quenched with addition of 1 µL of 0.6 M ribose to

60 mM final concentration and incubated for 5 minutes. Next 5 μL of freshly prepared 100 mM sodium tetraborate, pH 9.5 was added for a final concentration of 33 mM. This mixture was incubated for 30 min at 45 °C. To stop β-elimination and perform 3' end repair, 5 μL of T4 PNK mix (200 mMTrisHCl pH 6.8, 40 mM $MgCl_2$, 4 U/μL T4 PNK, from New England Biolabs) was added to the reaction, and incubated at 37 °C for 20 min. T4 PNK was heat inactivated by incubating at 65 °C for 10 min. This 20 μL reaction mixture can be used directly in the first bar-code ligation by adding 30 μL of a ligation master mix described below.

4.5.2. Standard tRNA Deacylation

Total RNA was prepared for library construction by first deacylating in a solution of 100 mMTris-HCl, pH 9.0 at 37 °C for 30 minutes, then neutralized by addition of sodium acetate, pH 4.8 to a final concentration of 180 mM. Deacylated RNA was then ethanol precipitated and resuspended in water, or desalted using a Zymo Research Oligo Clean-and-Concentrator spin column.

4.5.3. General protocol for msRNA-seq

First bar-code ligation: Depending on the nature of the experiment described in the main text, input RNA or total nucleic acid samples were either deacylated or had undergone one-pot deacylation and β-elimination as described above. Up to 1 μg of total RNA input was used in a ligation reaction of 50 μL with the following components: 1 U/μL T4 RNA ligase I (NEB), 1x NEB T4 RNA ligase I buffer, 15% PEG 8000, 50 μM ATP, 1 mM hexaamine cobalt chloride, and

5% DMSO. After adding the ligation mix to the sample, the capture hairpin oligo (CHO, **Table 4.S2**) was added to a final concentration of 1 μM and the samples were incubated at 16 °C overnight (12+ hours).

Binding to Dynabeads: The ligation mixture was diluted by adding an equal volume of water to reduce the viscosity of the solution. Next, streptavidin-coated MyOne C1 Dynabeads (ThermoFisher) were added to each sample in a 1.2:1 excess over CHO (for example, a 50 μL reaction had 50 pmolcapture hairpin oligo; beads were supplied at 10 mg/ml and had binding capacity of 500 pmol biotinylated oligo per mg, so use 12 μL beads). The bead-sample mixture was incubated at room temperature for 15 minutes. After binding, supernatants were removed, and the beads washed once with high salt wash buffer (1 M NaCl, 20 mM Tris-HCl, pH 7.4) and once with low salt wash buffer (100 mMNaCl, 20 mM Tris-HCl, pH 7.4). After washing, multiple individually barcoded samples can be combined for downstream steps. At this stage, enzymatic or chemical treatments can be incorporated to the library preparation protocol such as AlkB demethylase reaction or CMC treatments (see below).

Dephosphorylation: A 50 μL dephosphorylation mix containing the following was added to the multiplexed sample on bead: 0.04 U/μL calf intestine phosphatase (Roche), 10 mM $MgCl_2$, 0.5 mM $ZnCl_2$, 20 mM HEPES, pH 7.3. The sample was incubated at 37 °C for 30 minutes. The sample was then washed once with high salt wash buffer and once with low salt wash buffer, then resuspended in 20 μL water.

Reverse transcription: 5 μL of SuperScript IV VILO 5x master mix (ThermoFisher) was added to the dephosphorylated sample (final volume of 25 μL) and then incubated at 55 °C for

10 minutes. The sample was then washed once with high salt wash buffer and once with low salt wash buffer. Identical results were obtained upon extending the reaction time to 60 minutes. For overnight reverse transcription, after the initial 10 min incubation at 55 °C, the samples are further incubated at 35 °C overnight.

RNase H digestion: Beads were then resuspended into 50 µL of RNase H master mix containing 0.4 U/uL RNase H (NEB) and 1x NEB RNase H buffer and incubated at 37 °C for 15 minutes. The sample was then washed once with high salt wash buffer and once with low salt wash buffer. The sample was then resuspended in 40 µL water.

Periodate oxidation: 10 µLof 250 mM freshly prepared sodium periodate, 0.5 M sodium acetate, pH 5 were added to the RNase H digested sample and incubated at room temperature for 30 minutes. Afterwards, ribose was added to a final concentration of 167 mM to quench excess periodate at room temperature for 5 minutes. The sample was then washed once with high salt wash buffer and once with low salt wash buffer.

Second ligation: Beads were resuspended into 50 µL of a ligation master mix with the following components: 2 U/µL T4 RNA ligase I (NEB), 1x NEB T4 RNA ligase I buffer, 2 µM second ligation oligo (**Table 4.S2**), 25% PEG 8000, 50 µM ATP, 7.5% DMSO, and 1 mM hexaamine cobalt chloride. After incubation at room temperature overnight (12+ hours), the reaction was diluted with 50 µL water to reduce viscosity, washed once with high salt wash buffer and once with low salt wash buffer, and then resuspended in water. The amount of water was 6 µL per sample in the first ligation reaction, before pooling the barcoded samples. For example, if the second ligation mixture contains a pool of 6 samples, the amount of water used

for resuspension would be 36 µL. Samples can be stored at 4 °C or frozen at -20 °C; both can be used for the next PCR step.

PCR: A 50 µL PCR reaction was run using 5-10% of the bead slurry products from the second ligation reaction using Q5 DNA polymerase (NEB) and following the manufacturer's instructions: 0.02 U/µL Q5 DNA polymerase, 1x Q5 reaction buffer, 0.2 mM dNTPs, 0.5 µM Illumina index primer (**Table 4.S2**), and 0.5 µM Illumina multiplex primer (**Table 4.S2**). Typical PCR cycles were 9-15 cycles at 10 seconds at 98 °C, 15 seconds at 55 °C, and 72 °C for 20 seconds. PCR reactions were then processed through the DNA Clean and Concentrate kit (Zymo Research).

TBE-PAGE gel extraction: Following desalting, PCR products were run on 10% non-denaturing TBE gel with dsDNA size markers; lanes were cut according to the desired product size, mashed by pipette tip, and then resuspended in crush-and-soak buffer (500 mM sodium acetate, pH 5.0). The gel fragments were extracted overnight and then ethanol precipitated.

4.5.4. Oligonucleotide sequences

See **Table 4.S5**

4.5.5. m^3C poisoned primer extension

100 ng of total RNA sample was added to a tube containing 20 pmol (2 µM final concentration) of RT primer and 2 µL of 5x annealing buffer (10 mMKCl and 150 mMTris-HCl,

pH 7.5); water was added for a total volume of 5 µL. Samples were heated to 93 °C for 2 minutes and then directly placed on ice. 5 µL of a Post-annealing mix, containing the following components, was added to each sample tube (10 µL final volume): 2x AMV Buffer; 2 U/µL AMV RT [New England Biolabs]; 2x poisoned dHTP mix (2 mMdATP, 2 mMdCTP, and 4 mMddTTP); and 2 µCi/µL α-^{32}P dGTP [Perkin Elmer]. The samples were incubated at 37 °C for 30 minutes; and then mixed with 10 µL of 2x urea loading dye (9 M urea, 2 mM EDTA, 0.2% xylene cyanol, 0.2 % bromophenol blue) and incubated at 93 °C for 2 minutes before loading on a 15% denaturing polyacrylamide gels. The primer sequence for tRNA^{Ser}(GCT) was 5'TGGCGACGAGGATGGGATTCGAACCCACGCGT

4.5.6. AlkB and AlkB D135S purification

These were adapted from the previously described protocols for DM-tRNA-seq [154]. Briefly, NEB T7 Expression cells were grown in LB media at 37 °C, in the presence of 50 µM kanamycin, to an A_{600} of 0.6-0.8. Once the cells reached the desired density, IPTG and iron sulfate were added to final concentrations of 1 mM and 5 µM, respectively. After induction, the cells were incubated overnight at 30 °C. Cells were collected, pelleted and then resuspended in lysis buffer (10 mMTris, pH 7.4, 5% glycerol, 2 mM $CaCl_2$, 10 mM $MgCl_2$, 10 mM 2-mercaptoethanol) plus 300 mM NaCl. The cells were lysed by sonication and then centrifuged at 17,400 rcf for 20 min. The soluble proteins were first purified using a Ni-NTA superflow cartridge (Qiagen) with buffers A (lysis buffer plus 1 M NaCl for washing) and B (lysis buffer plus 1 M NaCl and 500 mM imidazole for elution) and then further purified by ion-exchange

(Mono S GL, GE Healthcare) with buffers A (lysis buffer plus 100 mMNaCl) for column loading and B (lysis buffer plus 1.5 M NaCl) for elution.

4.5.7. AlkB treatment

Demethylase buffer conditions were modified from Li et al [187]. Three stock solutions are made fresh immediately before reaction: L-ascorbic acid 200 mM, 2-ketogluterate 3 mM, and ammonium iron sulfate 5 mM. The final reaction mixture contained 2 mM L-ascorbic acid, 1 mM 2-ketogluterate, 0.3 mM ammonium iron sulfate, 100 mM KCl, 50 mM MES pH 6, 50 ng/µL BSA, 4 µM wild-type AlkB, and 4 µM AlkB-D135S. 50 µL of the reaction mixture was added to 5-20 µL of decanted streptavidin bead slurry after ligation, immobilization, and washing. Reaction continued for 30 min at 37 °C. Following the reaction, beads were washed once with high salt wash buffer (1 M NaCl, 20 mM Tris-HCl pH 7.4) and once with low salt wash buffer (100 mM NaCl, 20 mM Tris-HCl pH 7.4).

4.5.8. HEK cell culture and RNA extraction

HEK293T cells were cultured with complete DMEM medium under standard conditions according to ATCC. Briefly, HEK293T cells were grown in Hyclone DMEM medium (GE Healthcare Life Sciences, SH30022.01) with 10% FBS and 1% Pen-Strep (Penicillin-Streptomycin) to 80% confluency and passaged. Cells were collected and total RNA was extracted using TRIzol (ThermoFisher, 15596026) by following the manufacturer's protocol when cells reached 80-90% confluency.

4.5.9. Stress treatments

HEK293T cells were cultured in DMEM medium (GE Healthcare Life Sciences, SH30022.01) with 10% FBS and 1% Pen–Strep (Penicillin–Streptomycin). Twenty-four 15-cm plates of HEK293T cells (5×10^6 cells each) were seeded three days before collection. On the day of polysome profiling, 6 plates of cells (2 plates for 1 sample) were treated with different stress conditions: (1) unstressed control; (2) 42 °C heat shock, 1h; (3) 0.6 mM H_2O_2, 2h; (4) 300 μM $NaAsO_2$, 2h. Polysome profiling was immediately performed after stress treatment.

4.5.10. Polysome profiling

Polysome profiling procedures were adapted from reference [188]. Briefly, cells were treated with 100 μg/ml cycloheximide (CHX) in DMEM for 7 mins right after stress treatments. DMEM medium was removed. Cells were then collected using 10 ml ice-cold PBS with 100 μg/ml CHX and cell lifter. Cells were pelleted by centrifugation at 3000 RPM for 5 minutes. Cell pellet was washed twice with 5 ml ice-cold PBS with 100 μg/ml CHX. Cells from two plates were combined for one sample. Cells were resuspended in 1 ml ice-cold PBS and transferred to microcentrifuge tubes. 200 μl cell suspension from each sample was saved as input. Cells were pelleted by centrifugation at 3000 RPM for 5 mins. For input cells samples, 500 μl TRIzol reagent was added to extract the total RNA. For polysome cells samples, cell pellet was resuspended by 4 volumes of lysis buffer (20 mM HEPES, pH 7.6, 100 mM KCl, 5 mM $MgCl_2$, 1% Triton X-100, 100 μg/ml CHX, freshly added 1 × protease inhibitor (11873580001, Roche),

40 U/µl RNase inhibitor (AM2696, Thermo)). Cells were rotated and lysed at 4 °C cold room for 30 mins. Lysed samples were centrifuged at 16000g for 15 mins to collect the clear lysate (~600-700 µl). 4 ul Turbo DNase was added to each lysate and the samples were incubated at room temperature for 15 mins. The samples were centrifuged again at 16000g for 15 mins to get clear lysate. Absorbance at 260 nm of each sample was measured. Samples were adjusted to the same absorbance using lysis buffer. 5%-50% sucrose gradient (20 mM HEPES, pH 7.6, 100 mMKCl, 5 mM $MgCl_2$, 100 µg/ml CHX, freshly added 1 × protease inhibitor, 40 U/µl RNase inhibitor) was perpared using a Biocomp gradient station. 600 µl gradient buffer was removed from the top of the balanced sucrose gradient. 600 µl lysate was loaded onto the top of the gradient slowly while gently rotating the tube. The samples were centrifuged at 28000 RPM for 3 hours at 4 °C using a Beckman SW28.1 rotor. After centrifugation, fractions were collected and measured using Biocomp gradient station (30 fractions total). Fractions were flash frozen and stored at –80 °C before RNA extraction and library construction. For polysome RNA extraction, fractions from disome and higher were combined and 2 volumes of TRIzol reagent was added to extract the RNA. PolyA+ RNA was extracted from the input and polysome RNA using polyA+ RNA extraction kit from Promega (Z5310) or NEB (E7490S), respectively.

Poly(A)-selection was done with NEBNext Poly(A) mRNA Magnetic Isolation Module (NEB, E7490S) according to manufacturer's instructions.

1 µg of input polyA+ RNA samples and 100 ng polysome polyA+ RNA samples were used to build sequencing libraries. The RNA fragmentation and end repair steps are the same as the CMC sequencing libraries construction. Briefly, polyA+ RNA in 18 µl were added to PCR tubes

and 2 µl Magnesium RNA fragmentation buffer (NEB, E6150S) was added to each tube. The tubes were incubated at 94°C in a thermocycler for 5 mins to fragment the RNA to ~200 nt. The tubes were transferred to ice and 2 µl RNA fragmentation stop solution was then added to each tube to stop the fragmentation. Samples were spun down and diluted to 50 µl using sterile H_2O. The fragmented RNA was purified using Zymo RNA clean and concentrator columns and eluted in 16 µl sterile H_2O. 2 µl T4 PNK buffer and 2 µl T4 PNK were added to the tubes and the tubes were incubated at 37 °C for 30 min to repair the ends of the fragmented RNA. MSR-seq method was then used to build sequencing libraries with the fragmented RNA. Slight modifications were made to the MSR-Seq protocol. After the first ligation step, ligation reaction was quenched by adding 50 mM EDTA. Samples were combined and ligation products over 200nt long was purified using Zymo RNA clean and concentrator columns twice. Target cDNA products were purified using AMPure XP beads with 1:1 ratio after PCR.

4.5.11. mRNA transcriptome mapping

Raw 100 bp paired-end sequencing reads were obtained from Illumina Nova-Seq platform. Reads processing and trimming was the same as CMC sequencing libraries. The reads were mapped to human transcriptome (hg38) obtained from Ensembl. The mapped "bam" files were then analyzed using bamCoverage tool of the "deeptools" [189] (https://deeptools.readthedocs.io/en/develop/) with bin size as 1 to get the bigwig sequencing depth coverage files. The bigwig coverage files were visualized using IGV and coverage track images were obtained.

4.5.12. Northern blots

Northern blot method was adapted from reference [190] using ^{32}P radiolabeled probes. 500 ng of each polysome RNA sample were diluted to 9 µl in microcentrifuge tubes. 1 µl 1M Tris-HCl, pH 9 was added to each tube and mixed well. The samples were incubated at 37 °C for 30 mins to deacylate the tRNAs. 10 µl 2 × RNA loading buffer ((9 M Urea, 100 mM EDTA, pH 8, 0.2% Bromophenol blue, 0.2% Xylene cyanol)) were added. All RNA samples were loaded onto a 10% pre-run denaturing PAGE gel. The gel was stopped when the Xylene cyanol band passed the middle of the gel. RNA was transferred to Hybond-XL Membrane (RPN303S, GE Healthcare) at 80 °C for 4 hours using gel dryer (Bio-Rad). The membrane was soaked in deionized water with the membrane side on the top to separate the gel and the membrane. The gel was stained with SYBR gold (S11494, Thermo) and scanned using ChemiDoc imaging system (Bio-Rad). The membrane was UV-crosslinked twice (254 nm for 1200 mJ). The membrane was then prehybridized for 30 mins twice with hybridization buffer (20 mM phosphate, pH 7, 300 mMNaCl, 1% SDS). 40 pmol of the tRNA probes were radiolabeled by T4 PNK with γ-^{32}P-ATP in a 10 µl reaction. The labeling mixture were diluted to 50 µl and cleaned by IllustraMicroSpin G-25 Columns (27532501, Cytiva). The membrane was incubated with 15 µl ^{32}P radiolabeled probes for 16 hours at 60 °C in the UVP Hybridizer Oven (95-0030-01, Analytik Jena). The membrane was washed twice using 50 ml washing buffer (20 mM phosphate, pH 7, 300 mMNaCl, 2 mM EDTA, and 0.1% SDS) for 30 mins each. The membrane was wrapped in plastic wrap and exposed to phosphorimager screen for 1-2 days depending on the

signal strength. The screen was then scanned using personal molecular imager (Bio-Rad). The image was analyzed using ImageLab software.

Northern blot probes were from Integrated DNA Technologies (IDT) and gel purified. Sequences of the probes were (Y= C/T; R= A/G; W= A/T, M=A/C):

Gly:

5'-TGCATTGGCCRGGAATYGAACCCGGGYCTCCCRCGTGGWAGGCGAGAATTCTACC ACTGMACCACCMAYGC-3'

IleAAT:

5'-TGGCCMGTACGGGGATCGAACCCGCGACCTTGGCGTTATTAGCACCACGCTCTAAC CAACTGAGCTAACCRGCC-3'

4.5.13. Gene ontology analysis

Gene ontology analysis was performed using the default setting in reference [191] (http://geneontology.org/).

4.5.14. Western blots of eIF2α phosphorylation

All samples were incubated at 95 °C for 10 minutes, separated on a 4–12% polyacrylamide Bis-Tris protein gel (NP0322BOX, Thermo), and transferred to polyvinylidene fluoride membranes (IPVH00010, Millipore). The membranes were blocked in 10% w/v milk (1706404, Bio-Rad). The blots were probed with 1/1000 v/v EIF2S1 antibody (AHO0802, Invitrogen) or 1/500 v/v Phospho-EIF2S1 (Ser51) antibody (MA5-15133, Invitrogen), followed by 1/10000 v/v

sheep anti-mouse IgG (NA931V, Cytiva) or 1/10000 v/v donkey anti-rabbit IgG conjugated to horseradish peroxidase (NA934V, Cytiva). The blots were visualized with ECL Prime Western Blotting Detection Reagents (RPN2232, Amersham) using a BioRad ChemiDoc MP.

4.5.15. MCF7 growth and RNA extraction

MCF7 cells were cultured in EMEM medium (ATCC, 30-2003) with 10% FBS (ThermoFisher, 10082147), 0.01 mg/ml bovine insulin (Sigma-Aldrich, I0516), and 10 nM β-estradiol (Sigma- Aldrich, E2758) to 80% confluency and passaged at ratios of 1:3. Total RNA were extracted using TRIzol.

4.5.16. CMC treatment / library construction

MCF7 total RNA sequencing libraries were constructed as follows. Small RNA (<200nt) was first removed from 1 µg MCF7 total RNA using spin columns (Zymo Research RNA Clean & Concentrator-5, R1016) and the large RNA (>200 nt) was eluted with 18 µl sterile H_2O in a microcentrifuge tube. The RNA was transferred to PCR tubes and 2 µl Magnesium RNA fragmentation buffer (NEB, E6150S) was added to each tube and the tubes were incubated at 94 °C in a thermocycler for 5 minutes to fragment the RNA to ~200 nt. 2 µl RNA fragmentation stop solution was then added to each tube. The samples were diluted to 50 µl with H_2O and Zymo Research spin columns were used to purify the fragmented RNA; the RNA were eluted in 16 µl sterile H_2O in a microcentrifuge tube. For 3' end repair of the RNA fragments, 2 µl 10x T4 PNK buffer and 2 µl T4 PNK at 10U/µl (ThermoFisher, EK0032) were added and the mixture

incubated at 37°C for 30 minutes. The fragmented, end-repaired RNA was used to build sequencing libraries using the MSRNA-seq protocol described above with the following modifications. The fragmented RNA was ligated to bar-coded capture hairpin oligonucleotides and bound to streptavidin beads. The samples were then pooled, mixed and split into two parts for ±CMC (N-cyclohexyl-N′-(2-morpholinoethyl)carbodiimide) treatment (+CMC:-CMC=1.5 : 1 ratio). 12 µl sterile H_2O and 24 µl TEU buffer (50 mMTris-HCl (pH 8.3), 4 mM EDTA, 7 M urea) were first added to each tube, then 4 µl freshly prepared 1M CMC in TEU buffer was added to +CMC samples and 4 µl sterile H_2O was added -CMC samples. The samples were incubated at 30 °C for16 hours at 1400 rpm on an Eppendorf ThermoMixer. The samples were washed twice with high salt buffer and once with low salt buffer. The samples were then resuspended with 40 µl of 50 mM sodium carbonate and 2 mM EDTA (pH 10.4) buffer and incubated at 37 °C for 6 hours at 1400 rpm. The beads were washed twice with high salt buffer and once with low salt buffer and then proceeded to the MSRNA-seq steps such as phosphatase treatment and reverse transcription.

4.5.17. Read processing and mapping

Libraries were sequenced on Illumina Hi-Seq or NEXT-seq platform. First, paired end reads were split by barcode sequence using Je demultiplex with options BPOS=BOTH BM=READ_1 LEN=4:6 FORCE=true C=false[192]. BM and LEN options were adjusted for samples with a 3 nt barcode instead of 4, and for samples where the barcode is located in read 2. Barcode sequences are listed in **Table 4.S5**. Next, only the read beginning with the barcode (usually read

2) was used to map with bowtie2 (version 2.3.3.1) with the following parameters: "-q -p 10 --local --no-unal". For human sample reads were mapped to the human transcriptome, with tRNA genes shaped for a curated, non-redundant, set of high-scoring tRNA genes. This reference was a combination of HG19 ORFs, ncRNAs, and our curated tRNA list based on HG19 tRNAs curated to be non-redundant, tRNA-scan SE with score >47, and 3' "CCA" appended. Bowtie2 output sam files were converted to bam files, then sorted using samtools. Next IGV was used to collapse reads into 1 nt window. IGV output .wig files were reformatted using custom python scripts (available on GitHub). The bowtie2 output Sam files were also used as input for a custom python script using PySam, a python wrapper for SAMTools ([193],https://github.com/pysam-developers/pysam) to sum all reads that mapped to each gene. Related custom scripts were used to divide reads based on which 10nt window the 3' end mapped to for each tRNA; this is for fragment analysis. Data was visualized with custom R scripts. All custom scripts are available on GitHub (https://github.com/ckatanski/CHRIS-seq).

4.5.18. Translational efficiency and mRNA codon usage analysis

For each gene, read counts mapping to all transcript variants were summed together. Read counts were normalized for total detection in each sample (i.e. reads per million) among mRNA-detection reads (only genes with "gene_biotype" as "protein_coding" were included for normalization). After normalization, genes were filtered to have more than 100 counts. Next translational efficiency (TE) was calculated as the normalized gene counts in the polysome fraction divided by the input fraction for each replicate and each stress. Next, analysis was

limited to a set of well detected genes: this set of genes was defined as genes were TE could be calculated in all 4 treatments (control, heat, H_2O_2, and AsO_2) for one replicate. This gave a set of ~1500 gene, with small fluctuations in detection in other replicates. TE calculations were confirmed to be roughly log-normally distributed. A Z-score was calculated for each sample based on log10(TE) value. The mean Z-score from the control replicates was used as a reference for stress-dependent change.

For each CDS transcript in our HG19-derived reference genome, the occurrence of each codon was tallied - frequency was calculated as number of codon instances divided by protein length. For genes with several transcripts, the median value for each codon was used. Calculation was done with custom python script, available on GitHub. This data was combined with our TE calculations.

Next, genes were divided into 3 groups: low TE, average TE, and high TE. Divisions were based on the 33rd percentile and 66th percentile rank for TE in each sample. For each codon, frequency was used to assign a percentile rank to each gene in each sample (e.g. a gene with abundant "AAA" Lys usage may be in the 99th percentile for "AAA" and the 5thpercentile for "CCT" Pro). Percentile ranks were used to calculate statistical differences between gene groups for each sample and each codon; tests were calculated via two-sided wilcox test. Codon usage frequency is not normally distributed, so a non-parametric hypothesis test is appropriate.

Next, for each sample, genes were again divided into 3 groups, but based on percentile of change in Z-score from the mean of control replicates: decreased TE, no change in TE, and increased TE. Percentile group thresholds were again 33rd and 66th. Percentile ranking in codon

usage was again used for hypothesis testing between groups for each sample and each codon with a two-sided wilcox test as above.

4.5.19. Read processing from CMC reaction

Raw 100 bp paired-end sequencing reads were obtained from Illumina Hi-Seq platform. Read1 reads were separated by barcodes with the barcodes sequence on paired read2 reads using custom python scripts. Read2 reads were separated by barcodes using fastx_barcode_splitter (fastx_toolkit, http://hannonlab.cshl.edu/fastx_toolkit/). For read1 reads, the random 6 nucleotides unique molecular identifier (UMI) sequence at the start of the reads and the barcoded adaptor sequence at the end of the reads were removed using Trimmomatic [194] using single-end mode with a 15 nt cutoff. For read2 reads, the 7 nt barcode sequence at the start of the reads and the UMI and adaptor sequence at the end of the reads were removed by Trimmomatic using paired-end mode with a 15 nt cutoff. The reads were then mapped to human rRNA transcripts using bowtie2. The output sam files were converted to bam files and then sorted and indexed using samtools. Command-line version of "igvtools count" (IGV, http://software.broadinstitute.org/software/igv/download) were used to count nucleotide composition, insertions, and deletions at single base resolution. "Bedtools genomecov" (bedtools, https://bedtools.readthedocs.io/en/latest/) was used to count the start and end of all reads at each position. All the output files and reference sequence were combined into a single file for each sample, the mutation rate and the stop rate were computed by custom python scripts. The output files were analyzed to identify target pseudouridine sites.

5. Conclusions

5.1. Sensitive and convenient quantification of Ψ modification fraction

Since the initial discovery of Ψ, several methods have been developed for the detecting Ψ including low-throughput or high-throughput and quantitative or qualitative approaches. Each method is useful in certain applications. For example, HPLC-MS and spectroscopy methods are crucial for validating the presence of Ψ but are not ideal for quantitatively measuring Ψ fractions at specific sites. High-throughput sequencing methods are effective for transcriptome-wide profiling of Ψ sites and investigating Ψ status change under various cellular stimulus conditions. Low-throughput methods including CLAP are useful for locus-specific validation and quantification of candidate Ψ sites but cannot be used for Ψ mapping. After the initial profiling of Ψ sites in the whole transcriptome with high-throughput methods, we further investigate the functional roles of these sites. When it comes to the examination of the functions of specific Ψ sites, a convenient, rapid and low-cost quantification method is necessary. High-throughput sequencing methods are not ideal in this case due to the high cost, long waiting time and data analysis steps. CLAP provides convenient, single-base resolution quantification of Ψ at specific sites within 2-3 days. The Ψ modification fraction can be obtained by quantifying two bands in the same lane. CLAP is also very sensitive for Ψ analysis of low abundant RNAs. For the control oligos containing a single U or Ψ site, CLAP still retains its quantitative feature at the fmole amount in the background of 1 μg total human RNA. CLAP successfully measured the modification fractions of two Ψ sites in low abundant mRNAs in three human cell lines, indicating that CLAP is very useful for elucidating the functions of specific Ψ sites in

low-abundant mRNAs. The principal idea of CLAP should also be useful to study other modifications that stop the RT reaction such as m^1A, m^1G, and m^3C. Moreover, CLAP has potential for other applications when two differently sized RNA fragments are generated from the same source of RNA, such as quantifying the ratio of different fragments cleaved from the same RNA.

5.2. Efficient detection and quantification of glcosylated Q

Very few methods are available for the detection of glycosylated Q modifications beyond the HPLC-MS/MS method. HPLC-MS/MS is good for validating the presence of glycosylated Q modification, but is not convenient for routine detection of glycosylated Q modification due to the large amount of input RNA required and the involvement of expensive mass spectroscopy instruments.We developed an acid gel based Northern blot for glycosylated Q modification detection using common lab equipment. Although glycosylated Q modification was discovered around 50 years ago [74-76], no huge leaps have been made on their studies. The enzymes responsible for the glycosylation of Q in $tRNA^{Tyr}$ and $tRNA^{Asp}$ and the roles of the glycosylation still remain elusive. The efficient and quantitative acidgel based Northern blot for the detection of glycosylated Q will help uncover the functions and biological significance of Q glycosylation.Acid denaturing gel-based Northern blot also eliminates the use of ^{32}P for labeling the probes. Instead, biotinylated probes are used which are much more convenient. This method has the potential to detect other modifications such as the known acp^3U modification in tRNA with amine groups that can be protonated under acidic conditions.

5.3. Multiplexed sequencing for multiple types of RNA

Building next-generation, high-throughput sequencing libraries can be time-consuming and may involve size selection steps throughout the procedure. The current goal is to develop a multiplexed, small RNA sequencing method that allows for simultaneous library construction of many samples with low input amounts. After the incorporation of streptavidin magnetic beads to the library construction design, we successfully developed a multiplexed RNA library construction method named MSR-seq. MSR-seq is powerful for building small RNA libraries efficiently. We can sequence tRNA, tRNA fragments, snRNA and other small RNAs in one sample at the same time. MSR-seq is compatible with the detection of RNA modifications. MSR-seq has proven to be compatible with demethylase treatment and efficient for the analysis of RNA methylations such as m^3C, m^1G, m^1A, and $m^2{}_2G$. Chemical treatment-assisted RNA modification detection is also compatible with MSR-seq. We applied MSR-seq to CMC-based Ψ detection and successfully identified Ψ sites in rRNAs. MSR-seq may be effective for the studies of more RNA modification as long as the performance of the magnetic beads is not significantly affected by harsh chemical or enzyme treatments. In addition to enabling efficient detection of multiple RNA modifications, MSR-seq has the potential of building multiplexed mRNA libraries. We applied MSR-seq to sequence both tRNA and mRNA from stress treated polysome and input samples. MSR-seq performed very well for both tRNA sequencing and mRNA sequencing. From the sequencing data of input and polysome associated tRNAs and mRNAs, we identified two tRNA modifications of m^3C32 and m^3C47d that showed synergistic changes under different

stress conditions. The mRNA expression profiles of stress-related genes show heat shock protein transcripts as expected. By comparing the tRNA and mRNA sequencing data, we performed the codon usage analysis on stress treated samples and correlated the codon usage with tRNA profiles. This explained the down-regulation of translation in stress treated samples through tRNA-dependent regulation of translation elongation. In conclusion, MSR-seqenables the study of biological functions at low input sample amounts and multiplexing of small RNA-seq library construction.

5.4. Summary and future directions

In my thesis work, we developed sensitive and quantitative detection methods for Ψ, Q, glycosylated Q and tRNA methylations. These efficient and quantitative analysis methods help elucidate the biological functions of each modification. Method development is a crucial part of epi-transcriptomics. During the last few decades, various methods have been invented for the investigation and characterization of RNA modifications. These methods have greatly facilitated the study of the functions and mechanisms of RNA modifications. The methods we developed will further advance the understanding of the diverse biological functions of Ψ, Q, glycosylated Q and tRNA methylations. Our future studies will focus on more specific functions of Ψ, Q, glycosylated Q and tRNA m^3C modification. A potential avenue for further investigation is to identify the writer enzymes and functions of Q glycosylation in tRNA utilizing our acid denaturing gel based Northern blot methods.

References

[1] P.P. Chan, T.M. Lowe, GtRNAdb 2.0: an expanded database of transfer RNA genes identified in complete and draft genomes, Nucleic Acids Res 44(D1) (2016) D184-9.

[2] J.N. Wells, R. Buschauer, T. Mackens-Kiani, K. Best, H. Kratzat, O. Berninghausen, T. Becker, W. Gilbert, J. Cheng, R. Beckmann, Structure and function of yeast Lso2 and human CCDC124 bound to hibernating ribosomes, PLoS Biol 18(7) (2020) e3000780.

[3] W.E. Cohn, E. Volkin, Nucleoside-5′-Phosphates from Ribonucleic Acid, Nature 167(4247) (1951) 483-484.

[4] P. Boccaletto, M.A. Machnicka, E. Purta, P. Piatkowski, B. Baginski, T.K. Wirecki, V. de Crecy-Lagard, R. Ross, P.A. Limbach, A. Kotter, M. Helm, J.M. Bujnicki, MODOMICS: a database of RNA modification pathways. 2017 update, Nucleic Acids Res 46(D1) (2018) D303-D307.

[5] T. Pan, Modifications and functional genomics of human transfer RNA, Cell Res 28(4) (2018) 395-404.

[6] M. Taoka, Y. Nobe, Y. Yamaki, K. Sato, H. Ishikawa, K. Izumikawa, Y. Yamauchi, K. Hirota, H. Nakayama, N. Takahashi, T. Isobe, Landscape of the complete RNA chemical modifications in the human 80S ribosome, Nucleic Acids Res 46(18) (2018) 9289-9298.

[7] X. Jiang, B. Liu, Z. Nie, L. Duan, Q. Xiong, Z. Jin, C. Yang, Y. Chen, The role of m6A modification in the biological functions and diseases, Signal Transduct Target Ther 6(1) (2021) 74.

[8] J. Song, C. Yi, Chemical Modifications to RNA: A New Layer of Gene Expression Regulation, ACS Chem Biol 12(2) (2017) 316-325.

[9] L. Trixl, A. Lusser, The dynamic RNA modification 5-methylcytosine and its emerging role as an epitranscriptomic mark, Wiley Interdiscip Rev RNA 10(1) (2019) e1510.

[10] H.M. Goodman, J. Abelson, A. Landy, S. Brenner, J.D. Smith, Amber suppression: a nucleotide change in the anticodon of a tyrosine transfer RNA, Nature 217(5133) (1968) 1019-24.

[11] X. Li, X. Xiong, M. Zhang, K. Wang, Y. Chen, J. Zhou, Y. Mao, J. Lv, D. Yi, X.W. Chen, C. Wang, S.B. Qian, C. Yi, Base-Resolution Mapping Reveals Distinct m(1)A Methylome in Nuclear- and Mitochondrial-Encoded Transcripts, Mol Cell 68(5) (2017) 993-1005 e9.

[12] X. Li, P. Zhu, S. Ma, J. Song, J. Bai, F. Sun, C. Yi, Chemical pulldown reveals dynamic pseudouridylation of the mammalian transcriptome, Nat Chem Biol 11(8) (2015) 592-7.

[13] T.M. Carlile, M.F. Rojas-Duran, B. Zinshteyn, H. Shin, K.M. Bartoli, W.V. Gilbert, Pseudouridine profiling reveals regulated mRNA pseudouridylation in yeast and human cells, Nature 515(7525) (2014) 143-6.

[14] S. Schwartz, D.A. Bernstein, M.R. Mumbach, M. Jovanovic, R.H. Herbst, B.X. Leon-Ricardo, J.M. Engreitz, M. Guttman, R. Satija, E.S. Lander, G. Fink, A. Regev, Transcriptome-wide mapping reveals widespread dynamic-regulated pseudouridylation of ncRNA and mRNA, Cell 159(1) (2014) 148-162.

[15] A.F. Lovejoy, D.P. Riordan, P.O. Brown, Transcriptome-wide mapping of pseudouridines: pseudouridine synthases modify specific mRNAs in S. cerevisiae, PLoS One 9(10) (2014) e110799.

[16] M. Schaefer, T. Pollex, K. Hanna, F. Lyko, RNA cytosine methylation analysis by bisulfite sequencing, Nucleic Acids Res 37(2) (2009) e12.

[17] T. Amort, D. Rieder, A. Wille, D. Khokhlova-Cubberley, C. Riml, L. Trixl, X.Y. Jia, R. Micura, A. Lusser, Distinct 5-methylcytosine profiles in poly(A) RNA from mouse embryonic stem cells and brain, Genome Biol 18(1) (2017) 1.

[18] J. Cui, Q. Liu, E. Sendinc, Y. Shi, R.I. Gregory, Nucleotide resolution profiling of m3C RNA modification by HAC-seq, Nucleic Acids Res 49(5) (2021) e27.

[19] M. Heiss, S. Kellner, Detection of nucleic acid modifications by chemical reagents, RNA Biol 14(9) (2017) 1166-1174.

[20] I. Behm-Ansmant, M. Helm, Y. Motorin, Use of specific chemical reagents for detection of modified nucleotides in RNA, J Nucleic Acids 2011 (2011) 408053.

[21] G. Zheng, Y. Qin, W.C. Clark, Q. Dai, C. Yi, C. He, A.M. Lambowitz, T. Pan, Efficient and quantitative high-throughput tRNA sequencing, Nat Methods 12(9) (2015) 835-837.

[22] W.C. Clark, M.E. Evans, D. Dominissini, G. Zheng, T. Pan, tRNA base methylation identification and quantification via high-throughput sequencing, RNA 22(11) (2016) 1771-1784.

[23] D. Dominissini, S. Moshitch-Moshkovitz, S. Schwartz, M. Salmon-Divon, L. Ungar, S. Osenberg, K. Cesarkas, J. Jacob-Hirsch, N. Amariglio, M. Kupiec, R. Sorek, G. Rechavi, Topology of the human and mouse m6A RNA methylomes revealed by m6A-seq, Nature 485(7397) (2012) 201-6.

[24] M.T. Parker, K. Knop, A.V. Sherwood, N.J. Schurch, K. Mackinnon, P.D. Gould, A.J. Hall, G.J. Barton, G.G. Simpson, Nanopore direct RNA sequencing maps the complexity of Arabidopsis mRNA processing and m(6)A modification, Elife 9 (2020).

[25] L. Xu, M. Seki, Recent advances in the detection of base modifications using the Nanopore sequencer, J Hum Genet 65(1) (2020) 25-33.

[26] D.A. Lorenz, S. Sathe, J.M. Einstein, G.W. Yeo, Direct RNA sequencing enables m(6)A detection in endogenous transcript isoforms at base-specific resolution, RNA 26(1) (2020) 19-28.

[27] E.K. Borchardt, N.M. Martinez, W.V. Gilbert, Regulation and Function of RNA Pseudouridylation in Human Cells, Annu Rev Genet 54 (2020) 309-336.

[28] X. Li, S. Ma, C. Yi, Pseudouridine: the fifth RNA nucleotide with renewed interests, Curr Opin Chem Biol 33 (2016) 108-16.

[29] M. Safra, R. Nir, D. Farouq, I. Vainberg Slutskin, S. Schwartz, TRUB1 is the predominant pseudouridine synthase acting on mammalian mRNA via a predictable and conserved code, Genome Res 27(3) (2017) 393-406.

[30] M. Penzo, L. Montanaro, Turning Uridines around: Role of rRNA Pseudouridylation in Ribosome Biogenesis and Ribosomal Function, Biomolecules 8(2) (2018).

[31] A.C. Rintala-Dempsey, U. Kothe, Eukaryotic stand-alone pseudouridine synthases - RNA modifying enzymes and emerging regulators of gene expression?, RNA Biol 14(9) (2017) 1185-1196.

[32] P.G. Foster, L. Huang, D.V. Santi, R.M. Stroud, The structural basis for tRNA recognition and pseudouridine formation by pseudouridine synthase I, Nat Struct Biol 7(1) (2000) 23-7.

[33] T.M. Carlile, N.M. Martinez, C. Schaening, A. Su, T.A. Bell, B. Zinshteyn, W.V. Gilbert, mRNA structure determines modification by pseudouridine synthase 1, Nat Chem Biol 15(10) (2019) 966-974.

[34] S. Mukhopadhyay, M. Deogharia, R. Gupta, Mammalian nuclear TRUB1, mitochondrial

TRUB2, and cytoplasmic PUS10 produce conserved pseudouridine 55 in different sets of tRNA, RNA 27(1) (2021) 66-79.

[35] R. Kurimoto, T. Chiba, Y. Ito, T. Matsushima, Y. Yano, K. Miyata, Y. Yashiro, T. Suzuki, K. Tomita, H. Asahara, The tRNA pseudouridine synthase TruB1 regulates the maturation of let-7 miRNA, EMBO J 39(20) (2020) e104708.

[36] D.R. Davis, Stabilization of RNA stacking by pseudouridine, Nucleic Acids Res 23(24) (1995) 5020-6.

[37] E. Kierzek, M. Malgowska, J. Lisowiec, D.H. Turner, Z. Gdaniec, R. Kierzek, The contribution of pseudouridine to stabilities and structure of RNAs, Nucleic Acids Res 42(5) (2014) 3492-501.

[38] P. Morais, H. Adachi, Y.T. Yu, Spliceosomal snRNA Epitranscriptomics, Front Genet 12 (2021) 652129.

[39] Y. Zhao, W. Dunker, Y.T. Yu, J. Karijolich, The Role of Noncoding RNA Pseudouridylation in Nuclear Gene Expression Events, Front Bioeng Biotechnol 6 (2018) 8.

[40] H. Antonicka, K. Choquet, Z.Y. Lin, A.C. Gingras, C.L. Kleinman, E.A. Shoubridge, A pseudouridine synthase module is essential for mitochondrial protein synthesis and cell viability, EMBO Rep 18(1) (2017) 28-38.

[41] S. Zaganelli, P. Rebelo-Guiomar, K. Maundrell, A. Rozanska, S. Pierredon, C.A. Powell, A.A. Jourdain, N. Hulo, R.N. Lightowlers, Z.M. Chrzanowska-Lightowlers, M. Minczuk, J.C. Martinou, The Pseudouridine Synthase RPUSD4 Is an Essential Component of Mitochondrial RNA Granules, J Biol Chem 292(11) (2017) 4519-4532.

[42] I. Laptev, O. Dontsova, P. Sergiev, Epitranscriptomics of Mammalian Mitochondrial Ribosomal RNA, Cells 9(10) (2020).

[43] J. Karijolich, Y.T. Yu, Converting nonsense codons into sense codons by targeted pseudouridylation, Nature 474(7351) (2011) 395-8.

[44] H. Adachi, Y.T. Yu, Pseudouridine-mediated stop codon readthrough in S. cerevisiae is sequence context-independent, RNA 26(9) (2020) 1247-1256.

[45] B. Addepalli, P.A. Limbach, Pseudouridine in the Anticodon of Escherichia coli tRNATyr(QPsiA) Is Catalyzed by the Dual Specificity Enzyme RluF, J Biol Chem 291(42) (2016) 22327-22337.

[46] M. Tagel, H. Ilves, M. Leppik, K. Jurgenstein, J. Remme, M. Kivisaar, Pseudouridines of tRNA Anticodon Stem-Loop Have Unexpected Role in Mutagenesis in Pseudomonas sp, Microorganisms 9(1) (2020).

[47] O. Levi, Y.S. Arava, Pseudouridine-mediated translation control of mRNA by methionine aminoacyl tRNA synthetase, Nucleic Acids Res 49(1) (2021) 432-443.

[48] B.R. Anderson, H. Muramatsu, S.R. Nallagatla, P.C. Bevilacqua, L.H. Sansing, D. Weissman, K. Kariko, Incorporation of pseudouridine into mRNA enhances translation by diminishing PKR activation, Nucleic Acids Res 38(17) (2010) 5884-92.

[49] K.J. Kauffman, F.F. Mir, S. Jhunjhunwala, J.C. Kaczmarek, J.E. Hurtado, J.H. Yang, M.J. Webber, P.S. Kowalski, M.W. Heartlein, F. DeRosa, D.G. Anderson, Efficacy and immunogenicity of unmodified and pseudouridine-modified mRNA delivered systemically with lipid nanoparticles in vivo, Biomaterials 109 (2016) 78-87.

[50] D.E. Eyler, M.K. Franco, Z. Batool, M.Z. Wu, M.L. Dubuke, M. Dobosz-Bartoszek, J.D. Jones, Y.S. Polikanov, B. Roy, K.S. Koutmou, Pseudouridinylation of mRNA coding sequences alters translation, Proc Natl Acad Sci U S A 116(46) (2019) 23068-23074.

[51] N. Guzzi, M. Ciesla, P.C.T. Ngoc, S. Lang, S. Arora, M. Dimitriou, K. Pimkova, M.N.E. Sommarin, R. Munita, M. Lubas, Y. Lim, K. Okuyama, S. Soneji, G. Karlsson, J. Hansson, G. Jonsson, A.H. Lund, M. Sigvardsson, E. Hellstrom-Lindberg, A.C. Hsieh, C. Bellodi, Pseudouridylation of tRNA-Derived Fragments Steers Translational Control in Stem Cells, Cell 173(5) (2018) 1204-1216 e26.

[52] Y.V. Svitkin, Y.M. Cheng, T. Chakraborty, V. Presnyak, M. John, N. Sonenberg, N1-methyl-pseudouridine in mRNA enhances translation through eIF2alpha-dependent and independent mechanisms by increasing ribosome density, Nucleic Acids Res 45(10) (2017) 6023-6036.

[53] J.A. Stockert, R. Weil, K.K. Yadav, N. Kyprianou, A.K. Tewari, Pseudouridine as a novel biomarker in prostate cancer, Urol Oncol 39(1) (2021) 63-71.

[54] J.A. Stockert, A. Gupta, B. Herzog, S.S. Yadav, A.K. Tewari, K.K. Yadav, Predictive value of pseudouridine in prostate cancer, Am J Clin Exp Urol 7(4) (2019) 262-272.

[55] P. Nombela, B. Miguel-Lopez, S. Blanco, The role of m(6)A, m(5)C and Psi RNA modifications in cancer: Novel therapeutic opportunities, Mol Cancer 20(1) (2021) 18.

[56] N.W. Ho, P.T. Gilham, Reaction of pseudouridine and inosine with N-cyclohexyl-N'-beta-(4-methylmorpholinium)ethylcarbodiimide, Biochemistry 10(20) (1971) 3651-7.

[57] A. Bakin, J. Ofengand, Four newly located pseudouridylate residues in Escherichia coli 23S ribosomal RNA are all at the peptidyltransferase center: analysis by the application of a new sequencing technique, Biochemistry 32(37) (1993) 9754-62.

[58] M. Zaringhalam, F.N. Papavasiliou, Pseudouridylation meets next-generation sequencing, Methods 107 (2016) 63-72.

[59] K.I. Zhou, W.C. Clark, D.W. Pan, M.J. Eckwahl, Q. Dai, T. Pan, Pseudouridines have context-dependent mutation and stop rates in high-throughput sequencing, RNA Biol 15(7) (2018) 892-900.

[60] Z. Lei, C. Yi, A Radiolabeling-Free, qPCR-Based Method for Locus-Specific Pseudouridine Detection, Angew Chem Int Ed Engl 56(47) (2017) 14878-14882.

[61] V. Khoddami, A. Yerra, T.L. Mosbruger, A.M. Fleming, C.J. Burrows, B.R. Cairns, Transcriptome-wide profiling of multiple RNA modifications simultaneously at single-base resolution, Proc Natl Acad Sci U S A 116(14) (2019) 6784-6789.

[62] A.M. Fleming, A. Alenko, J.P. Kitt, A.M. Orendt, P.F. Flynn, J.M. Harris, C.J. Burrows, Structural Elucidation of Bisulfite Adducts to Pseudouridine That Result in Deletion Signatures during Reverse Transcription of RNA, J Am Chem Soc 141(41) (2019) 16450-16460.

[63] V. Marchand, F. Pichot, P. Neybecker, L. Ayadi, V. Bourguignon-Igel, L. Wacheul, D.L.J. Lafontaine, A. Pinzano, M. Helm, Y. Motorin, HydraPsiSeq: a method for systematic and quantitative mapping of pseudouridines in RNA, Nucleic Acids Res 48(19) (2020) e110.

[64] A.M. Smith, M. Jain, L. Mulroney, D.R. Garalde, M. Akeson, Reading canonical and modified nucleobases in 16S ribosomal RNA using nanopore native RNA sequencing, PLoS One 14(5) (2019) e0216709.

[65] A.Z.B. Aziz, M.A.M. Hasan, J. Shin, Identification of RNA pseudouridine sites using deep learning approaches, PLoS One 16(2) (2021) e0247511.

[66] W. Chen, H. Tang, J. Ye, H. Lin, K.C. Chou, iRNA-PseU: Identifying RNA pseudouridine sites, Mol Ther Nucleic Acids 5 (2016) e332.

[67] Z. Lv, J. Zhang, H. Ding, Q. Zou, RF-PseU: A Random Forest Predictor for RNA

Pseudouridine Sites, Front Bioeng Biotechnol 8 (2020) 134.

[68] Y. Bi, D. Jin, C. Jia, EnsemPseU: identifying pseudouridine sites with an ensemble approach, Ieee Access 8 (2020) 79376-79382.

[69] K. Liu, W. Chen, H. Lin, XG-PseU: an eXtreme Gradient Boosting based method for identifying pseudouridine sites, Mol Genet Genomics 295(1) (2020) 13-21.

[70] L. Dou, X. Li, H. Ding, L. Xu, H. Xiang, Is There Any Sequence Feature in the RNA Pseudouridine Modification Prediction Problem?, Mol Ther Nucleic Acids 19 (2020) 293-303.

[71] B. Song, Y. Tang, Z. Wei, G. Liu, J. Su, J. Meng, K. Chen, PIANO: A Web Server for Pseudouridine-Site (Psi) Identification and Functional Annotation, Front Genet 11 (2020) 88.

[72] C. Fergus, D. Barnes, M.A. Alqasem, V.P. Kelly, The queuine micronutrient: charting a course from microbe to man, Nutrients 7(4) (2015) 2897-929.

[73] H. Kasai, Z. Oashi, F. Harada, S. Nishimura, N.J. Oppenheimer, P.F. Crain, J.G. Liehr, D.L. von Minden, J.A. McCloskey, Structure of the modified nucleoside Q isolated from Escherichia coli transfer ribonucleic acid. 7-(4,5-cis-Dihydroxy-1-cyclopenten-3-ylaminomethyl)-7-deazaguanosine, Biochemistry 14(19) (1975) 4198-208.

[74] H. Kasai, K. Nakanishi, R.D. Macfarlane, D.F. Torgerson, Z. Ohashi, J.A. McCloskey, H.J. Gross, S. Nishimura, Letter: The structure of Q* nucleoside isolated from rabbit liver transfer ribonucleic acid, J Am Chem Soc 98(16) (1976) 5044-6.

[75] N. Okada, N. Shindo-Okada, S. Nishimura, Isolation of mammalian tRNAAsp and tRNATyr by lectin-Sepharose affinity column chromatography, Nucleic Acids Res 4(2) (1977) 415-23.

[76] H. Kasai, Y. Kuchino, K. Nihei, S. Nishimura, Distribution of the modified nucleoside Q and its derivatives in animal and plant transfer RNA's, Nucleic Acids Res 2(10) (1975) 1931-9.

[77] M. Kang, R. Peterson, J. Feigon, Structural Insights into riboswitch control of the biosynthesis of queuosine, a modified nucleotide found in the anticodon of tRNA, Mol Cell 33(6) (2009) 784-90.

[78] R.K. Slany, M. Bosl, P.F. Crain, H. Kersten, A new function of S-adenosylmethionine: the ribosyl moiety of AdoMet is the precursor of the cyclopentenediol moiety of the tRNA wobble base queuine, Biochemistry 32(30) (1993) 7811-7.

[79] M. Marchetti, D. Capela, R. Poincloux, N. Benmeradi, M.C. Auriac, A. Le Ru, I. Maridonneau-Parini, J. Batut, C. Masson-Boivin, Queuosine biosynthesis is required for sinorhizobium meliloti-induced cytoskeletal modifications on HeLa Cells and symbiosis with Medicago truncatula, PLoS One 8(2) (2013) e56043.

[80] J.P. Reyniers, J.R. Pleasants, B.S. Wostmann, J.R. Katze, W.R. Farkas, Administration of exogenous queuine is essential for the biosynthesis of the queuosine-containing transfer RNAs in the mouse, J Biol Chem 256(22) (1981) 11591-4.

[81] M.A. Alqasem, C. Fergus, J.M. Southern, S.J. Connon, V.P. Kelly, The eukaryotic tRNA-guanine transglycosylase enzyme inserts queuine into tRNA via a sequential bi-bi mechanism, Chem Commun (Camb) 56(27) (2020) 3915-3918.

[82] C. Boland, P. Hayes, I. Santa-Maria, S. Nishimura, V.P. Kelly, Queuosine formation in eukaryotic tRNA occurs via a mitochondria-localized heteromeric transglycosylase, J Biol Chem 284(27) (2009) 18218-27.

[83] W. Langgut, T. Reisser, Involvement of protein kinase C in the control of tRNA modification with queuine in HeLa cells, Nucleic Acids Res 23(13) (1995) 2488-91.

[84] C. Romier, J.E. Meyer, D. Suck, Slight sequence variations of a common fold explain the substrate specificities of tRNA-guanine transglycosylases from the three kingdoms, FEBS Lett 416(1) (1997) 93-8.

[85] I. Biela, N. Tidten-Luksch, F. Immekus, S. Glinca, T.X. Nguyen, H.D. Gerber, A. Heine, G. Klebe, K. Reuter, Investigation of specificity determinants in bacterial tRNA-guanine transglycosylase reveals queuine, the substrate of its eucaryotic counterpart, as inhibitor, PLoS One 8(5) (2013) e64240.

[86] R. Zallot, C. Brochier-Armanet, K.W. Gaston, F. Forouhar, P.A. Limbach, J.F. Hunt, V. de Crecy-Lagard, Plant, animal, and fungal micronutrient queuosine is salvaged by members of the DUF2419 protein family, ACS Chem Biol 9(8) (2014) 1812-25.

[87] Y. Yuan, R. Zallot, T.L. Grove, D.J. Payan, I. Martin-Verstraete, S. Sepic, S. Balamkundu, R. Neelakandan, V.K. Gadi, C.F. Liu, M.A. Swairjo, P.C. Dedon, S.C. Almo, J.A. Gerlt, V. de Crecy-Lagard, Discovery of novel bacterial queuine salvage enzymes and pathways in human pathogens, Proc Natl Acad Sci U S A 116(38) (2019) 19126-19135.

[88] R.P. Singhal, V.N. Vakharia, The role of queuine in the aminoacylation of mammalian aspartate transfer RNAs, Nucleic Acids Res 11(12) (1983) 4257-72.

[89] F. Meier, B. Suter, H. Grosjean, G. Keith, E. Kubli, Queuosine modification of the wobble base in tRNAHis influences 'in vivo' decoding properties, EMBO J 4(3) (1985) 823-7.

[90] M. Muller, C. Legrand, F. Tuorto, V.P. Kelly, Y. Atlasi, F. Lyko, A.E. Ehrenhofer-Murray, Queuine links translational control in eukaryotes to a micronutrient from bacteria, Nucleic Acids Res 47(7) (2019) 3711-3727.

[91] A.E. Ehrenhofer-Murray, Cross-Talk between Dnmt2-Dependent tRNA Methylation and Queuosine Modification, Biomolecules 7(1) (2017).

[92] F. Tuorto, C. Legrand, C. Cirzi, G. Federico, R. Liebers, M. Muller, A.E. Ehrenhofer-Murray, G. Dittmar, H.J. Grone, F. Lyko, Queuosine-modified tRNAs confer nutritional control of protein translation, EMBO J 37(18) (2018).

[93] M. Muller, M. Hartmann, I. Schuster, S. Bender, K.L. Thuring, M. Helm, J.R. Katze, W. Nellen, F. Lyko, A.E. Ehrenhofer-Murray, Dynamic modulation of Dnmt2-dependent tRNA methylation by the micronutrient queuine, Nucleic Acids Res 43(22) (2015) 10952-62.

[94] S. Nagaraja, M.W. Cai, J. Sun, H. Varet, L. Sarid, M. Trebicz-Geffen, Y. Shaulov, M. Mazumdar, R. Legendre, J.Y. Coppee, T.J. Begley, P.C. Dedon, S. Gourinath, N. Guillen, Y. Saito-Nakano, C. Shimokawa, H. Hisaeda, S. Ankri, Queuine Is a Nutritional Regulator of Entamoeba histolytica Response to Oxidative Stress and a Virulence Attenuator, mBio 12(2) (2021).

[95] Y. Chiari, K. Dion, J. Colborn, A. Parmakelis, J.R. Powell, On the possible role of tRNA base modifications in the evolution of codon usage: queuosine and Drosophila, J Mol Evol 70(4) (2010) 339-45.

[96] J.M. Zaborske, V.L. DuMont, E.W. Wallace, T. Pan, C.F. Aquadro, D.A. Drummond, A nutrient-driven tRNA modification alters translational fidelity and genome-wide protein coding across an animal genus, PLoS Biol 12(12) (2014) e1002015.

[97] X. Wang, Z. Matuszek, Y. Huang, M. Parisien, Q. Dai, W. Clark, M.H. Schwartz, T. Pan, Queuosine modification protects cognate tRNAs against ribonuclease cleavage, RNA 24(10) (2018) 1305-1313.

[98] T. Marks, W.R. Farkas, Effects of a diet deficient in tyrosine and queuine on germfree mice, Biochem Biophys Res Commun 230(2) (1997) 233-7.

[99] T. Rakovich, C. Boland, I. Bernstein, V.M. Chikwana, D. Iwata-Reuyl, V.P. Kelly, Queuosine deficiency in eukaryotes compromises tyrosine production through increased

tetrahydrobiopterin oxidation, J Biol Chem 286(22) (2011) 19354-63.

[100] J. Zhang, R. Lu, Y. Zhang, Z. Matuszek, W. Zhang, Y. Xia, T. Pan, J. Sun, tRNA Queuosine Modification Enzyme Modulates the Growth and Microbiome Recruitment to Breast Tumors, Cancers (Basel) 12(3) (2020).

[101] P. Hayes, C. Fergus, M. Ghanim, C. Cirzi, L. Burtnyak, C.J. McGrenaghan, F. Tuorto, D.P. Nolan, V.P. Kelly, Queuine Micronutrient Deficiency Promotes Warburg Metabolism and Reversal of the Mitochondrial ATP Synthase in Hela Cells, Nutrients 12(3) (2020).

[102] C. Pathak, Y.K. Jaiswal, M. Vinayak, Possible involvement of queuine in regulation of cell proliferation, Biofactors 29(4) (2007) 159-73.

[103] G. Dirheimer, W. Baranowski, G. Keith, Variations in tRNA modifications, particularly of their queuine content in higher eukaryotes. Its relation to malignancy grading, Biochimie 77(1-2) (1995) 99-103.

[104] C. Pathak, M. Vinayak, Modulation of lactate dehydrogenase isozymes by modified base queuine, Mol Biol Rep 32(3) (2005) 191-6.

[105] C. Pathak, Y.K. Jaiswal, M. Vinayak, Queuine mediated inhibition in phosphorylation of tyrosine phosphoproteins in cancer, Mol Biol Rep 35(3) (2008) 369-74.

[106] C. Pathak, Y.K. Jaiswal, M. Vinayak, Modulation in the activity of lactate dehydrogenase and level of c-Myc and c-Fos by modified base queuine in cancer, Cancer Biol Ther 7(1) (2008) 85-91.

[107] C. Pathak, Y.K. Jaiswal, M. Vinayak, Queuine promotes antioxidant defence system by activating cellular antioxidant enzyme activities in cancer, Bioscience Rep 28(2) (2008) 73-81.

[108] Q. Ma, J. He, Enhanced expression of queuine tRNA-ribosyltransferase 1 (QTRT1) predicts poor prognosis in lung adenocarcinoma, Ann Transl Med 8(24) (2020) 1658.

[109] A. Costa, J.P. Pais de Barros, G. Keith, W. Baranowski, J. Desgres, Determination of queuosine derivatives by reverse-phase liquid chromatography for the hypomodification study of Q-bearing tRNAs from various mammal liver cells, J Chromatogr B Analyt Technol Biomed Life Sci 801(2) (2004) 237-47.

[110] G.L. Igloi, H. Kossel, Affinity electrophoresis for monitoring terminal phosphorylation and the presence of queuosine in RNA. Application of polyacrylamide containing a covalently bound boronic acid, Nucleic Acids Res 13(19) (1985) 6881-98.

[111] R.H. Hall, Isolation of 3-Methyluridine and 3-Methylcytidine from Solubleribonucleic Acid, Biochem Biophys Res Commun 12 (1963) 361-4.

[112] V. de Crecy-Lagard, P. Boccaletto, C.G. Mangleburg, P. Sharma, T.M. Lowe, S.A. Leidel, J.M. Bujnicki, Matching tRNA modifications in humans to their known and predicted enzymes, Nucleic Acids Res 47(5) (2019) 2143-2159.

[113] S. D'Silva, S.J. Haider, E.M. Phizicky, A domain of the actin binding protein Abp140 is the yeast methyltransferase responsible for 3-methylcytidine modification in the tRNA anti-codon loop, RNA 17(6) (2011) 1100-10.

[114] A. Noma, S. Yi, T. Katoh, Y. Takai, T. Suzuki, T. Suzuki, Actin-binding protein ABP140 is a methyltransferase for 3-methylcytidine at position 32 of tRNAs in Saccharomyces cerevisiae, RNA 17(6) (2011) 1111-9.

[115] L. Han, E. Marcus, S. D'Silva, E.M. Phizicky, S. cerevisiae Trm140 has two recognition modes for 3-methylcytidine modification of the anticodon loop of tRNA substrates, RNA 23(3) (2017) 406-419.

[116] A.G. Arimbasseri, J. Iben, F.Y. Wei, K. Rijal, K. Tomizawa, M. Hafner, R.J. Maraia, Evolving specificity of tRNA 3-methyl-cytidine-32 (m3C32) modification: a subset of tRNAsSer requires N6-isopentenylation of A37, RNA 22(9) (2016) 1400-10.

[117] L. Xu, X. Liu, N. Sheng, K.S. Oo, J. Liang, Y.H. Chionh, J. Xu, F. Ye, Y.G. Gao, P.C. Dedon, X.Y. Fu, Three distinct 3-methylcytidine (m(3)C) methyltransferases modify tRNA and mRNA in mice and humans, J Biol Chem 292(35) (2017) 14695-14703.

[118] Y. Iwanami, G.M. Brown, Methylated bases of ribosomal ribonucleic acid from HeLa cells, Arch Biochem Biophys 126(1) (1968) 8-15.

[119] C.J. Ma, J.H. Ding, T.T. Ye, B.F. Yuan, Y.Q. Feng, AlkB Homologue 1 Demethylates N(3)-Methylcytidine in mRNA of Mammals, ACS Chem Biol 14(7) (2019) 1418-1425.

[120] S. Mao, P. Haruehanroengra, S.V. Ranganathan, F. Shen, T.J. Begley, J. Sheng, Base Pairing and Functional Insights into N(3)-Methylcytidine (m(3)C) in RNA, ACS Chem Biol 16(1) (2021) 76-85.

[121] L.H. Zhang, X.Y. Zhang, T. Hu, X.Y. Chen, J.J. Li, M. Raida, N. Sun, Y. Luo, X. Gao, The SUMOylated METTL8 Induces R-loop and Tumorigenesis via m3C, iScience 23(3) (2020) 100968.

[122] V.V. Ignatova, S. Kaiser, J.S.Y. Ho, X. Bing, P. Stolz, Y.X. Tan, C.L. Lee, F.P.H. Gay, P.R. Lastres, R. Gerlini, B. Rathkolb, A. Aguilar-Pimentel, A. Sanz-Moreno, T. Klein-Rodewald, J. Calzada-Wack, E. Ibragimov, M. Valenta, S. Lukauskas, A. Pavesi, S. Marschall, S. Leuchtenberger, H. Fuchs, V. Gailus-Durner, M.H. de Angelis, S. Bultmann, O.J. Rando, E. Guccione, S.M. Kellner, R. Schneider, METTL6 is a tRNA m(3)C methyltransferase that regulates pluripotency and tumor cell growth, Sci Adv 6(35) (2020) eaaz4551.

[123] V. Marchand, L. Ayadi, F.G.M. Ernst, J. Hertler, V. Bourguignon-Igel, A. Galvanin, A. Kotter, M. Helm, D.L.J. Lafontaine, Y. Motorin, AlkAniline-Seq: Profiling of m(7) G and m(3) C RNA Modifications at Single Nucleotide Resolution, Angew Chem Int Ed Engl 57(51) (2018) 16785-16790.

[124] S. Delaunay, M. Frye, RNA modifications regulating cell fate in cancer, Nat Cell Biol 21(5) (2019) 552-559.

[125] M. Charette, M.W. Gray, Pseudouridine in RNA: what, where, how, and why, IUBMB Life 49(5) (2000) 341-51.

[126] J. Ge, Y.T. Yu, RNA pseudouridylation: new insights into an old modification, Trends Biochem Sci 38(4) (2013) 210-8.

[127] G. Wu, M. Xiao, C. Yang, Y.T. Yu, U2 snRNA is inducibly pseudouridylated at novel sites by Pus7p and snR81 RNP, EMBO J 30(1) (2011) 79-89.

[128] G. Wu, H. Adachi, J. Ge, D. Stephenson, C.C. Query, Y.T. Yu, Pseudouridines in U2 snRNA stimulate the ATPase activity of Prp5 during spliceosome assembly, EMBO J 35(6) (2016) 654-67.

[129] T.M. Carlile, M.F. Rojas-Duran, B. Zinshteyn, H. Shin, K.M. Bartoli, W.V. Gilbert, Pseudouridine profiling reveals regulated mRNA pseudouridylation in yeast and human cells, Nature 515 (2014) 143-6.

[130] S. Schwartz, D.A. Bernstein, M.R. Mumbach, M. Jovanovic, R.H. Herbst, B.X. Leon-Ricardo, J.M. Engreitz, M. Guttman, R. Satija, E.S. Lander, G. Fink, A. Regev, Transcriptome-wide Mapping Reveals Widespread Dynamic-Regulated Pseudouridylation of ncRNA and mRNA, Cell 159 (2014) 148-62.

[131] X. Zhao, Y.T. Yu, Detection and quantitation of RNA base modifications, RNA 10(6) (2004) 996-1002.

[132] N. Liu, M. Parisien, Q. Dai, G. Zheng, C. He, T. Pan, Probing N6-methyladenosine RNA modification status at single nucleotide resolution in mRNA and long noncoding RNA, RNA 19(12) (2013) 1848-56.

[133] Vandenbroucke, II, J. Vandesompele, A.D. Paepe, L. Messiaen, Quantification of splice variants using real-time PCR, Nucleic Acids Res 29(13) (2001) E68-8.

[134] R.P. Singh, X. Nie, M. Singh, Duplex RT-PCR: reagent concentrations at reverse transcription stage affect the PCR performance, J Virol Methods 86(2) (2000) 121-9.

[135] D. Piekna-Przybylska, W.A. Decatur, M.J. Fournier, The 3D rRNA modification maps database: with interactive tools for ribosome analysis, Nucleic Acids Res 36(Database issue) (2008) D178-83.

[136] B.B. Mughal, M. Leemans, P. Spirhanzlova, B. Demeneix, J.B. Fini, Reference gene identification and validation for quantitative real-time PCR studies in developing Xenopus laevis, Sci Rep 8(1) (2018) 496.

[137] A.M. Gentile, S. Lhamyani, L. Coin-Araguez, W. Oliva-Olivera, H. Zayed, A. Vega-Rioja, J. Monteseirin, S.Y. Romero-Zerbo, F.J. Tinahones, F.J. Bermudez-Silva, R. El Bekay, RPL13A and EEF1A1 Are Suitable Reference Genes for qPCR during Adipocyte Differentiation of Vascular Stromal Cells from Patients with Different BMI and HOMA-IR, PLoS One 11(6) (2016) e0157002.

[138] X. Zhang, M.H. Hamblin, K.J. Yin, The long noncoding RNA Malat1: Its physiological and pathophysiological functions, RNA Biol 14(12) (2017) 1705-1714.

[139] N. Liu, K.I. Zhou, M. Parisien, Q. Dai, L. Diatchenko, T. Pan, N6-methyladenosine alters RNA structure to regulate binding of a low-complexity protein, Nucleic Acids Res 45(10) (2017) 6051-6063.

[140] A.M. Waterhouse, J.B. Procter, D.M. Martin, M. Clamp, G.J. Barton, Jalview Version 2--a multiple sequence alignment editor and analysis workbench, Bioinformatics 25(9) (2009) 1189-91.

[141] D. Dominissini, S. Nachtergaele, S. Moshitch-Moshkovitz, E. Peer, N. Kol, M.S. Ben-Haim, Q. Dai, A. Di Segni, M. Salmon-Divon, W.C. Clark, G. Zheng, T. Pan, O. Solomon, E. Eyal, V. Hershkovitz, D. Han, L.C. Dore, N. Amariglio, G. Rechavi, C. He, The dynamic N(1)-methyladenosine methylome in eukaryotic messenger RNA, Nature 530(7591) (2016) 441-6.

[142] M.A. Machnicka, K. Milanowska, O. Osman Oglou, E. Purta, M. Kurkowska, A. Olchowik, W. Januszewski, S. Kalinowski, S. Dunin-Horkawicz, K.M. Rother, M. Helm, J.M. Bujnicki, H. Grosjean, MODOMICS: a database of RNA modification pathways--2013 update, Nucleic Acids Res 41(Database issue) (2013) D262-7.

[143] J.P. Reyniers, J.R. Pleasants, B.S. Wostmann, J.R. Katze, W.R. Farkas, Administration of Exogenous Queuine Is Essential for the Biosynthesis of the Queuosine-Containing Transfer-Rnas in the Mouse, J Biol Chem 256(22) (1981) 1591-1594.

[144] M. Vinayak, C. Pathak, Queuosine modification of tRNA: its divergent role in cellular machinery, Biosci Rep 30(2) (2009) 135-48.

[145] C. Pathak, Y.K. Jaiswal, M. Vinayak, Queuine promotes antioxidant defence system by activating cellular antioxidant enzyme activities in cancer, Biosci Rep 28(2) (2008) 73-81.

[146] A. Bednarova, M. Hanna, I. Durham, T. VanCleave, A. England, A. Chaudhuri, N. Krishnan, Lost in Translation: Defects in Transfer RNA Modifications and Neurological Disorders, Front Mol Neurosci 10 (2017) 135.

[147] U. Varshney, C.P. Lee, U.L. RajBhandary, Direct analysis of aminoacylation levels of tRNAs in vivo. Application to studying recognition of Escherichia coli initiator tRNA mutants by glutaminyl-tRNA synthetase, J Biol Chem 266(36) (1991) 24712-8.

[148] J.R. Katze, B. Basile, J.A. McCloskey, Queuine, a modified base incorporated posttranscriptionally into eukaryotic transfer RNA: wide distribution in nature, Science 216(4541) (1982) 55-6.

[149] E.Y. Chen, B.A. Roe, Structural comparison of human, bovine, rat, and Walker 256 carcinosarcoma asparaginyl-tRNA, Biochim Biophys Acta 610(2) (1980) 272-84.

[150] N. Okada, S. Nishimura, Enzymatic synthesis of Q nucleoside containing mannose in the anticodon of tRNA: isolation of a novel mannosyltransferase from a cell-free extract of rat liver, Nucleic Acids Res 4(8) (1977) 2931-8.

[151] E.M. Phizicky, A.K. Hopper, tRNA biology charges to the front, Genes Dev 24(17) (2010) 1832-60.

[152] B. El Yacoubi, M. Bailly, V. de Crecy-Lagard, Biosynthesis and Function of Posttranscriptional Modifications of Transfer RNAs, Annu Rev Genet 46 (2012) 69-95.

[153] T. Suzuki, The expanding world of tRNA modifications and their disease relevance, Nat

Rev Mol Cell Biol (2021).

[154] G. Zheng, Y. Qin, W.C. Clark, Q. Dai, C. Yi, C. He, A.M. Lambowitz, T. Pan, Efficient and quantitative high-throughput tRNA sequencing, Nat Methods 12 (2015) 835-7.

[155] A.E. Cozen, E. Quartley, A.D. Holmes, E. Hrabeta-Robinson, E.M. Phizicky, T.M. Lowe, ARM-seq: AlkB-facilitated RNA methylation sequencing reveals a complex landscape of modified tRNA fragments, Nat Methods 12(9) (2015) 879-84.

[156] O. Pinkard, S. McFarland, T. Sweet, J. Coller, Quantitative tRNA-sequencing uncovers metazoan tissue-specific tRNA regulation, Nat Commun 11(1) (2020) 4104.

[157] A. Behrens, G. Rodschinka, D.D. Nedialkova, High-resolution quantitative profiling of tRNA abundance and modification status in eukaryotes by mim-tRNAseq, Mol Cell (2021).

[158] Y.L. Pang, R. Abo, S.S. Levine, P.C. Dedon, Diverse cell stresses induce unique patterns of tRNA up- and down-regulation: tRNA-seq for quantifying changes in tRNA copy number, Nucleic Acids Res 42(22) (2014) e170.

[159] T. Gogakos, M. Brown, A. Garzia, C. Meyer, M. Hafner, T. Tuschl, Characterizing Expression and Processing of Precursor and Mature Human tRNAs by Hydro-tRNAseq and PAR-CLIP, Cell Rep 20(6) (2017) 1463-1475.

[160] F. Ma, B.K. Fuqua, Y. Hasin, C. Yukhtman, C.D. Vulpe, A.J. Lusis, M. Pellegrini, A comparison between whole transcript and 3' RNA sequencing methods using Kapa and Lexogen library preparation methods, BMC Genomics 20(1) (2019) 9.

[161] D. Balchin, M. Hayer-Hartl, F.U. Hartl, In vivo aspects of protein folding and quality control, Science 353(6294) (2016) aac4354.

[162] H. Sies, D.P. Jones, Reactive oxygen species (ROS) as pleiotropic physiological signalling agents, Nat Rev Mol Cell Biol 21(7) (2020) 363-383.

[163] N. Medda, S.K. De, S. Maiti, Different mechanisms of arsenic related signaling in cellular proliferation, apoptosis and neo-plastic transformation, Ecotoxicol Environ Saf 208 (2021) 111752.

[164] M. Helm, Y. Motorin, Detecting RNA modifications in the epitranscriptome: predict and validate, Nat Rev Genet 18(5) (2017) 275-291.

[165] W.V. Gilbert, T.A. Bell, C. Schaening, Messenger RNA modifications: Form, distribution,

and function, Science 352(6292) (2016) 1408-12.

[166] D. Piekna-Przybylska, W.A. Decatur, M.J. Fournier, The 3D rRNA modification maps database: with interactive tools for ribosome analysis, Nucleic Acids Res 36 (2007) D178-83.

[167] Z. Chen, M. Qi, B. Shen, G. Luo, Y. Wu, J. Li, Z. Lu, Z. Zheng, Q. Dai, H. Wang, Transfer RNA demethylase ALKBH3 promotes cancer progression via induction of tRNA-derived small RNAs, Nucleic Acids Res 47 (2019) 2533-2545.

[168] Y. Ueda, I. Ooshio, Y. Fusamae, K. Kitae, M. Kawaguchi, K. Jingushi, H. Hase, K. Harada, K. Hirata, K. Tsujikawa, AlkB homolog 3-mediated tRNA demethylation promotes protein synthesis in cancer cells, Sci Rep 7 (2017) 42271.

[169] C.T. Chan, Y.L. Pang, W. Deng, I.R. Babu, M. Dyavaiah, T.J. Begley, P.C. Dedon, Reprogramming of tRNA modifications controls the oxidative stress response by codon-biased translation of proteins, Nat Commun 3 (2012) 937.

[170] W. Deng, I.R. Babu, D. Su, S. Yin, T.J. Begley, P.C. Dedon, Trm9-Catalyzed tRNA Modifications Regulate Global Protein Expression by Codon-Biased Translation, PLoS Genet 11(12) (2015) e1005706.

[171] P. Anderson, P. Ivanov, tRNA fragments in human health and disease, FEBS Lett 588(23) (2014) 4297-304.

[172] P. Schimmel, The emerging complexity of the tRNA world: mammalian tRNAs beyond protein synthesis, Nat Rev Mol Cell Biol 19 (2018) 45–58.

[173] S. Yamasaki, P. Ivanov, G.F. Hu, P. Anderson, Angiogenin cleaves tRNA and promotes stress-induced translational repression, J Cell Biol 185(1) (2009) 35-42.

[174] S. Rashad, X. Han, K. Sato, E. Mishima, T. Abe, T. Tominaga, K. Niizuma, The stress specific impact of ALKBH1 on tRNA cleavage and tiRNA generation, RNA Biol 17(8) (2020) 1092-1103.

[175] S. Blanco, S. Dietmann, J.V. Flores, S. Hussain, C. Kutter, P. Humphreys, M. Lukk, P. Lombard, L. Treps, M. Popis, S. Kellner, S.M. Holter, L. Garrett, W. Wurst, L. Becker, T. Klopstock, H. Fuchs, V. Gailus-Durner, M. Hrabe de Angelis, R.T. Karadottir, M. Helm, J. Ule, J.G. Gleeson, D.T. Odom, M. Frye, Aberrant methylation of tRNAs links cellular stress to neuro-developmental disorders, EMBO J 33(18) (2014) 2020-39.

[176] C. Cosentino, S. Toivonen, E. Diaz Villamil, M. Atta, J.L. Ravanat, S. Demine, A.A.

Schiavo, N. Pachera, J.P. Deglasse, J.C. Jonas, D. Balboa, T. Otonkoski, E.R. Pearson, P. Marchetti, D.L. Eizirik, M. Cnop, M. Igoillo-Esteve, Pancreatic beta-cell tRNA hypomethylation and fragmentation link TRMT10A deficiency with diabetes, Nucleic Acids Res 46(19) (2018) 10302-10318.

[177] E. Hrabeta-Robinson, E. Marcus, A.E. Cozen, E.M. Phizicky, T.M. Lowe, High-Throughput Small RNA Sequencing Enhanced by AlkB-Facilitated RNA de-Methylation (ARM-Seq), Methods Mol Biol 1562 (2017) 231-243.

[178] J.H. Song, Y. Zhuang, C.X. Zhu, H.W. Meng, B. Lu, B.T. Xie, J.Y. Peng, M. Li, C.Q. Yi, Differential roles of human PUS10 in miRNA processing and tRNA pseudouridylation, Nat. Chem. Biol. 16 (2020) 160-169.

[179] Z. Zhang, L.Q. Chen, Y.L. Zhao, C.G. Yang, I.A. Roundtree, Z. Zhang, J. Ren, W. Xie, C. He, G.Z. Luo, Single-base mapping of m(6)A by an antibody-independent method, Sci Adv 5(7) (2019) eaax0250.

[180] M.A. Garcia-Campos, S. Edelheit, U. Toth, M. Safra, R. Shachar, S. Viukov, R. Winkler, R. Nir, L. Lasman, A. Brandis, J.H. Hanna, W. Rossmanith, S. Schwartz, Deciphering the "m(6)A Code" via Antibody-Independent Quantitative Profiling, Cell 178(3) (2019) 731-747 e16.

[181] S. Lin, Q. Liu, V.S. Lelyveld, J. Choe, J.W. Szostak, R.I. Gregory, Mettl1/Wdr4-Mediated m(7)G tRNA Methylome Is Required for Normal mRNA Translation and Embryonic Stem Cell Self-Renewal and Differentiation, Mol Cell 71(2) (2018) 244-255 e5.

[182] D. Chen, J.T. Patton, Reverse transcriptase adds nontemplated nucleotides to cDNAs during 5'-RACE and primer extension, Biotechniques 30(3) (2001) 574-80, 582.

[183] L. Endres, P.C. Dedon, T.J. Begley, Codon-biased translation can be regulated by wobble-base tRNA modification systems during cellular stress responses, RNA Biol 12(6) (2015) 603-14.

[184] B. Liu, S.B. Qian, Translational reprogramming in cellular stress response, Wiley Interdiscip Rev RNA 5(3) (2014) 301-15.

[185] C.W. Chen, M. Tanaka, Genome-wide Translation Profiling by Ribosome-Bound tRNA Capture, Cell Rep 23(2) (2018) 608-621.

[186] C.C. Wu, B. Zinshteyn, K.A. Wehner, R. Green, High-Resolution Ribosome Profiling Defines Discrete Ribosome Elongation States and Translational Regulation during Cellular Stress, Mol Cell 73(5) (2019) 959-970 e5.

[187] M. Li, E. Kao, D. Malone, X. Gao, J.Y.J. Wang, M. David, DNA damage-induced cell death relies on SLFN11-dependent cleavage of distinct type II tRNAs, Nat Struct Mol Biol 25(11) (2018) 1047-1058.

[188] X. Wang, Z. Lu, A. Gomez, G.C. Hon, Y. Yue, D. Han, Y. Fu, M. Parisien, Q. Dai, G. Jia, B. Ren, T. Pan, C. He, N6-methyladenosine-dependent regulation of messenger RNA stability, Nature 505(7481) (2014) 117-20.

[189] F. Ramirez, D.P. Ryan, B. Gruning, V. Bhardwaj, F. Kilpert, A.S. Richter, S. Heyne, F. Dundar, T. Manke, deepTools2: a next generation web server for deep-sequencing data analysis, Nucleic Acids Res 44(W1) (2016) W160-5.

[190] W. Zhang, R. Xu, Z. Matuszek, Z. Cai, T. Pan, Detection and quantification of glycosylated queuosine modified tRNAs by acid denaturing and APB gels, RNA 26 (2020) 1291-1298.

[191] H. Mi, A. Muruganujan, D. Ebert, X. Huang, P.D. Thomas, PANTHER version 14: more genomes, a new PANTHER GO-slim and improvements in enrichment analysis tools, Nucleic Acids Res 47(D1) (2019) D419-D426.

[192] C. Girardot, J. Scholtalbers, S. Sauer, S.Y. Su, E.E. Furlong, Je, a versatile suite to handle multiplexed NGS libraries with unique molecular identifiers, BMC Bioinformatics 17(1) (2016) 419.

[193] H. Li, B. Handsaker, A. Wysoker, T. Fennell, J. Ruan, N. Homer, G. Marth, G. Abecasis, R. Durbin, S. Genome Project Data Processing, The Sequence Alignment/Map format and SAMtools, Bioinformatics 25(16) (2009) 2078-9.

[194] A.M. Bolger, M. Lohse, B. Usadel, Trimmomatic: a flexible trimmer for Illumina sequence data, Bioinformatics 30(15) (2014) 2114-20.

Appendix-Supplementary information

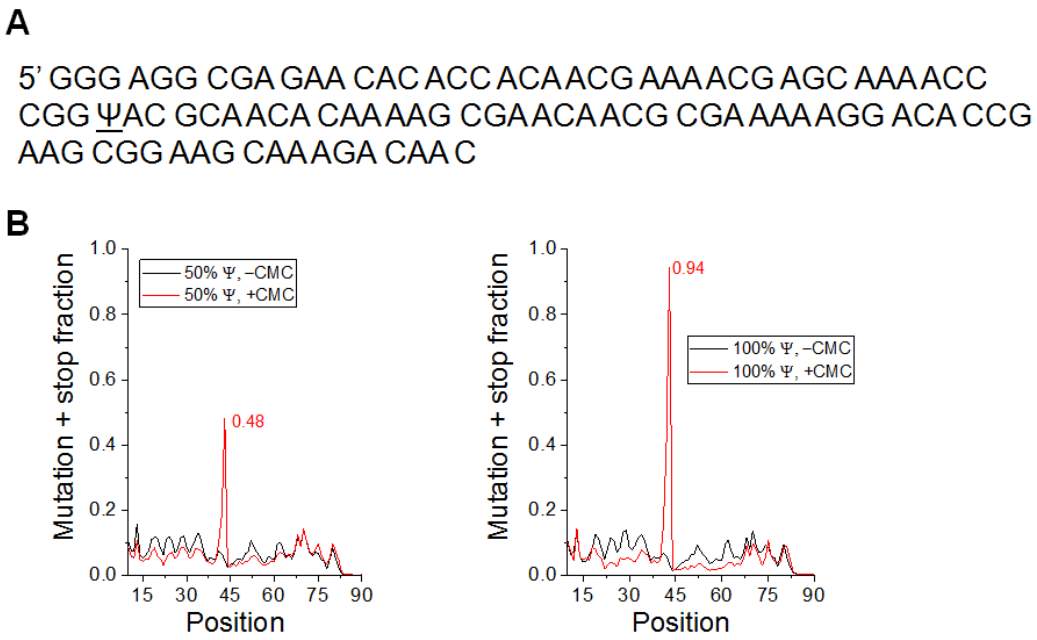

Fig. 2.S1: RNA standard used for calibration. (A) The 100mer RNA contains a single U or Ψ at the underlined position. (B) Sequencing results using this RNA spiked-in total HEK293T RNA (data from GSE110247, NCBI GEO) showing a near complete conversion of Ψ to Ψ-CMC under our condition.

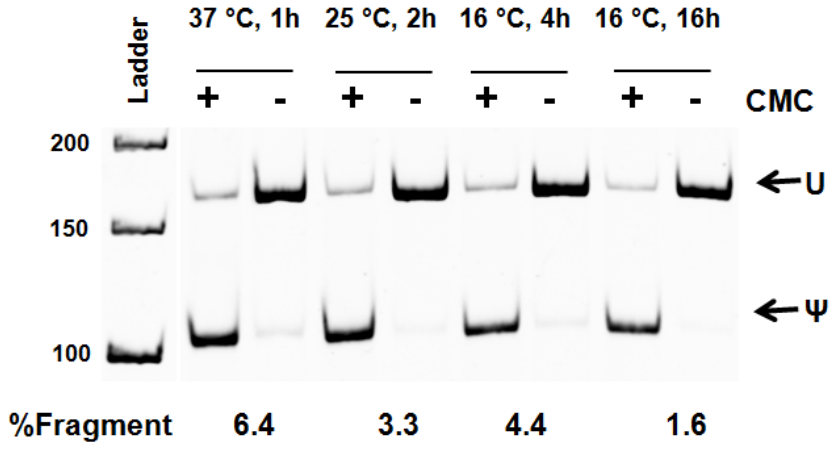

Fig. 2.S2: Optimization of RNA-5 ligation conditions to reduce background. MALAT1 Ψ5590 site was tested here upon varying the incubation condition of the blocking 5mer RNA (RNA-5) ligation. The 16 °C, 16h condition was used for subsequent experiments.

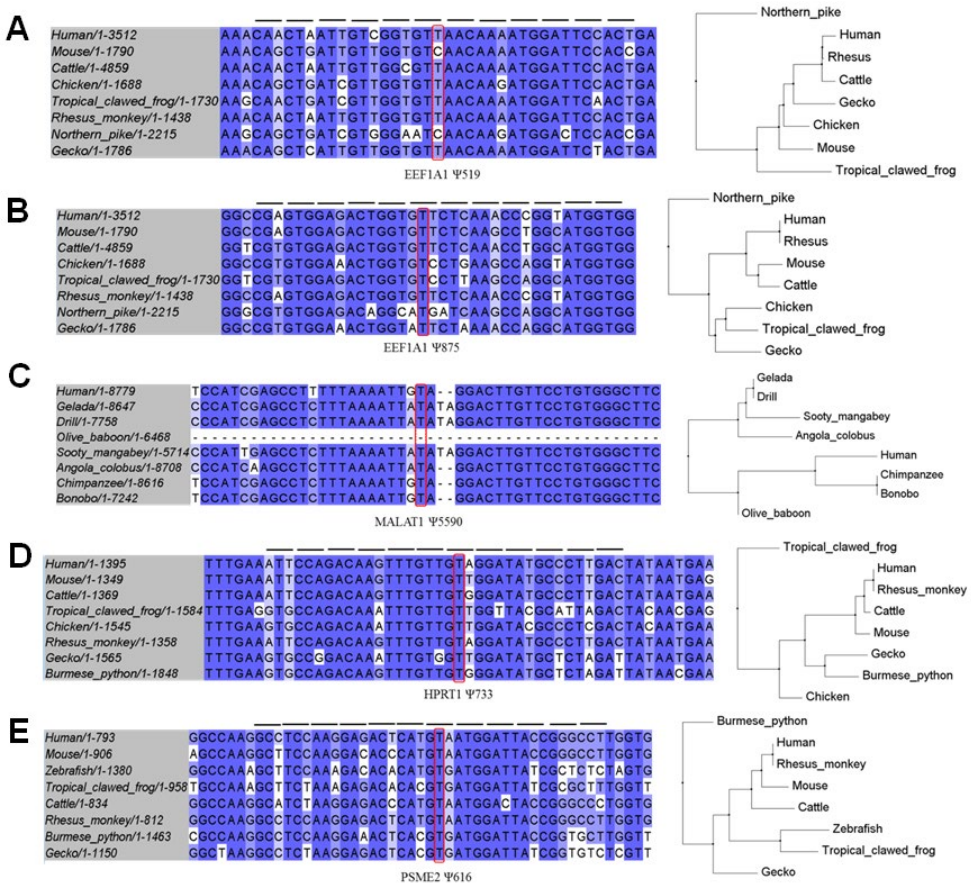

Fig. 2.S3: Conservation in vertebrates of the mRNA/lncRNA Ψ sites in this study. Sequence alignment around each target Ψ sites (boxed) are shown. The phylogenetic relationship of the organisms is shown on the right. For the 4 mRNA sites the codon positions are marked by lines on top. (A) eEF1A1 Ψ519; (B) eEF1A1 Ψ875; (C) MALAT1 Ψ5590; (D) HPRT1 Ψ733; (E) PSME2 Ψ616.

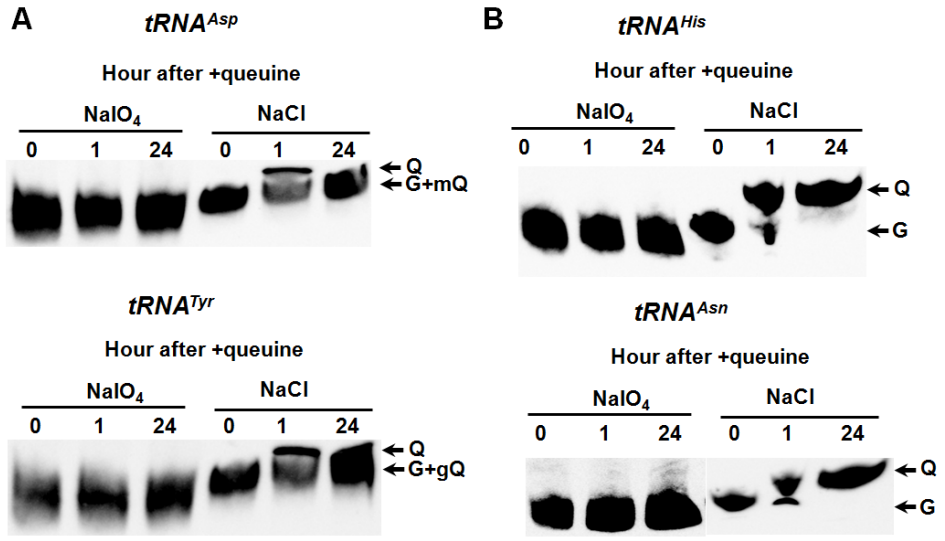

Fig. 3.S1: Analysis of Q and glycosylated Q-modified tRNAs using APB gels. Individual tRNA with ($NaIO_4$) and without (NaCl) periodate treatment. 0: total RNA from 0Q cells; 1, 24: total RNA from cells 1 and 24 hours after the addition of queuine to 0Q cells. Total RNA was from MCF7 cells.

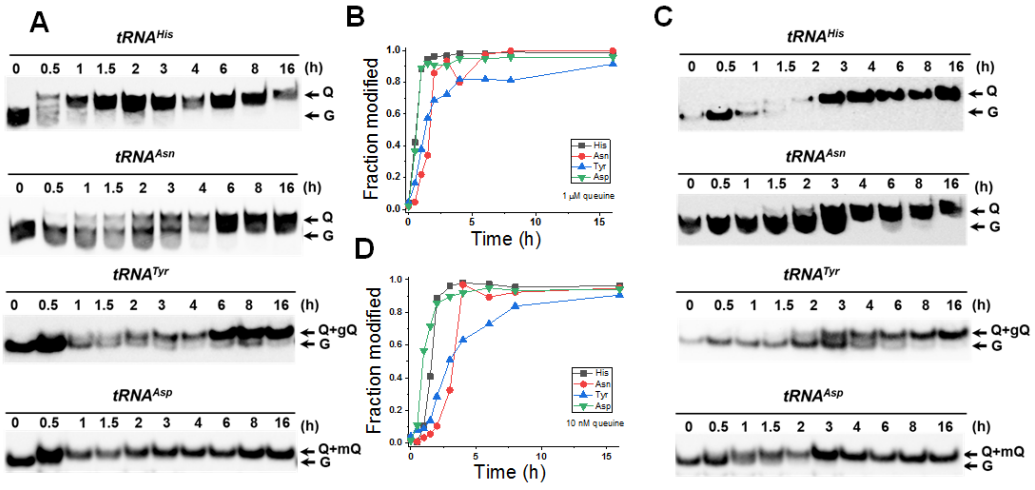

Fig. 3.S2: Q and glycosylated Q-modification kinetics of HeLa cells by APB (tRNAHis and tRNAAsn) and acid denaturing (tRNATyr and tRNAAsp) gels.(A) At t = 0, 1 μM queuine was added to the medium of 0Q cells, total RNA was extracted after designated time points in hours. G: unmodified tRNA, Q: Q-modified tRNA, mQ: mannosyl-Q, gQ: galactosyl-Q. (B) Quantitative modification fraction over time for individual tRNAs, from 1 μM queuine data. For $tRNA^{His}$ and $tRNA^{Asn}$, the modification fraction represents Q; for $tRNA^{Asp}$ and $tRNA^{Tyr}$, the modification fraction represents the sum of the Q and glycosylated Q modifications. (C), (D) Same as (A), (B) except at t = 0, 10 nM queuine was added to the medium of 0Q cells.

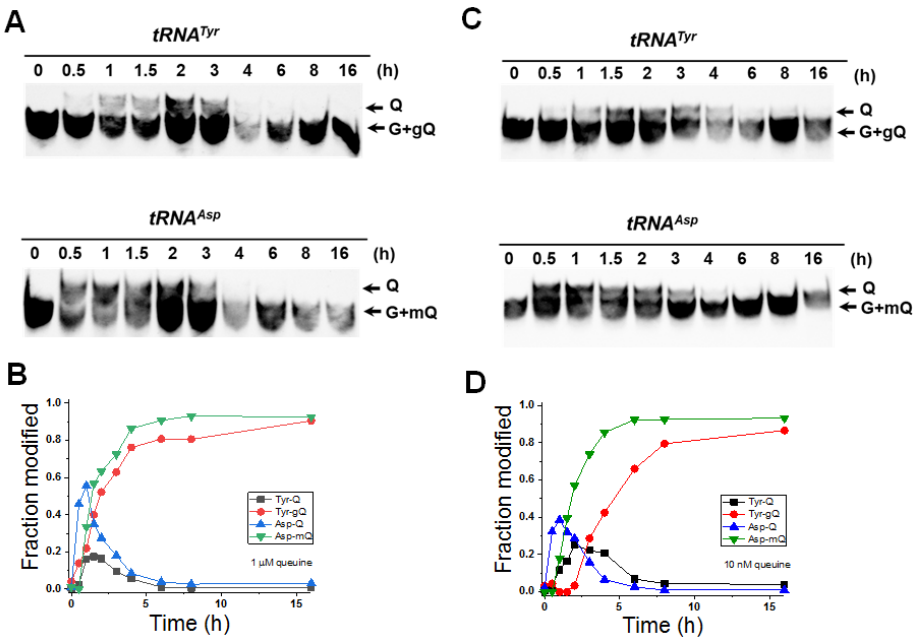

Fig. 3.S3: Q-modification kinetics of tRNAAsp and tRNATyr in HeLa cells by APB gels.(A) At t = 0, 1 µM queuine was added to the medium of 0Q cells, total RNA was extracted after designated time points in hours. G: unmodified tRNA, Q: Q-modified tRNA, mQ: mannosyl-Q, gQ: galactosyl-Q. The reversal to fast migration in later time points corresponds to gQ or mQ products as indicated by the acid denaturing gel results from Figure S2. (B) Quantitative modification fraction over time for individual tRNAs, from 1 µM queuine data. For comparison the total modification fraction from acid denaturing gel results in Figure S2 are also shown. (C), (D) Same as (A), (B) except at t = 0, 10 nM queuine was added to the medium of 0Q cells.

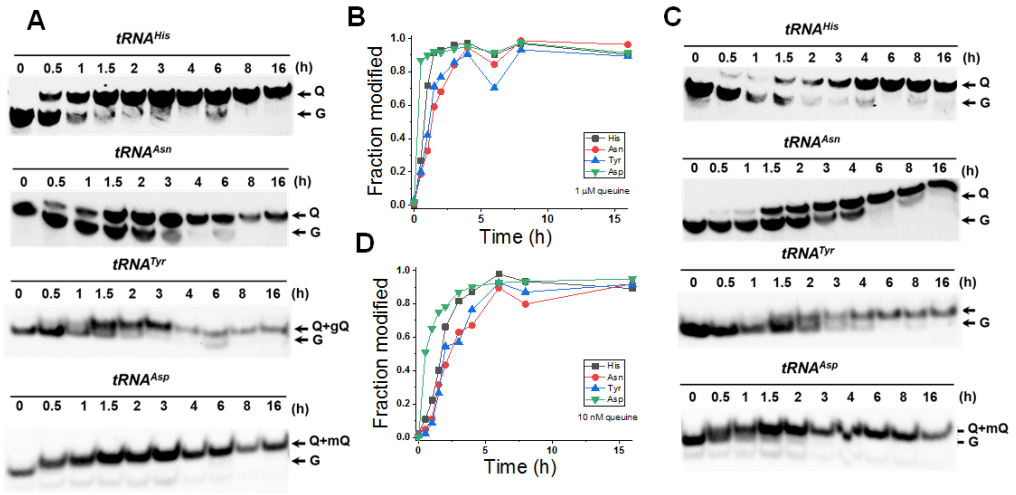

Fig. 3.S4: Q and glycosylated Q-modification kinetics of MCF7 cells by APB (tRNAHis and tRNAAsn) and acid denaturing (tRNATyr and tRNAAsp) gels.(A) At t = 0, 1 μM queuine was added to the medium of 0Q cells, total RNA was extracted after designated time points in hours. G: unmodified tRNA, Q: Q-modified tRNA, mQ: mannosyl-Q, gQ: galactosyl-Q. (B) Quantitative modification fraction over time for individual tRNAs, from 1 μM queuine data. For $tRNA^{His}$ and $tRNA^{Asn}$, the modification fraction represents Q; for $tRNA^{Asp}$ and $tRNA^{Tyr}$, the modification fraction represents the sum of the Q and glycosylated Q modifications. (C), (D) Same as (A), (B) except at t = 0, 10 nM queuine was added to the medium of 0Q cells.

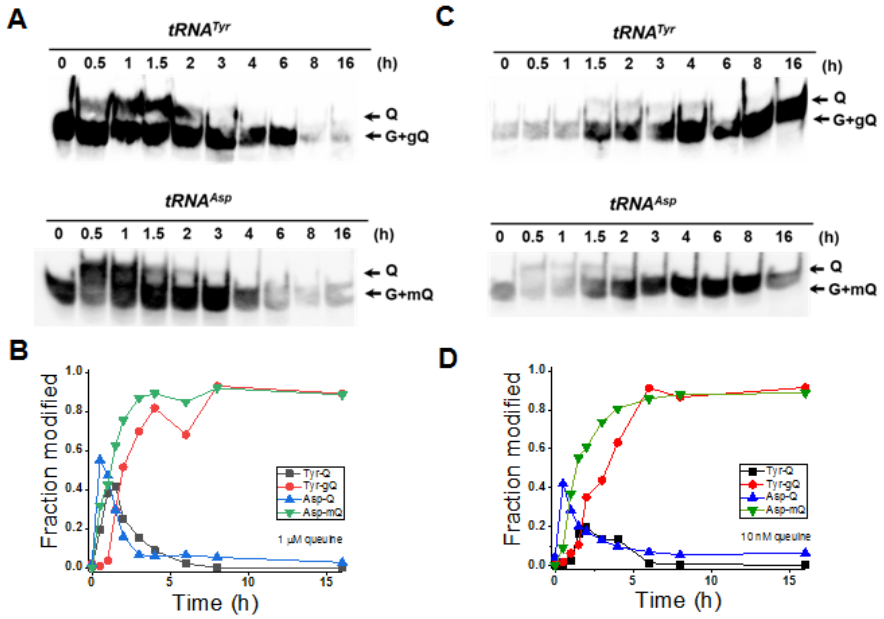

Fig. 3.S5: Q-modification kinetics of tRNAAsp and tRNATyr in MCF7 cells by APB gels.(A) At t = 0, 1 μM queuine was added to the medium of 0Q cells, total RNA was extracted after designated time points in hours. G: unmodified tRNA, Q: Q-modified tRNA, mQ: mannosyl-Q, gQ: galactosyl-Q. The reversal to fast migration in later time points corresponds to gQ or mQ products as indicated by the acid denaturing gel results from Figure S4. (B) Quantitative modification fraction over time for individual tRNAs, from 1 μM queuine data. For comparison the total modification fraction from acid denaturing gel results in Figure S4 are also shown. (C), (D) Same as (A), (B) except at t = 0, 10 nM queuine was added to the medium of 0Q cells.

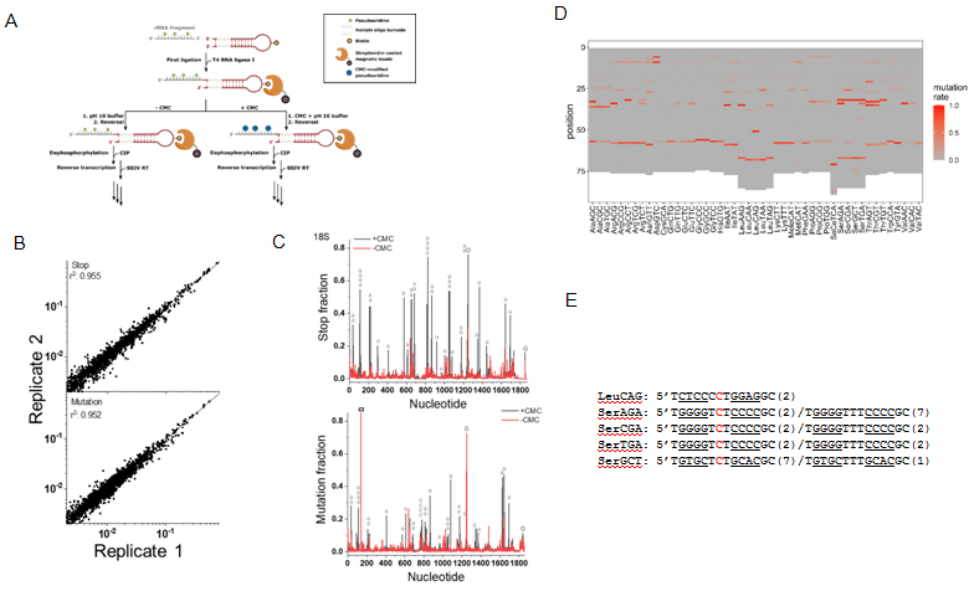

Fig. 4.S1: Chemical treatment, enzyme treatment and other results. (A-C) Pseudouridine identification by CMC reaction on bead. (A) Schematic representation of incorporating CMC reaction in MSR-seq. Total RNA was fragmented, 3' end repaired and ligated to the capture hairpin oligonucleotide. CMC reaction was done on-bead before cDNA synthesis. (B) RNA library Stop and mutation fraction at each nucleotide position in human 18S rRNA among biological replicates. (C) Stop and mutation fraction of the18S rRNA. Known Ψ sites are indicated by filled gray ovals, known $m^1acp^3\Psi$ and $m^6{}_2A$ sites by open ovals. (D) Mutation pattern for most abundant tRNA isodecoder in each isoacceptor familyusing overnight RT condition for library construction, no demethylase treatment. (E) Variable loop sequences of $tRNA^{Leu}$(CAG), $tRNA^{Ser}$(AGA/CGA/TGA/GCT). The variable stem is underlined, and the C47d residue is in red. Gene copy numbers are in parenthesis. C47d and T47d $tRNA^{Ser}$ can also be distinguished in the sequences elsewhere in the tRNA body.

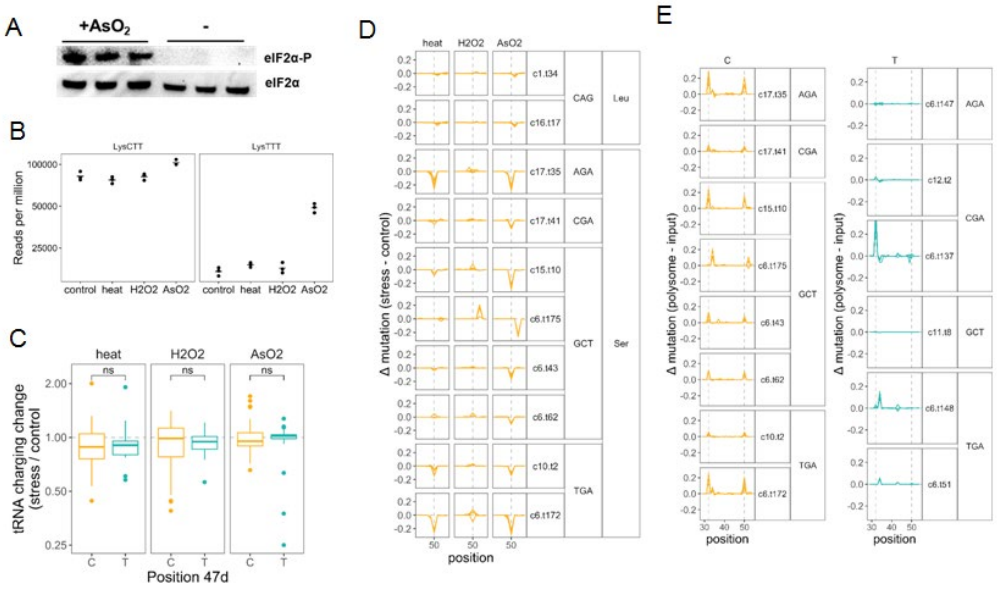

Fig. 4.S2: tRNA analysis without and with stress on the polysome.(A) Western blot showing eIF2α phosphorylation increase in arsenite stress. (B) $tRNA^{Lys}$ abundance change on the polysome.(C) $tRNA^{Ser}$ charging change on the polysome. (D) $tRNA^{Ser}$ m^3C32 and m^3C47d change for polysome-total, unstressed control. Shown are all tRNA isodecoders containing m^3C47d. (E) $tRNA^{Ser}m^3C32$ and m^3C47d change for polysome, stress-control. C47d-$tRNA^{Ser}$isodecoders in orange, T47d-$tRNA^{Ser}$ in blue.

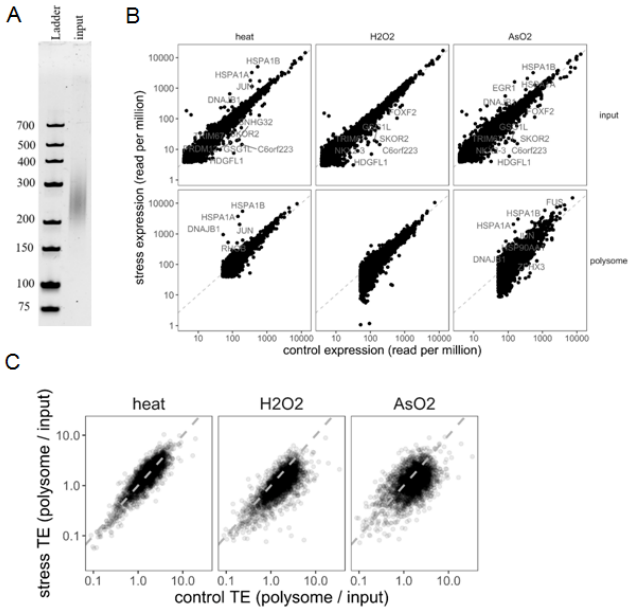

Fig. 4.S3: More polysome profiling mRNA results. (A) Final PCR product of MSR-seq libraries of polyA+ RNA. (B) Stress (y) versus control (x) mRNA analysis for total RNA input and for polysome. (C) Translation efficiency (TE) between stress (y) and unstressed control (x).

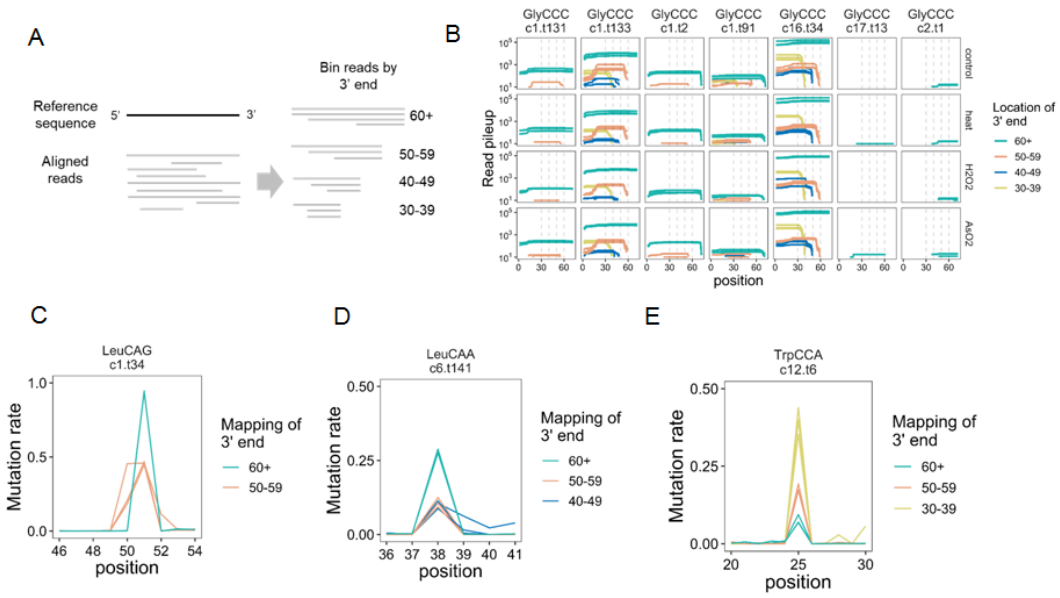

Fig. 4.S4: more tRNA and tRNA fragment analysis.(A) Schematics of tRF analysis. (B) Read pile-up of all $tRNA^{Gly}$(CCC) isodecoders, biological triplicates are shown. (C-E) Mutation rate of the cognate full-length tRNA in red and for tRF in blue,biological triplicates are shown. (C) m^3C47 of $tRNA^{Leu}$(CAG). (D) m^1G37 of $tRNA^{Leu}$(CAA). (E) $m^2{}_2G26$ of $tRNA^{Trp}$.

Table 4.S1: input tRNA abundance

treatment	sample	anticodon	AA	rpm_1	rpm_2	rpm_3	sum_count_1	sum_count_2	sum_count_3
AsO2	input	AGC	Ala	0.0421	0.0359	0.0403	337438	227810	230796
AsO2	input	CGC	Ala	0.0120	0.0113	0.0116	96331	71444	66720
AsO2	input	TGC	Ala	0.0296	0.0287	0.0298	237317	182136	170517
AsO2	input	ACG	Arg	0.0178	0.0138	0.0158	142831	87258	90511
AsO2	input	CCG	Arg	0.0268	0.0293	0.0277	214752	185530	158407
AsO2	input	CCT	Arg	0.0087	0.0087	0.0087	69898	54915	50046
AsO2	input	TCG	Arg	0.0462	0.0435	0.0448	370734	275887	256699
AsO2	input	TCT	Arg	0.0202	0.0206	0.0179	161646	130721	102509
AsO2	input	GTT	Asn	0.0389	0.0416	0.0420	311933	263906	240640
AsO2	input	GTC	Asp	0.0596	0.0672	0.0612	477480	425990	350442
AsO2	input	GCA	Cys	0.0013	0.0013	0.0014	10410	8131	7890
AsO2	input	CTG	Gln	0.0102	0.0082	0.0091	81854	51890	52164
AsO2	input	TTG	Gln	0.0040	0.0032	0.0033	31758	20557	18886
AsO2	input	CTC	Glu	0.0493	0.0594	0.0602	395161	376672	344857
AsO2	input	TTC	Glu	0.0145	0.0179	0.0173	116403	113608	99098
AsO2	input	CCC	Gly	0.0179	0.0158	0.0173	143214	99927	99269
AsO2	input	GCC	Gly	0.0255	0.0271	0.0289	204316	171608	165549
AsO2	input	TCC	Gly	0.0181	0.0183	0.0187	145442	116093	107387
AsO2	input	GTG	His	0.0031	0.0028	0.0034	25142	17668	19727
AsO2	input	AAT	Ile	0.0446	0.0418	0.0426	357390	264769	244233
AsO2	input	TAT	Ile	0.0230	0.0215	0.0211	184183	135973	120717
AsO2	input	AAG	Leu	0.0158	0.0166	0.0171	126491	105291	98045
AsO2	input	CAA	Leu	0.0123	0.0120	0.0120	98944	76250	68481
AsO2	input	CAG	Leu	0.0107	0.0101	0.0109	85816	64282	62225
AsO2	input	TAA	Leu	0.0044	0.0042	0.0043	34962	26732	24782
AsO2	input	TAG	Leu	0.0111	0.0112	0.0114	89346	70691	65347
AsO2	input	CTT	Lys	0.0848	0.0939	0.0924	679751	595368	529436
AsO2	input	TTT	Lys	0.0191	0.0223	0.0208	153167	141186	118917
AsO2	input	CAT	Mete	0.0491	0.0452	0.0463	393625	286516	265041
AsO2	input	CAT	Meti	0.0117	0.0092	0.0118	93895	58556	67676
AsO2	input	TGC	mtAla	0.0018	0.0018	0.0017	14476	11283	9626
AsO2	input	TCG	mtArg	0.0005	0.0004	0.0005	4345	2593	3033
AsO2	input	GTT	mtAsn	0.0011	0.0009	0.0009	8518	5803	5289
AsO2	input	GTC	mtAsp	0.0003	0.0002	0.0003	2281	1448	1441

Table 4.S1: input tRNA abundance (continued)

treatment	sample	anticodon	AA	rpm_1	rpm_2	rpm_3	sum_count_1	sum_count_2	sum_count_3
AsO2	input	GCA	mtCys	0.0012	0.0012	0.0012	9856	7744	6805
AsO2	input	TTG	mtGln	0.0022	0.0022	0.0020	17662	13892	11697
AsO2	input	TTC	mtGlu	0.0088	0.0065	0.0063	70695	41292	36270
AsO2	input	TCC	mtGly	0.0005	0.0004	0.0005	4217	2409	2784
AsO2	input	GTG	mtHis	0.0009	0.0007	0.0008	7053	4174	4516
AsO2	input	GAT	mtIle	0.0006	0.0004	0.0006	4918	2735	3302
AsO2	input	TAA	mtLeu	0.0024	0.0022	0.0022	19181	13646	12661
AsO2	input	TAG	mtLeu	0.0007	0.0005	0.0007	5436	3442	3733
AsO2	input	TTT	mtLys	0.0011	0.0009	0.0010	8750	5984	5962
AsO2	input	CAT	mtMet	0.0010	0.0009	0.0010	8106	5568	5496
AsO2	input	GAA	mtPhe	0.0021	0.0023	0.0021	17130	14318	11989
AsO2	input	TGG	mtPro	0.0009	0.0008	0.0008	7269	4790	4859
AsO2	input	GCT	mtSer	0.0006	0.0004	0.0005	4483	2810	2643
AsO2	input	TGA	mtSer	0.0054	0.0050	0.0046	43230	31951	26611
AsO2	input	TGT	mtThr	0.0011	0.0010	0.0011	8982	6379	6128
AsO2	input	TCA	mtTrp	0.0012	0.0010	0.0010	9918	6631	5965
AsO2	input	GTA	mtTyr	0.0028	0.0024	0.0025	22303	15357	14167
AsO2	input	TAC	mtVal	0.0102	0.0096	0.0083	81654	61101	47794
AsO2	input	GAA	Phe	0.0266	0.0276	0.0246	213240	174829	140808
AsO2	input	AGG	Pro	0.0027	0.0024	0.0025	21280	15106	14583
AsO2	input	CGG	Pro	0.0046	0.0042	0.0044	36690	26319	25361
AsO2	input	TGG	Pro	0.0080	0.0072	0.0080	64135	45639	45606
AsO2	input	TCA	SeCe	0.0028	0.0031	0.0032	22301	19832	18292
AsO2	input	AGA	Ser	0.0067	0.0062	0.0061	53781	39285	35187
AsO2	input	CGA	Ser	0.0017	0.0019	0.0019	14030	12258	10892
AsO2	input	GCT	Ser	0.0375	0.0404	0.0367	300832	256096	210008
AsO2	input	TGA	Ser	0.0116	0.0113	0.0108	93185	71532	62103
AsO2	input	AGT	Thr	0.0156	0.0160	0.0154	125379	101201	88340
AsO2	input	CGT	Thr	0.0043	0.0044	0.0046	34313	28201	26417
AsO2	input	TGT	Thr	0.0047	0.0043	0.0048	37450	27339	27529
AsO2	input	CCA	Trp	0.0203	0.0181	0.0180	162410	114799	103270
AsO2	input	GTA	Tyr	0.0391	0.0394	0.0362	313379	249616	207336
AsO2	input	AAC	Val	0.0083	0.0066	0.0077	66596	41959	43907
AsO2	input	CAC	Val	0.0163	0.0142	0.0156	130520	90039	89525
AsO2	input	TAC	Val	0.0095	0.0083	0.0086	75809	52300	49179

Table 4.S1: input tRNA abundance (continued)

treatment	sample	anticodon	AA	rpm_1	rpm_2	rpm_3	sum_count_1	sum_count_2	sum_count_3
control	input	AGC	Ala	0.0401	0.0355	0.0322	438022	278179	199226
control	input	CGC	Ala	0.0140	0.0112	0.0106	152458	87616	65654
control	input	TGC	Ala	0.0357	0.0283	0.0273	389673	221795	169261
control	input	ACG	Arg	0.0167	0.0146	0.0150	182584	114346	93088
control	input	CCG	Arg	0.0295	0.0265	0.0284	322080	207386	175705
control	input	CCT	Arg	0.0075	0.0082	0.0092	81901	63994	56657
control	input	TCG	Arg	0.0440	0.0431	0.0436	481005	337533	269740
control	input	TCT	Arg	0.0201	0.0161	0.0202	219933	125666	124781
control	input	GTT	Asn	0.0358	0.0353	0.0366	391297	276586	226682
control	input	GTC	Asp	0.0620	0.0646	0.0746	677417	505770	461823
control	input	GCA	Cys	0.0012	0.0016	0.0014	12610	12895	8660
control	input	CTG	Gln	0.0083	0.0113	0.0087	90144	88215	53676
control	input	TTG	Gln	0.0033	0.0039	0.0033	35753	30604	20589
control	input	CTC	Glu	0.0578	0.0549	0.0571	631282	430053	353315
control	input	TTC	Glu	0.0146	0.0164	0.0163	159665	128292	100929
control	input	CCC	Gly	0.0164	0.0161	0.0146	179156	126318	90196
control	input	GCC	Gly	0.0284	0.0344	0.0264	309655	269580	163483
control	input	TCC	Gly	0.0198	0.0180	0.0174	216682	140763	107970
control	input	GTG	His	0.0027	0.0037	0.0028	29970	28815	17447
control	input	AAT	Ile	0.0434	0.0371	0.0358	474448	290525	221660
control	input	TAT	Ile	0.0205	0.0184	0.0176	223399	144016	109061
control	input	AAG	Leu	0.0177	0.0182	0.0161	193619	142131	99830
control	input	CAA	Leu	0.0129	0.0141	0.0126	140492	110732	77794
control	input	CAG	Leu	0.0107	0.0130	0.0103	117013	102011	63514
control	input	TAA	Leu	0.0042	0.0056	0.0049	45888	44070	30208
control	input	TAG	Leu	0.0124	0.0126	0.0109	134892	98795	67411
control	input	CTT	Lys	0.0878	0.0861	0.0954	958859	674083	590616
control	input	TTT	Lys	0.0197	0.0203	0.0249	214630	158748	154022
control	input	CAT	Mete	0.0482	0.0451	0.0439	526257	352942	271596
control	input	CAT	Meti	0.0090	0.0153	0.0127	98377	120067	78474
control	input	TGC	mtAla	0.0015	0.0025	0.0020	16255	19570	12592
control	input	TCG	mtArg	0.0005	0.0008	0.0008	5559	6326	4924
control	input	GTT	mtAsn	0.0007	0.0014	0.0012	8058	11014	7163
control	input	GTC	mtAsp	0.0003	0.0005	0.0005	3624	4083	2840
control	input	GCA	mtCys	0.0013	0.0019	0.0017	14086	15058	10602
control	input	TTG	mtGln	0.0018	0.0028	0.0026	20135	21765	15825

Table 4.S1: input tRNA abundance (continued)

treatment	sample	anticodon	AA	rpm_1	rpm_2	rpm_3	sum_count_1	sum_count_2	sum_count_3
control	input	TTC	mtGlu	0.0067	0.0083	0.0075	73049	65165	46354
control	input	TCC	mtGly	0.0005	0.0009	0.0008	5232	7084	5183
control	input	GTG	mtHis	0.0006	0.0011	0.0009	6939	8598	5554
control	input	GAT	mtIle	0.0005	0.0008	0.0012	5043	6075	7549
control	input	TAA	mtLeu	0.0022	0.0031	0.0029	24314	23997	18099
control	input	TAG	mtLeu	0.0005	0.0010	0.0009	5860	7875	5261
control	input	TTT	mtLys	0.0010	0.0013	0.0014	10399	10372	8871
control	input	CAT	mtMet	0.0012	0.0018	0.0048	13338	14082	29428
control	input	GAA	mtPhe	0.0025	0.0028	0.0029	27561	21913	17707
control	input	TGG	mtPro	0.0007	0.0012	0.0011	7710	9777	6919
control	input	GCT	mtSer	0.0006	0.0008	0.0007	6674	6533	4211
control	input	TGA	mtSer	0.0060	0.0069	0.0063	65276	53626	39158
control	input	TGT	mtThr	0.0011	0.0013	0.0013	11594	9997	8086
control	input	TCA	mtTrp	0.0010	0.0012	0.0014	10407	9596	8839
control	input	GTA	mtTyr	0.0024	0.0027	0.0028	25739	20907	17550
control	input	TAC	mtVal	0.0096	0.0171	0.0113	105026	134204	69977
control	input	GAA	Phe	0.0259	0.0227	0.0279	282856	177830	172450
control	input	AGG	Pro	0.0021	0.0029	0.0024	23093	22775	14667
control	input	CGG	Pro	0.0038	0.0049	0.0041	41169	38735	25366
control	input	TGG	Pro	0.0065	0.0092	0.0073	70708	71622	45441
control	input	TCA	SeCe	0.0026	0.0032	0.0032	28809	25153	19753
control	input	AGA	Ser	0.0065	0.0061	0.0062	70846	47572	38069
control	input	CGA	Ser	0.0018	0.0020	0.0019	19407	15755	11650
control	input	GCT	Ser	0.0368	0.0352	0.0394	401810	275836	243599
control	input	TGA	Ser	0.0113	0.0104	0.0108	123551	81171	66802
control	input	AGT	Thr	0.0158	0.0146	0.0171	172540	113998	105638
control	input	CGT	Thr	0.0043	0.0043	0.0046	46956	33941	28501
control	input	TGT	Thr	0.0043	0.0052	0.0046	46735	40354	28699
control	input	CCA	Trp	0.0203	0.0190	0.0169	222223	148537	104524
control	input	GTA	Tyr	0.0386	0.0327	0.0385	421185	255851	238462
control	input	AAC	Val	0.0074	0.0091	0.0062	80799	71145	38230
control	input	CAC	Val	0.0155	0.0169	0.0131	169137	132471	81292
control	input	TAC	Val	0.0091	0.0094	0.0081	98938	73620	49987
H2O2	input	AGC	Ala	0.0300	0.0360	0.0340	199617	208346	212308
H2O2	input	CGC	Ala	0.0098	0.0113	0.0112	65516	65289	69939
H2O2	input	TGC	Ala	0.0256	0.0290	0.0284	170560	167663	177272

Table 4.S1: input tRNA abundance (continued)

treatment	sample	anticodon	AA	rpm_1	rpm_2	rpm_3	sum_count_1	sum_count_2	sum_count_3
H2O2	input	ACG	Arg	0.0155	0.0168	0.0162	102770	97511	101260
H2O2	input	CCG	Arg	0.0294	0.0289	0.0300	195878	167323	187130
H2O2	input	CCT	Arg	0.0096	0.0090	0.0093	63891	52208	57837
H2O2	input	TCG	Arg	0.0456	0.0450	0.0429	303080	260408	267664
H2O2	input	TCT	Arg	0.0187	0.0206	0.0198	124556	119327	123548
H2O2	input	GTT	Asn	0.0392	0.0418	0.0408	261012	241872	254621
H2O2	input	GTC	Asp	0.0690	0.0691	0.0654	459292	399979	408005
H2O2	input	GCA	Cys	0.0013	0.0011	0.0012	8480	6621	7685
H2O2	input	CTG	Gln	0.0082	0.0080	0.0081	54732	46295	50744
H2O2	input	TTG	Gln	0.0032	0.0032	0.0030	21036	18531	18580
H2O2	input	CTC	Glu	0.0644	0.0595	0.0608	428245	344379	379440
H2O2	input	TTC	Glu	0.0185	0.0155	0.0164	122970	89674	102294
H2O2	input	CCC	Gly	0.0152	0.0150	0.0162	101001	86709	100882
H2O2	input	GCC	Gly	0.0276	0.0255	0.0284	183306	147498	177388
H2O2	input	TCC	Gly	0.0175	0.0167	0.0179	116524	96654	112006
H2O2	input	GTG	His	0.0029	0.0029	0.0030	19437	16952	18437
H2O2	input	AAT	Ile	0.0364	0.0404	0.0383	242111	233990	239033
H2O2	input	TAT	Ile	0.0177	0.0191	0.0188	118062	110822	117499
H2O2	input	AAG	Leu	0.0163	0.0162	0.0170	108133	93875	105808
H2O2	input	CAA	Leu	0.0124	0.0119	0.0123	82279	68903	76980
H2O2	input	CAG	Leu	0.0103	0.0101	0.0104	68783	58663	64698
H2O2	input	TAA	Leu	0.0049	0.0045	0.0044	32392	26205	27547
H2O2	input	TAG	Leu	0.0109	0.0111	0.0111	72731	64065	69522
H2O2	input	CTT	Lys	0.0973	0.0917	0.0918	646983	530709	572966
H2O2	input	TTT	Lys	0.0224	0.0223	0.0221	148819	129233	137905
H2O2	input	CAT	Mete	0.0442	0.0454	0.0438	294262	262522	273328
H2O2	input	CAT	Meti	0.0123	0.0114	0.0110	81582	66222	68431
H2O2	input	TGC	mtAla	0.0027	0.0024	0.0024	17702	13964	14927
H2O2	input	TCG	mtArg	0.0007	0.0007	0.0006	4979	3918	3737
H2O2	input	GTT	mtAsn	0.0014	0.0014	0.0012	9524	8001	7750
H2O2	input	GTC	mtAsp	0.0006	0.0006	0.0005	3793	3461	2960
H2O2	input	GCA	mtCys	0.0018	0.0016	0.0016	11873	9104	9684
H2O2	input	TTG	mtGln	0.0034	0.0029	0.0029	22720	16585	18096
H2O2	input	TTC	mtGlu	0.0095	0.0089	0.0089	63260	51225	55742
H2O2	input	TCC	mtGly	0.0007	0.0006	0.0006	4711	3483	3584
H2O2	input	GTG	mtHis	0.0011	0.0009	0.0009	7189	5112	5318

Table 4.S1: input tRNA abundance (continued)

treatment	sample	anticodon	AA	rpm_1	rpm_2	rpm_3	sum_count_1	sum_count_2	sum_count_3
H2O2	input	GAT	mtIle	0.0008	0.0007	0.0006	5106	3855	3632
H2O2	input	TAA	mtLeu	0.0037	0.0029	0.0028	24478	16515	17323
H2O2	input	TAG	mtLeu	0.0009	0.0008	0.0007	6142	4468	4344
H2O2	input	TTT	mtLys	0.0016	0.0013	0.0012	10325	7537	7615
H2O2	input	CAT	mtMet	0.0019	0.0015	0.0016	12513	8878	9829
H2O2	input	GAA	mtPhe	0.0032	0.0028	0.0029	21180	16409	17967
H2O2	input	TGG	mtPro	0.0010	0.0009	0.0009	6875	5307	5446
H2O2	input	GCT	mtSer	0.0007	0.0007	0.0007	4847	3785	4575
H2O2	input	TGA	mtSer	0.0079	0.0069	0.0077	52458	39986	47754
H2O2	input	TGT	mtThr	0.0015	0.0013	0.0012	9722	7449	7753
H2O2	input	TCA	mtTrp	0.0016	0.0013	0.0012	10817	7353	7670
H2O2	input	GTA	mtTyr	0.0036	0.0030	0.0030	24050	17274	19009
H2O2	input	TAC	mtVal	0.0144	0.0127	0.0128	95698	73756	79913
H2O2	input	GAA	Phe	0.0250	0.0265	0.0274	166251	153613	170702
H2O2	input	AGG	Pro	0.0024	0.0021	0.0023	15703	12429	14662
H2O2	input	CGG	Pro	0.0043	0.0038	0.0041	28571	21920	25369
H2O2	input	TGG	Pro	0.0073	0.0066	0.0071	48249	38135	44306
H2O2	input	TCA	SeCe	0.0038	0.0035	0.0036	24964	20488	22499
H2O2	input	AGA	Ser	0.0056	0.0060	0.0061	37157	34493	37810
H2O2	input	CGA	Ser	0.0020	0.0018	0.0019	13132	10643	12139
H2O2	input	GCT	Ser	0.0388	0.0397	0.0407	258066	229792	253810
H2O2	input	TGA	Ser	0.0101	0.0107	0.0108	66948	61646	67674
H2O2	input	AGT	Thr	0.0142	0.0151	0.0147	94594	87626	91913
H2O2	input	CGT	Thr	0.0042	0.0043	0.0042	28140	24660	26311
H2O2	input	TGT	Thr	0.0044	0.0042	0.0041	29251	24340	25822
H2O2	input	CCA	Trp	0.0168	0.0171	0.0166	111643	98966	103764
H2O2	input	GTA	Tyr	0.0346	0.0359	0.0382	230267	207964	238273
H2O2	input	AAC	Val	0.0059	0.0061	0.0062	39492	35568	38628
H2O2	input	CAC	Val	0.0122	0.0127	0.0132	81374	73683	82575
H2O2	input	TAC	Val	0.0075	0.0078	0.0079	49876	45336	49006
heat	input	AGC	Ala	0.0397	0.0369	0.0377	387520	215407	187179
heat	input	CGC	Ala	0.0139	0.0124	0.0125	135899	72291	61808
heat	input	TGC	Ala	0.0348	0.0311	0.0319	339686	181268	158035
heat	input	ACG	Arg	0.0166	0.0155	0.0160	161757	90236	79477
heat	input	CCG	Arg	0.0291	0.0286	0.0293	284163	166796	145157
heat	input	CCT	Arg	0.0077	0.0081	0.0080	75536	47279	39869

Table 4.S1: input tRNA abundance (continued)

treatment	sample	anticodon	AA	rpm_1	rpm_2	rpm_3	sum_count_1	sum_count_2	sum_count_3
heat	input	TCG	Arg	0.0455	0.0416	0.0415	443928	242584	205720
heat	input	TCT	Arg	0.0190	0.0197	0.0196	184953	114725	97213
heat	input	GTT	Asn	0.0328	0.0387	0.0376	319893	225640	186709
heat	input	GTC	Asp	0.0677	0.0725	0.0686	660554	423123	340219
heat	input	GCA	Cys	0.0010	0.0012	0.0011	10177	7111	5670
heat	input	CTG	Gln	0.0078	0.0082	0.0084	75654	47840	41694
heat	input	TTG	Gln	0.0033	0.0033	0.0033	31996	19248	16324
heat	input	CTC	Glu	0.0602	0.0632	0.0662	587538	368407	328122
heat	input	TTC	Glu	0.0146	0.0155	0.0146	142908	90675	72540
heat	input	CCC	Gly	0.0143	0.0140	0.0143	139950	81568	70826
heat	input	GCC	Gly	0.0255	0.0291	0.0301	249235	169840	149150
heat	input	TCC	Gly	0.0182	0.0173	0.0181	177956	101158	89926
heat	input	GTG	His	0.0025	0.0029	0.0029	24827	17088	14267
heat	input	AAT	Ile	0.0476	0.0388	0.0428	464187	226237	212144
heat	input	TAT	Ile	0.0208	0.0187	0.0193	203239	108846	95699
heat	input	AAG	Leu	0.0184	0.0169	0.0181	179751	98443	89624
heat	input	CAA	Leu	0.0124	0.0126	0.0129	120877	73756	63851
heat	input	CAG	Leu	0.0100	0.0109	0.0112	97860	63312	55613
heat	input	TAA	Leu	0.0041	0.0045	0.0043	40202	26286	21261
heat	input	TAG	Leu	0.0125	0.0112	0.0123	121494	65230	60917
heat	input	CTT	Lys	0.0906	0.0888	0.0897	883485	518279	444966
heat	input	TTT	Lys	0.0209	0.0234	0.0206	203604	136317	102012
heat	input	CAT	Mete	0.0516	0.0426	0.0441	502998	248450	218704
heat	input	CAT	Meti	0.0084	0.0109	0.0103	81827	63764	50996
heat	input	TGC	mtAla	0.0013	0.0021	0.0020	13106	12337	9785
heat	input	TCG	mtArg	0.0005	0.0005	0.0005	5144	2825	2285
heat	input	GTT	mtAsn	0.0007	0.0012	0.0010	6382	6721	4725
heat	input	GTC	mtAsp	0.0004	0.0004	0.0004	3621	2246	1805
heat	input	GCA	mtCys	0.0013	0.0015	0.0015	12942	8832	7618
heat	input	TTG	mtGln	0.0018	0.0026	0.0022	17605	15343	11108
heat	input	TTC	mtGlu	0.0061	0.0068	0.0077	59890	39414	38212
heat	input	TCC	mtGly	0.0005	0.0005	0.0005	4807	2855	2408
heat	input	GTG	mtHis	0.0006	0.0007	0.0007	6322	4280	3333
heat	input	GAT	mtIle	0.0005	0.0005	0.0005	4979	2936	2473
heat	input	TAA	mtLeu	0.0024	0.0023	0.0023	23363	13301	11550
heat	input	TAG	mtLeu	0.0006	0.0006	0.0006	5590	3487	2895

Table 4.S1: input tRNA abundance (continued)

treatment	sample	anticodon	AA	rpm_1	rpm_2	rpm_3	sum_count_1	sum_count_2	sum_count_3
heat	input	TTT	mtLys	0.0011	0.0011	0.0010	10349	6501	5013
heat	input	CAT	mtMet	0.0011	0.0012	0.0012	10783	7106	5981
heat	input	GAA	mtPhe	0.0022	0.0024	0.0026	21135	13921	12692
heat	input	TGG	mtPro	0.0006	0.0008	0.0008	6068	4807	3878
heat	input	GCT	mtSer	0.0005	0.0006	0.0006	5093	3390	2870
heat	input	TGA	mtSer	0.0061	0.0063	0.0064	59270	36579	31936
heat	input	TGT	mtThr	0.0011	0.0011	0.0010	10853	6468	5013
heat	input	TCA	mtTrp	0.0010	0.0010	0.0011	9754	5847	5237
heat	input	GTA	mtTyr	0.0025	0.0023	0.0025	24614	13395	12170
heat	input	TAC	mtVal	0.0098	0.0149	0.0109	95321	87121	54030
heat	input	GAA	Phe	0.0250	0.0274	0.0246	243635	159782	122124
heat	input	AGG	Pro	0.0020	0.0022	0.0024	19131	13120	11761
heat	input	CGG	Pro	0.0035	0.0039	0.0041	33891	22723	20304
heat	input	TGG	Pro	0.0059	0.0068	0.0071	57263	39732	34993
heat	input	TCA	SeCe	0.0027	0.0027	0.0026	26129	15930	12683
heat	input	AGA	Ser	0.0062	0.0060	0.0063	60892	35040	31304
heat	input	CGA	Ser	0.0017	0.0018	0.0018	16867	10426	8996
heat	input	GCT	Ser	0.0341	0.0394	0.0388	332948	229875	192578
heat	input	TGA	Ser	0.0108	0.0107	0.0111	105192	62328	55204
heat	input	AGT	Thr	0.0163	0.0158	0.0157	158602	92384	77747
heat	input	CGT	Thr	0.0046	0.0043	0.0044	44751	25347	21621
heat	input	TGT	Thr	0.0048	0.0045	0.0045	46727	26260	22311
heat	input	CCA	Trp	0.0204	0.0174	0.0172	198570	101730	85454
heat	input	GTA	Tyr	0.0346	0.0373	0.0344	337247	217826	170534
heat	input	AAC	Val	0.0074	0.0066	0.0068	72570	38772	33903
heat	input	CAC	Val	0.0158	0.0139	0.0143	154331	81275	71136
heat	input	TAC	Val	0.0098	0.0086	0.0089	95809	49938	43962

Table 4.S2: input tRNA charging

sample	source	treatment	AA	anticodon	rep_1_charging	rep_2_charging	rep_3_charging
input	cytosolic	AsO2	Ala	AGC	0.519644	0.472524	0.494666
input	cytosolic	AsO2	Ala	CGC	0.528997	0.488031	0.508069
input	cytosolic	AsO2	Ala	TGC	0.563487	0.518773	0.543121
input	cytosolic	AsO2	Arg	ACG	0.585328	0.575546	0.598759
input	cytosolic	AsO2	Arg	CCG	0.705162	0.720064	0.718576
input	cytosolic	AsO2	Arg	CCT	0.81592	0.787258	0.808088
input	cytosolic	AsO2	Arg	TCG	0.674744	0.673209	0.683344
input	cytosolic	AsO2	Arg	TCT	0.590229	0.565582	0.618921
input	cytosolic	AsO2	Asn	GTT	0.673835	0.66389	0.652379
input	cytosolic	AsO2	Asp	GTC	0.792548	0.759803	0.789453
input	cytosolic	AsO2	Cys	GCA	0.804558	0.791128	0.815974
input	cytosolic	AsO2	Gln	CTG	0.678432	0.655848	0.698232
input	cytosolic	AsO2	Gln	TTG	0.615538	0.584403	0.641727
input	cytosolic	AsO2	Glu	CTC	0.799313	0.789986	0.786097
input	cytosolic	AsO2	Glu	TTC	0.748302	0.699283	0.727234
input	cytosolic	AsO2	Gly	CCC	0.615904	0.606955	0.602968
input	cytosolic	AsO2	Gly	GCC	0.706082	0.719245	0.694434
input	cytosolic	AsO2	Gly	TCC	0.621205	0.590627	0.616274
input	cytosolic	AsO2	His	GTG	0.71446	0.68176	0.689864
input	cytosolic	AsO2	Ile	AAT	0.534517	0.488194	0.525938
input	cytosolic	AsO2	Ile	TAT	0.629199	0.6157	0.641481
input	cytosolic	AsO2	Leu	AAG	0.668333	0.643995	0.649279
input	cytosolic	AsO2	Leu	CAA	0.667468	0.642398	0.654349
input	cytosolic	AsO2	Leu	CAG	0.628959	0.606278	0.623168
input	cytosolic	AsO2	Leu	TAA	0.660215	0.608038	0.640822
input	cytosolic	AsO2	Leu	TAG	0.635158	0.609203	0.617545
input	cytosolic	AsO2	Lys	CTT	0.66726	0.678075	0.685004
input	cytosolic	AsO2	Lys	TTT	0.70732	0.688091	0.70314
input	cytosolic	AsO2	Mete	CAT	0.650195	0.644721	0.659709
input	cytosolic	AsO2	Meti	CAT	0.678588	0.648138	0.660424
input	mitochondrial	AsO2	mtAla	TGC	0.788138	0.785133	0.798476
input	mitochondrial	AsO2	mtArg	TCG	0.735815	0.746285	0.703892
input	mitochondrial	AsO2	mtAsn	GTT	0.883841	0.885276	0.871184
input	mitochondrial	AsO2	mtAsp	GTC	0.670498	0.689597	0.680769

Table 4.S2: input tRNA charging (continued)

sample	source	treatment	AA	anticodon	rep_1_charging	rep_2_charging	rep_3_charging
input	mitochondrial	AsO2	mtCys	GCA	0.747008	0.691041	0.73939
input	mitochondrial	AsO2	mtGln	TTG	0.823665	0.799694	0.846735
input	mitochondrial	AsO2	mtGlu	TTC	0.758249	0.744846	0.781658
input	mitochondrial	AsO2	mtGly	TCC	0.833333	0.839231	0.814454
input	mitochondrial	AsO2	mtHis	GTG	0.772877	0.800867	0.780872
input	mitochondrial	AsO2	mtIle	GAT	0.83391	0.808537	0.827474
input	mitochondrial	AsO2	mtLeu	TAA	0.764281	0.752221	0.77703
input	mitochondrial	AsO2	mtLeu	TAG	0.841358	0.824846	0.839631
input	mitochondrial	AsO2	mtLys	TTT	0.823257	0.815559	0.803726
input	mitochondrial	AsO2	mtMet	CAT	0.688078	0.651394	0.587264
input	mitochondrial	AsO2	mtPhe	GAA	0.757518	0.756026	0.743202
input	mitochondrial	AsO2	mtPro	TGG	0.78179	0.781368	0.76225
input	mitochondrial	AsO2	mtSer	GCT	0.638158	0.608629	0.610727
input	mitochondrial	AsO2	mtSer	TGA	0.746747	0.709584	0.729185
input	mitochondrial	AsO2	mtThr	TGT	0.716561	0.6934	0.730007
input	mitochondrial	AsO2	mtTrp	TCA	0.829468	0.844304	0.840409
input	mitochondrial	AsO2	mtTyr	GTA	0.739577	0.725878	0.734779
input	mitochondrial	AsO2	mtVal	TAC	0.741024	0.704076	0.725886
input	cytosolic	AsO2	Phe	GAA	0.649646	0.609053	0.637598
input	cytosolic	AsO2	Pro	AGG	0.829555	0.820205	0.821722
input	cytosolic	AsO2	Pro	CGG	0.80341	0.81578	0.812127
input	cytosolic	AsO2	Pro	TGG	0.810306	0.812976	0.801271
input	cytosolic	AsO2	SeCe	TCA	0.397004	0.357447	0.438914
input	cytosolic	AsO2	Ser	AGA	0.517686	0.523382	0.532344
input	cytosolic	AsO2	Ser	CGA	0.577747	0.565007	0.572673
input	cytosolic	AsO2	Ser	GCT	0.7362	0.734872	0.726363
input	cytosolic	AsO2	Ser	TGA	0.525943	0.520849	0.5273
input	cytosolic	AsO2	Thr	AGT	0.676559	0.635851	0.676872
input	cytosolic	AsO2	Thr	CGT	0.713825	0.67684	0.703896
input	cytosolic	AsO2	Thr	TGT	0.746577	0.735093	0.731106
input	cytosolic	AsO2	Trp	CCA	0.652705	0.641101	0.670635
input	cytosolic	AsO2	Tyr	GTA	0.721975	0.674479	0.709654
input	cytosolic	AsO2	Val	AAC	0.512279	0.506525	0.504297
input	cytosolic	AsO2	Val	CAC	0.510692	0.499923	0.50558
input	cytosolic	AsO2	Val	TAC	0.647916	0.615883	0.623267

Table 4.S2: input tRNA charging (continued)

sample	source	treatment	AA	anticodon	rep_1_charging	rep_2_charging	rep_3_charging
input	cytosolic	control	Ala	AGC	0.450942	0.51634	0.536865
input	cytosolic	control	Ala	CGC	0.450425	0.537802	0.553615
input	cytosolic	control	Ala	TGC	0.485252	0.553103	0.572798
input	cytosolic	control	Arg	ACG	0.551755	0.651316	0.599049
input	cytosolic	control	Arg	CCG	0.663634	0.747367	0.736024
input	cytosolic	control	Arg	CCT	0.78448	0.8127	0.795802
input	cytosolic	control	Arg	TCG	0.631896	0.7231	0.685443
input	cytosolic	control	Arg	TCT	0.537655	0.657447	0.592303
input	cytosolic	control	Asn	GTT	0.663483	0.688645	0.709001
input	cytosolic	control	Asp	GTC	0.734468	0.805555	0.788348
input	cytosolic	control	Cys	GCA	0.776122	0.813142	0.797161
input	cytosolic	control	Gln	CTG	0.629835	0.728489	0.68151
input	cytosolic	control	Gln	TTG	0.574275	0.680904	0.634568
input	cytosolic	control	Glu	CTC	0.746028	0.813824	0.804407
input	cytosolic	control	Glu	TTC	0.700719	0.767314	0.742478
input	cytosolic	control	Gly	CCC	0.54827	0.64943	0.640027
input	cytosolic	control	Gly	GCC	0.673603	0.710409	0.738201
input	cytosolic	control	Gly	TCC	0.554597	0.662535	0.648206
input	cytosolic	control	His	GTG	0.699213	0.700751	0.71893
input	cytosolic	control	Ile	AAT	0.479892	0.548092	0.542709
input	cytosolic	control	Ile	TAT	0.597075	0.653783	0.674339
input	cytosolic	control	Leu	AAG	0.640043	0.676532	0.6863
input	cytosolic	control	Leu	CAA	0.644385	0.67588	0.676673
input	cytosolic	control	Leu	CAG	0.622886	0.641398	0.664602
input	cytosolic	control	Leu	TAA	0.614484	0.666721	0.66314
input	cytosolic	control	Leu	TAG	0.590757	0.635003	0.6575
input	cytosolic	control	Lys	CTT	0.649047	0.731464	0.702604
input	cytosolic	control	Lys	TTT	0.666615	0.730995	0.707565
input	cytosolic	control	Mete	CAT	0.617432	0.709832	0.668824
input	cytosolic	control	Meti	CAT	0.629561	0.690274	0.792038
input	mitochondrial	control	mtAla	TGC	0.773508	0.805556	0.819536
input	mitochondrial	control	mtArg	TCG	0.727057	0.793546	0.742888
input	mitochondrial	control	mtAsn	GTT	0.859864	0.901062	0.887725
input	mitochondrial	control	mtAsp	GTC	0.781723	0.801162	0.809282
input	mitochondrial	control	mtCys	GCA	0.719042	0.776072	0.76351
input	mitochondrial	control	mtGln	TTG	0.797366	0.849966	0.824533

Table 4.S2: input tRNA charging (continued)

sample	source	treatment	AA	anticodon	rep_1_charging	rep_2_charging	rep_3_charging
input	mitochondrial	control	mtGlu	TTC	0.732125	0.789526	0.79259
input	mitochondrial	control	mtGly	TCC	0.805433	0.86349	0.862305
input	mitochondrial	control	mtHis	GTG	0.761521	0.77582	0.777054
input	mitochondrial	control	mtIle	GAT	0.815066	0.87277	0.926725
input	mitochondrial	control	mtLeu	TAA	0.746194	0.789597	0.769309
input	mitochondrial	control	mtLeu	TAG	0.824296	0.858131	0.871803
input	mitochondrial	control	mtLys	TTT	0.774392	0.824434	0.811176
input	mitochondrial	control	mtMet	CAT	0.752171	0.815805	0.960477
input	mitochondrial	control	mtPhe	GAA	0.721866	0.773484	0.763484
input	mitochondrial	control	mtPro	TGG	0.744067	0.829196	0.812807
input	mitochondrial	control	mtSer	GCT	0.628723	0.640202	0.69746
input	mitochondrial	control	mtSer	TGA	0.709244	0.789176	0.767005
input	mitochondrial	control	mtThr	TGT	0.690528	0.773331	0.719547
input	mitochondrial	control	mtTrp	TCA	0.794431	0.835258	0.836183
input	mitochondrial	control	mtTyr	GTA	0.684015	0.741763	0.748314
input	mitochondrial	control	mtVal	TAC	0.676353	0.751836	0.72043
input	cytosolic	control	Phe	GAA	0.581672	0.638978	0.615531
input	cytosolic	control	Pro	AGG	0.822149	0.820374	0.85423
input	cytosolic	control	Pro	CGG	0.797683	0.810702	0.845748
input	cytosolic	control	Pro	TGG	0.803105	0.811535	0.835431
input	cytosolic	control	SeCe	TCA	0.504762	0.441176	0.439834
input	cytosolic	control	Ser	AGA	0.506661	0.55305	0.543119
input	cytosolic	control	Ser	CGA	0.544058	0.631005	0.590096
input	cytosolic	control	Ser	GCT	0.71997	0.757643	0.75606
input	cytosolic	control	Ser	TGA	0.507303	0.559816	0.551882
input	cytosolic	control	Thr	AGT	0.626725	0.721092	0.654328
input	cytosolic	control	Thr	CGT	0.674223	0.732939	0.694545
input	cytosolic	control	Thr	TGT	0.713932	0.776594	0.734493
input	cytosolic	control	Trp	CCA	0.592628	0.705045	0.665344
input	cytosolic	control	Tyr	GTA	0.651928	0.732571	0.711752
input	cytosolic	control	Val	AAC	0.462668	0.554965	0.543859
input	cytosolic	control	Val	CAC	0.463702	0.547392	0.537053
input	cytosolic	control	Val	TAC	0.58808	0.664633	0.658201
input	cytosolic	H2O2	Ala	AGC	0.540903	0.470788	0.516354
input	cytosolic	H2O2	Ala	CGC	0.537474	0.481616	0.515273
input	cytosolic	H2O2	Ala	TGC	0.571242	0.515486	0.556881

Table 4.S2: input tRNA charging (continued)

sample	source	treatment	AA	anticodon	rep_1_charging	rep_2_charging	rep_3_charging
input	cytosolic	H2O2	Arg	ACG	0.609811	0.554526	0.607503
input	cytosolic	H2O2	Arg	CCG	0.749113	0.699461	0.733329
input	cytosolic	H2O2	Arg	CCT	0.819833	0.787463	0.797296
input	cytosolic	H2O2	Arg	TCG	0.705069	0.654498	0.683607
input	cytosolic	H2O2	Arg	TCT	0.610143	0.544925	0.586054
input	cytosolic	H2O2	Asn	GTT	0.685384	0.656192	0.688171
input	cytosolic	H2O2	Asp	GTC	0.77962	0.738385	0.759217
input	cytosolic	H2O2	Cys	GCA	0.827412	0.784577	0.792096
input	cytosolic	H2O2	Gln	CTG	0.716719	0.667155	0.641732
input	cytosolic	H2O2	Gln	TTG	0.662667	0.581276	0.590002
input	cytosolic	H2O2	Glu	CTC	0.80646	0.772548	0.809989
input	cytosolic	H2O2	Glu	TTC	0.721931	0.68469	0.720231
input	cytosolic	H2O2	Gly	CCC	0.648678	0.586618	0.628577
input	cytosolic	H2O2	Gly	GCC	0.743269	0.697389	0.735234
input	cytosolic	H2O2	Gly	TCC	0.635198	0.595822	0.633391
input	cytosolic	H2O2	His	GTG	0.716884	0.679823	0.7257
input	cytosolic	H2O2	Ile	AAT	0.569784	0.503445	0.557593
input	cytosolic	H2O2	Ile	TAT	0.68568	0.606419	0.64299
input	cytosolic	H2O2	Leu	AAG	0.675663	0.62716	0.678113
input	cytosolic	H2O2	Leu	CAA	0.670207	0.619304	0.662158
input	cytosolic	H2O2	Leu	CAG	0.649132	0.593513	0.642268
input	cytosolic	H2O2	Leu	TAA	0.641021	0.603344	0.602998
input	cytosolic	H2O2	Leu	TAG	0.644139	0.60289	0.645406
input	cytosolic	H2O2	Lys	CTT	0.703033	0.668356	0.701714
input	cytosolic	H2O2	Lys	TTT	0.702686	0.656932	0.689122
input	cytosolic	H2O2	Mete	CAT	0.697231	0.62139	0.662556
input	cytosolic	H2O2	Meti	CAT	0.687317	0.608673	0.649239
input	mitochondrial	H2O2	mtAla	TGC	0.787096	0.703628	0.781601
input	mitochondrial	H2O2	mtArg	TCG	0.755255	0.674089	0.755556
input	mitochondrial	H2O2	mtAsn	GTT	0.888713	0.868912	0.877111
input	mitochondrial	H2O2	mtAsp	GTC	0.834825	0.552609	0.828555
input	mitochondrial	H2O2	mtCys	GCA	0.769842	0.727011	0.724391
input	mitochondrial	H2O2	mtGln	TTG	0.818835	0.797136	0.813418
input	mitochondrial	H2O2	mtGlu	TTC	0.800879	0.7466	0.749089
input	mitochondrial	H2O2	mtGly	TCC	0.837928	0.803552	0.813624
input	mitochondrial	H2O2	mtHis	GTG	0.781398	0.776643	0.756667

Table 4.S2: input tRNA charging (continued)

sample	source	treatment	AA	anticodon	rep_1_charging	rep_2_charging	rep_3_charging
input	mitochondrial	H2O2	mtIle	GAT	0.84359	0.765651	0.842057
input	mitochondrial	H2O2	mtLeu	TAA	0.769792	0.753307	0.755834
input	mitochondrial	H2O2	mtLeu	TAG	0.838981	0.814605	0.839247
input	mitochondrial	H2O2	mtLys	TTT	0.802817	0.759358	0.785939
input	mitochondrial	H2O2	mtMet	CAT	0.785461	0.736387	0.769858
input	mitochondrial	H2O2	mtPhe	GAA	0.771454	0.743306	0.75045
input	mitochondrial	H2O2	mtPro	TGG	0.741995	0.693974	0.757028
input	mitochondrial	H2O2	mtSer	GCT	0.649437	0.619643	0.624699
input	mitochondrial	H2O2	mtSer	TGA	0.797792	0.75582	0.7466
input	mitochondrial	H2O2	mtThr	TGT	0.710645	0.700327	0.699173
input	mitochondrial	H2O2	mtTrp	TCA	0.820059	0.825075	0.809333
input	mitochondrial	H2O2	mtTyr	GTA	0.738841	0.710209	0.731255
input	mitochondrial	H2O2	mtVal	TAC	0.720745	0.672977	0.701428
input	cytosolic	H2O2	Phe	GAA	0.630563	0.591723	0.611604
input	cytosolic	H2O2	Pro	AGG	0.84209	0.832096	0.845615
input	cytosolic	H2O2	Pro	CGG	0.827804	0.803265	0.837618
input	cytosolic	H2O2	Pro	TGG	0.823787	0.798242	0.828566
input	cytosolic	H2O2	SeCe	TCA	0.483582	0.440191	0.412088
input	cytosolic	H2O2	Ser	AGA	0.533769	0.492123	0.54338
input	cytosolic	H2O2	Ser	CGA	0.585132	0.561776	0.586084
input	cytosolic	H2O2	Ser	GCT	0.742213	0.710002	0.737959
input	cytosolic	H2O2	Ser	TGA	0.532637	0.505335	0.540689
input	cytosolic	H2O2	Thr	AGT	0.712187	0.629376	0.664587
input	cytosolic	H2O2	Thr	CGT	0.734831	0.679174	0.699752
input	cytosolic	H2O2	Thr	TGT	0.767242	0.70968	0.731388
input	cytosolic	H2O2	Trp	CCA	0.701056	0.606236	0.661676
input	cytosolic	H2O2	Tyr	GTA	0.708783	0.645035	0.667188
input	cytosolic	H2O2	Val	AAC	0.562464	0.497182	0.538718
input	cytosolic	H2O2	Val	CAC	0.556729	0.502817	0.526208
input	cytosolic	H2O2	Val	TAC	0.655067	0.580752	0.628298
input	cytosolic	heat	Ala	AGC	0.494294	0.486629	0.454336
input	cytosolic	heat	Ala	CGC	0.480461	0.476839	0.451733
input	cytosolic	heat	Ala	TGC	0.516243	0.502693	0.492394
input	cytosolic	heat	Arg	ACG	0.567152	0.568386	0.543412
input	cytosolic	heat	Arg	CCG	0.667904	0.708681	0.688707
input	cytosolic	heat	Arg	CCT	0.796426	0.788678	0.783356

Table 4.S2: input tRNA charging (continued)

sample	source	treatment	AA	anticodon	rep_1_charging	rep_2_charging	rep_3_charging
input	cytosolic	heat	Arg	TCG	0.647517	0.656365	0.647558
input	cytosolic	heat	Arg	TCT	0.573546	0.568876	0.545998
input	cytosolic	heat	Asn	GTT	0.677507	0.672532	0.629614
input	cytosolic	heat	Asp	GTC	0.757856	0.766034	0.764245
input	cytosolic	heat	Cys	GCA	0.790335	0.791691	0.772845
input	cytosolic	heat	Gln	CTG	0.671352	0.642419	0.628977
input	cytosolic	heat	Gln	TTG	0.639874	0.573105	0.575833
input	cytosolic	heat	Glu	CTC	0.751945	0.786478	0.774813
input	cytosolic	heat	Glu	TTC	0.690985	0.717214	0.720877
input	cytosolic	heat	Gly	CCC	0.56927	0.605098	0.59075
input	cytosolic	heat	Gly	GCC	0.656614	0.708942	0.692119
input	cytosolic	heat	Gly	TCC	0.562672	0.62323	0.589224
input	cytosolic	heat	His	GTG	0.702247	0.711739	0.68858
input	cytosolic	heat	Ile	AAT	0.501939	0.531548	0.488178
input	cytosolic	heat	Ile	TAT	0.603049	0.618608	0.587477
input	cytosolic	heat	Leu	AAG	0.635362	0.643429	0.639672
input	cytosolic	heat	Leu	CAA	0.629898	0.642486	0.64013
input	cytosolic	heat	Leu	CAG	0.613263	0.621389	0.606854
input	cytosolic	heat	Leu	TAA	0.614415	0.593052	0.593937
input	cytosolic	heat	Leu	TAG	0.599487	0.610373	0.606131
input	cytosolic	heat	Lys	CTT	0.648441	0.681038	0.668876
input	cytosolic	heat	Lys	TTT	0.677512	0.677133	0.663601
input	cytosolic	heat	Mete	CAT	0.620208	0.639322	0.641194
input	cytosolic	heat	Meti	CAT	0.644692	0.631189	0.628481
input	mitochondrial	heat	mtAla	TGC	0.764289	0.76864	0.783848
input	mitochondrial	heat	mtArg	TCG	0.708055	0.71258	0.725236
input	mitochondrial	heat	mtAsn	GTT	0.85359	0.870062	0.866164
input	mitochondrial	heat	mtAsp	GTC	0.778777	0.823394	0.766854
input	mitochondrial	heat	mtCys	GCA	0.726532	0.706388	0.72678
input	mitochondrial	heat	mtGln	TTG	0.801451	0.78173	0.793424
input	mitochondrial	heat	mtGlu	TTC	0.718227	0.745011	0.740781
input	mitochondrial	heat	mtGly	TCC	0.801136	0.814696	0.807994
input	mitochondrial	heat	mtHis	GTG	0.747835	0.786487	0.745656
input	mitochondrial	heat	mtIle	GAT	0.829625	0.835301	0.84174
input	mitochondrial	heat	mtLeu	TAA	0.73893	0.768403	0.740197
input	mitochondrial	heat	mtLeu	TAG	0.802844	0.803455	0.796933

Table 4.S2: input tRNA charging (continued)

sample	source	treatment	AA	anticodon	rep_1_charging	rep_2_charging	rep_3_charging
input	mitochondrial	heat	mtLys	TTT	0.770746	0.775284	0.784802
input	mitochondrial	heat	mtMet	CAT	0.744457	0.794663	0.761167
input	mitochondrial	heat	mtPhe	GAA	0.714336	0.746772	0.730751
input	mitochondrial	heat	mtPro	TGG	0.750415	0.777354	0.76305
input	mitochondrial	heat	mtSer	GCT	0.61705	0.689524	0.653587
input	mitochondrial	heat	mtSer	TGA	0.722612	0.741168	0.732761
input	mitochondrial	heat	mtThr	TGT	0.689612	0.71388	0.709091
input	mitochondrial	heat	mtTrp	TCA	0.78509	0.815475	0.799282
input	mitochondrial	heat	mtTyr	GTA	0.68597	0.725207	0.67031
input	mitochondrial	heat	mtVal	TAC	0.679562	0.689445	0.681963
input	cytosolic	heat	Phe	GAA	0.617548	0.600143	0.564477
input	cytosolic	heat	Pro	AGG	0.807112	0.82268	0.823651
input	cytosolic	heat	Pro	CGG	0.792759	0.806025	0.799617
input	cytosolic	heat	Pro	TGG	0.792712	0.804063	0.797337
input	cytosolic	heat	SeCe	TCA	0.467626	0.428571	0.582677
input	cytosolic	heat	Ser	AGA	0.509775	0.532134	0.492559
input	cytosolic	heat	Ser	CGA	0.546811	0.588046	0.548424
input	cytosolic	heat	Ser	GCT	0.717957	0.717389	0.7147
input	cytosolic	heat	Ser	TGA	0.504858	0.533642	0.499336
input	cytosolic	heat	Thr	AGT	0.633485	0.634484	0.624033
input	cytosolic	heat	Thr	CGT	0.687697	0.666948	0.669765
input	cytosolic	heat	Thr	TGT	0.7289	0.715215	0.70949
input	cytosolic	heat	Trp	CCA	0.612957	0.607979	0.632365
input	cytosolic	heat	Tyr	GTA	0.693214	0.663801	0.651049
input	cytosolic	heat	Val	AAC	0.480979	0.514385	0.503049
input	cytosolic	heat	Val	CAC	0.464179	0.506121	0.501777
input	cytosolic	heat	Val	TAC	0.580341	0.622808	0.609048

Table 4.S3: polysome tRNA abundance

treatment	sample	anticodon	AA	rpm_1	rpm_2	rpm_3	sum_count_1	sum_count_2	sum_count_3
AsO2	polysome	AGC	Ala	4.0E-02	3.5E-02	4.1E-02	41981	42604	39282
AsO2	polysome	CGC	Ala	1.8E-02	1.6E-02	1.8E-02	19340	19793	17296
AsO2	polysome	TGC	Ala	3.2E-02	2.9E-02	3.1E-02	33253	34751	29333
AsO2	polysome	ACG	Arg	1.9E-02	1.5E-02	1.8E-02	20365	18436	17650
AsO2	polysome	CCG	Arg	1.7E-02	1.7E-02	1.8E-02	18070	20781	16796
AsO2	polysome	CCT	Arg	9.6E-03	1.1E-02	1.1E-02	10071	13073	10309
AsO2	polysome	TCG	Arg	2.1E-02	2.0E-02	2.2E-02	21747	24773	21216
AsO2	polysome	TCT	Arg	1.3E-02	1.4E-02	1.2E-02	13355	16622	11664
AsO2	polysome	GTT	Asn	4.6E-02	4.8E-02	5.4E-02	48584	57801	51977
AsO2	polysome	GTC	Asp	6.7E-02	8.2E-02	7.5E-02	70622	98940	71609
AsO2	polysome	GCA	Cys	1.0E-03	1.1E-03	9.5E-04	1063	1362	908
AsO2	polysome	CTG	Gln	7.5E-03	7.3E-03	7.2E-03	7847	8893	6853
AsO2	polysome	TTG	Gln	2.5E-03	2.3E-03	2.4E-03	2664	2800	2286
AsO2	polysome	CTC	Glu	4.0E-02	3.9E-02	4.2E-02	41813	46920	39883
AsO2	polysome	TTC	Glu	1.1E-02	1.2E-02	1.4E-02	11718	14359	13181
AsO2	polysome	CCC	Gly	1.2E-02	1.1E-02	1.1E-02	12720	13127	10690
AsO2	polysome	GCC	Gly	2.1E-02	1.9E-02	2.1E-02	22063	23273	20063
AsO2	polysome	TCC	Gly	2.5E-02	2.3E-02	2.6E-02	26202	27744	24340
AsO2	polysome	GTG	His	4.8E-03	4.7E-03	5.1E-03	5061	5681	4891
AsO2	polysome	AAT	Ile	1.4E-01	1.3E-01	1.2E-01	146898	163185	111881
AsO2	polysome	TAT	Ile	5.4E-02	5.5E-02	4.4E-02	56795	66396	41588
AsO2	polysome	AAG	Leu	7.6E-03	6.2E-03	7.6E-03	7944	7547	7286
AsO2	polysome	CAA	Leu	4.1E-03	4.1E-03	3.9E-03	4294	4925	3768
AsO2	polysome	CAG	Leu	3.7E-03	3.6E-03	3.5E-03	3851	4408	3333
AsO2	polysome	TAA	Leu	1.5E-03	1.4E-03	1.3E-03	1577	1644	1262
AsO2	polysome	TAG	Leu	3.4E-03	3.0E-03	3.0E-03	3520	3612	2890
AsO2	polysome	CTT	Lys	1.0E-01	1.0E-01	1.1E-01	104360	121827	103367
AsO2	polysome	TTT	Lys	4.5E-02	5.2E-02	4.9E-02	46839	63216	46787
AsO2	polysome	CAT	Mete	1.7E-02	1.6E-02	1.5E-02	17856	19141	14353
AsO2	polysome	CAT	Meti	2.3E-02	2.4E-02	2.9E-02	23717	28530	27456
AsO2	polysome	TGC	mtAla	4.0E-04	3.4E-04	3.0E-04	417	418	287
AsO2	polysome	TCG	mtArg	6.1E-05	6.1E-05	4.7E-05	64	74	45
AsO2	polysome	GTT	mtAsn	3.7E-04	3.5E-04	2.6E-04	388	428	249
AsO2	polysome	GTC	mtAsp	7.4E-05	8.3E-05	7.4E-05	77	101	71

Table 4.S3: polysome tRNA abundance (continued)

treatment	sample	anticodon	AA	rpm_1	rpm_2	rpm_3	sum_count_1	sum_count_2	sum_count_3
AsO2	polysome	GCA	mtCys	1.1E-04	1.2E-04	9.9E-05	119	151	94
AsO2	polysome	TTG	mtGln	3.5E-04	4.7E-04	3.8E-04	369	572	363
AsO2	polysome	TTC	mtGlu	3.0E-03	2.9E-03	2.3E-03	3115	3490	2195
AsO2	polysome	TCC	mtGly	6.0E-05	7.3E-05	6.2E-05	63	89	59
AsO2	polysome	GTG	mtHis	1.1E-04	1.1E-04	4.7E-05	115	137	45
AsO2	polysome	GAT	mtIle	1.3E-04	1.5E-04	1.3E-04	141	188	126
AsO2	polysome	TAA	mtLeu	2.1E-04	1.6E-04	1.6E-04	219	191	151
AsO2	polysome	TAG	mtLeu	1.3E-04	1.2E-04	1.1E-04	133	145	108
AsO2	polysome	TTT	mtLys	2.0E-04	1.8E-04	1.8E-04	213	221	173
AsO2	polysome	CAT	mtMet	6.1E-04	6.7E-04	4.7E-04	636	811	449
AsO2	polysome	GAA	mtPhe	8.6E-04	9.8E-04	6.8E-04	902	1190	650
AsO2	polysome	TGG	mtPro	3.4E-04	3.4E-04	3.8E-04	356	410	367
AsO2	polysome	GCT	mtSer	2.8E-04	2.6E-04	2.0E-04	296	314	187
AsO2	polysome	TGA	mtSer	1.1E-03	1.1E-03	9.3E-04	1175	1358	886
AsO2	polysome	TGT	mtThr	8.3E-05	1.1E-04	9.3E-05	87	130	89
AsO2	polysome	TCA	mtTrp	2.5E-04	2.6E-04	1.9E-04	258	312	182
AsO2	polysome	GTA	mtTyr	7.1E-04	6.5E-04	5.5E-04	748	787	529
AsO2	polysome	TAC	mtVal	1.8E-02	1.9E-02	1.3E-02	18806	23411	12833
AsO2	polysome	GAA	Phe	1.8E-02	1.8E-02	1.6E-02	18633	22023	15261
AsO2	polysome	AGG	Pro	2.3E-03	2.2E-03	2.2E-03	2409	2679	2071
AsO2	polysome	CGG	Pro	4.1E-03	4.3E-03	4.3E-03	4321	5232	4125
AsO2	polysome	TGG	Pro	5.4E-03	5.7E-03	5.8E-03	5643	6913	5544
AsO2	polysome	TCA	SeCe	1.5E-04	1.9E-04	1.4E-04	155	231	130
AsO2	polysome	AGA	Ser	5.5E-03	4.9E-03	5.5E-03	5785	5984	5264
AsO2	polysome	CGA	Ser	1.7E-03	1.6E-03	1.6E-03	1802	1951	1557
AsO2	polysome	GCT	Ser	2.3E-02	2.5E-02	2.2E-02	23932	29968	21201
AsO2	polysome	TGA	Ser	9.3E-03	8.5E-03	8.8E-03	9729	10307	8353
AsO2	polysome	AGT	Thr	2.1E-02	2.1E-02	2.5E-02	22001	25604	23985
AsO2	polysome	CGT	Thr	4.6E-03	4.7E-03	5.5E-03	4774	5656	5235
AsO2	polysome	TGT	Thr	3.4E-03	3.0E-03	3.2E-03	3535	3695	3014
AsO2	polysome	CCA	Trp	6.4E-03	5.8E-03	6.3E-03	6669	7028	5979
AsO2	polysome	GTA	Tyr	3.9E-02	4.3E-02	4.0E-02	40451	52423	38316
AsO2	polysome	AAC	Val	5.9E-03	5.6E-03	6.2E-03	6186	6798	5926
AsO2	polysome	CAC	Val	9.9E-03	8.8E-03	9.9E-03	10359	10711	9427
AsO2	polysome	TAC	Val	5.0E-03	4.3E-03	4.7E-03	5210	5219	4445

Table 4.S3: polysome tRNA abundance (continued)

treatment	sample	anticodon	AA	rpm_1	rpm_2	rpm_3	sum_count_1	sum_count_2	sum_count_3
control	polysome	AGC	Ala	4.9E-02	4.5E-02	3.8E-02	36108	26697	20486
control	polysome	CGC	Ala	2.2E-02	1.9E-02	1.6E-02	15980	10983	8687
control	polysome	TGC	Ala	3.2E-02	2.7E-02	2.4E-02	23556	16087	13121
control	polysome	ACG	Arg	1.8E-02	1.8E-02	1.7E-02	13114	10536	9117
control	polysome	CCG	Arg	2.3E-02	2.3E-02	2.3E-02	16751	13463	12675
control	polysome	CCT	Arg	1.0E-02	1.2E-02	1.4E-02	7455	7048	7570
control	polysome	TCG	Arg	2.2E-02	2.1E-02	2.1E-02	15982	12505	11678
control	polysome	TCT	Arg	1.7E-02	1.5E-02	1.5E-02	12704	8732	8412
control	polysome	GTT	Asn	4.1E-02	5.8E-02	4.8E-02	29890	34098	26360
control	polysome	GTC	Asp	9.9E-02	1.1E-01	1.6E-01	72960	65124	84949
control	polysome	GCA	Cys	1.4E-03	1.3E-03	1.4E-03	1028	753	790
control	polysome	CTG	Gln	1.0E-02	1.0E-02	1.1E-02	7591	6135	6056
control	polysome	TTG	Gln	2.8E-03	2.8E-03	2.6E-03	2037	1649	1394
control	polysome	CTC	Glu	6.6E-02	6.3E-02	6.5E-02	48615	37277	35217
control	polysome	TTC	Glu	1.8E-02	1.7E-02	1.8E-02	13029	9811	9998
control	polysome	CCC	Gly	1.7E-02	1.6E-02	1.4E-02	12252	9239	7504
control	polysome	GCC	Gly	4.3E-02	4.0E-02	3.3E-02	31330	23332	18100
control	polysome	TCC	Gly	2.3E-02	2.3E-02	2.4E-02	16889	13479	12909
control	polysome	GTG	His	6.1E-03	6.3E-03	5.7E-03	4518	3705	3132
control	polysome	AAT	Ile	4.5E-02	4.1E-02	3.6E-02	32753	24356	19657
control	polysome	TAT	Ile	1.6E-02	1.3E-02	1.3E-02	12064	7926	6915
control	polysome	AAG	Leu	1.2E-02	1.2E-02	1.0E-02	8658	6980	5541
control	polysome	CAA	Leu	5.9E-03	5.4E-03	4.7E-03	4311	3174	2562
control	polysome	CAG	Leu	6.2E-03	6.2E-03	5.2E-03	4546	3644	2840
control	polysome	TAA	Leu	2.7E-03	2.4E-03	2.4E-03	1970	1433	1286
control	polysome	TAG	Leu	6.3E-03	5.9E-03	5.2E-03	4642	3484	2832
control	polysome	CTT	Lys	7.7E-02	8.0E-02	8.9E-02	56895	47369	48487
control	polysome	TTT	Lys	1.8E-02	1.6E-02	1.7E-02	13242	9250	9311
control	polysome	CAT	Mete	2.4E-02	2.2E-02	1.9E-02	17770	12898	10112
control	polysome	CAT	Meti	3.0E-02	3.0E-02	2.6E-02	22061	17424	14155
control	polysome	TGC	mtAla	1.9E-04	2.1E-04	2.1E-04	139	123	116
control	polysome	TCG	mtArg	5.0E-05	4.1E-05	3.5E-05	37	24	19
control	polysome	GTT	mtAsn	3.0E-04	3.3E-04	3.8E-04	222	195	207
control	polysome	GTC	mtAsp	9.5E-06	1.5E-05	1.3E-05	7	9	7
control	polysome	GCA	mtCys	1.0E-04	1.1E-04	1.1E-04	77	65	60
control	polysome	TTG	mtGln	5.4E-04	6.3E-04	5.6E-04	396	370	306

Table 4.S3: polysome tRNA abundance (continued)

treatment	sample	anticodon	AA	rpm_1	rpm_2	rpm_3	sum_count_1	sum_count_2	sum_count_3
control	polysome	TTC	mtGlu	2.6E-03	2.4E-03	2.3E-03	1912	1428	1242
control	polysome	TCC	mtGly	3.9E-05	5.3E-05	8.6E-05	29	31	47
control	polysome	GTG	mtHis	6.7E-05	9.7E-05	1.2E-04	49	57	65
control	polysome	GAT	mtIle	2.1E-04	1.9E-04	2.2E-04	156	111	122
control	polysome	TAA	mtLeu	2.8E-04	3.2E-04	2.5E-04	205	187	138
control	polysome	TAG	mtLeu	9.1E-05	1.1E-04	1.2E-04	67	63	68
control	polysome	TTT	mtLys	7.2E-05	1.0E-04	1.2E-04	53	59	67
control	polysome	CAT	mtMet	4.1E-04	4.5E-04	9.5E-04	305	263	517
control	polysome	GAA	mtPhe	7.0E-04	6.4E-04	6.8E-04	514	375	372
control	polysome	TGG	mtPro	1.9E-04	1.7E-04	2.6E-04	141	102	141
control	polysome	GCT	mtSer	2.2E-04	1.3E-04	1.8E-04	163	75	98
control	polysome	TGA	mtSer	7.5E-04	7.0E-04	5.8E-04	554	412	319
control	polysome	TGT	mtThr	3.9E-05	5.9E-05	4.6E-05	29	35	25
control	polysome	TCA	mtTrp	2.1E-04	2.4E-04	3.3E-04	157	139	178
control	polysome	GTA	mtTyr	4.3E-04	2.7E-04	4.0E-04	316	157	220
control	polysome	TAC	mtVal	1.5E-02	2.2E-02	1.5E-02	11126	13041	8257
control	polysome	GAA	Phe	3.2E-02	2.8E-02	2.8E-02	23298	16440	15375
control	polysome	AGG	Pro	3.4E-03	3.6E-03	3.5E-03	2465	2134	1915
control	polysome	CGG	Pro	6.5E-03	6.5E-03	6.6E-03	4801	3857	3604
control	polysome	TGG	Pro	8.7E-03	8.3E-03	8.8E-03	6382	4870	4778
control	polysome	TCA	SeCe	1.3E-04	1.1E-04	1.3E-04	96	65	72
control	polysome	AGA	Ser	5.0E-03	4.3E-03	4.1E-03	3688	2563	2263
control	polysome	CGA	Ser	1.7E-03	1.6E-03	1.7E-03	1275	934	935
control	polysome	GCT	Ser	2.6E-02	2.6E-02	2.8E-02	18795	15245	15025
control	polysome	TGA	Ser	7.9E-03	7.1E-03	6.8E-03	5839	4188	3682
control	polysome	AGT	Thr	2.3E-02	2.8E-02	2.5E-02	16643	16582	13498
control	polysome	CGT	Thr	5.4E-03	6.3E-03	5.8E-03	3957	3702	3166
control	polysome	TGT	Thr	3.8E-03	3.8E-03	3.9E-03	2811	2266	2112
control	polysome	CCA	Trp	7.3E-03	6.1E-03	5.7E-03	5386	3594	3113
control	polysome	GTA	Tyr	5.9E-02	5.4E-02	5.3E-02	43361	31594	29134
control	polysome	AAC	Val	7.1E-03	7.3E-03	6.2E-03	5241	4315	3369
control	polysome	CAC	Val	1.4E-02	1.3E-02	1.1E-02	10064	7745	6142
control	polysome	TAC	Val	5.8E-03	5.8E-03	5.0E-03	4295	3391	2722
H2O2	polysome	AGC	Ala	4.0E-02	4.2E-02	4.0E-02	43239	28672	24900
H2O2	polysome	CGC	Ala	1.5E-02	1.6E-02	1.7E-02	16095	10995	10341
H2O2	polysome	TGC	Ala	2.5E-02	2.8E-02	2.8E-02	27488	19104	17268

Table 4.S3: polysome tRNA abundance (continued)

treatment	sample	anticodon	AA	rpm_1	rpm_2	rpm_3	sum_count_1	sum_count_2	sum_count_3
H2O2	polysome	ACG	Arg	1.4E-02	1.6E-02	1.5E-02	15254	10720	9396
H2O2	polysome	CCG	Arg	2.0E-02	2.1E-02	2.1E-02	21183	14553	13265
H2O2	polysome	CCT	Arg	1.3E-02	1.3E-02	1.3E-02	13575	8651	7922
H2O2	polysome	TCG	Arg	2.0E-02	2.1E-02	2.0E-02	21760	14369	12492
H2O2	polysome	TCT	Arg	1.6E-02	1.5E-02	1.6E-02	17603	10608	9865
H2O2	polysome	GTT	Asn	5.3E-02	6.2E-02	5.1E-02	57518	42584	31263
H2O2	polysome	GTC	Asp	1.3E-01	1.4E-01	1.3E-01	136237	96647	81551
H2O2	polysome	GCA	Cys	1.1E-03	1.0E-03	1.4E-03	1167	711	856
H2O2	polysome	CTG	Gln	8.3E-03	8.9E-03	9.4E-03	8917	6120	5806
H2O2	polysome	TTG	Gln	2.6E-03	2.5E-03	2.7E-03	2805	1730	1644
H2O2	polysome	CTC	Glu	6.6E-02	6.1E-02	6.8E-02	70868	41839	41898
H2O2	polysome	TTC	Glu	2.0E-02	1.5E-02	1.8E-02	21416	10655	10966
H2O2	polysome	CCC	Gly	1.4E-02	1.3E-02	1.5E-02	15105	9034	9040
H2O2	polysome	GCC	Gly	2.8E-02	2.9E-02	3.1E-02	29757	20118	19453
H2O2	polysome	TCC	Gly	2.0E-02	2.2E-02	2.2E-02	21632	15322	13556
H2O2	polysome	GTG	His	5.8E-03	6.1E-03	5.7E-03	6232	4234	3516
H2O2	polysome	AAT	Ile	6.7E-02	5.8E-02	5.6E-02	72092	39821	34461
H2O2	polysome	TAT	Ile	2.5E-02	2.1E-02	2.2E-02	27486	14409	13411
H2O2	polysome	AAG	Leu	1.1E-02	9.8E-03	9.3E-03	11521	6765	5772
H2O2	polysome	CAA	Leu	4.6E-03	4.4E-03	4.9E-03	4938	3004	2997
H2O2	polysome	CAG	Leu	4.7E-03	4.9E-03	5.2E-03	5110	3356	3241
H2O2	polysome	TAA	Leu	2.5E-03	2.2E-03	2.5E-03	2735	1504	1564
H2O2	polysome	TAG	Leu	5.0E-03	4.9E-03	4.7E-03	5405	3378	2908
H2O2	polysome	CTT	Lys	7.7E-02	8.5E-02	8.3E-02	82774	58682	51186
H2O2	polysome	TTT	Lys	2.0E-02	1.7E-02	1.8E-02	21199	11399	10877
H2O2	polysome	CAT	Mete	2.0E-02	1.8E-02	1.9E-02	21842	12640	11668
H2O2	polysome	CAT	Meti	2.1E-02	2.2E-02	2.3E-02	22612	15404	14229
H2O2	polysome	TGC	mtAla	1.5E-04	1.6E-04	1.9E-04	167	109	117
H2O2	polysome	TCG	mtArg	4.1E-05	5.1E-05	4.1E-05	44	35	25
H2O2	polysome	GTT	mtAsn	5.2E-04	4.5E-04	4.4E-04	562	313	271
H2O2	polysome	GTC	mtAsp	1.3E-05	1.3E-05	6.5E-06	14	9	4
H2O2	polysome	GCA	mtCys	8.5E-05	8.0E-05	1.1E-04	92	55	67
H2O2	polysome	TTG	mtGln	5.2E-04	4.7E-04	4.9E-04	557	324	302
H2O2	polysome	TTC	mtGlu	1.5E-03	1.6E-03	1.6E-03	1641	1116	993
H2O2	polysome	TCC	mtGly	3.7E-05	2.3E-05	2.3E-05	40	16	14
H2O2	polysome	GTG	mtHis	5.6E-05	9.1E-05	5.0E-05	60	63	31

Table 4.S3: polysome tRNA abundance (continued)

treatment	sample	anticodon	AA	rpm_1	rpm_2	rpm_3	sum_count_1	sum_count_2	sum_count_3
H2O2	polysome	GAT	mtIle	2.9E-04	2.0E-04	2.2E-04	311	139	136
H2O2	polysome	TAA	mtLeu	3.1E-04	2.2E-04	2.8E-04	330	149	173
H2O2	polysome	TAG	mtLeu	8.2E-05	7.6E-05	7.8E-05	88	52	48
H2O2	polysome	TTT	mtLys	1.0E-04	7.4E-05	9.1E-05	111	51	56
H2O2	polysome	CAT	mtMet	4.9E-04	5.4E-04	5.0E-04	528	375	311
H2O2	polysome	GAA	mtPhe	6.0E-04	5.8E-04	5.9E-04	650	399	367
H2O2	polysome	TGG	mtPro	2.0E-04	1.7E-04	1.8E-04	216	120	113
H2O2	polysome	GCT	mtSer	2.3E-04	1.3E-04	1.8E-04	251	92	110
H2O2	polysome	TGA	mtSer	1.1E-03	1.2E-03	1.3E-03	1196	854	828
H2O2	polysome	TGT	mtThr	4.8E-05	3.6E-05	4.7E-05	52	25	29
H2O2	polysome	TCA	mtTrp	9.6E-05	9.1E-05	9.6E-05	104	63	59
H2O2	polysome	GTA	mtTyr	3.0E-04	2.7E-04	2.8E-04	327	189	172
H2O2	polysome	TAC	mtVal	1.4E-02	1.4E-02	1.4E-02	15310	9391	8521
H2O2	polysome	GAA	Phe	3.3E-02	2.8E-02	3.1E-02	35804	19274	18941
H2O2	polysome	AGG	Pro	2.9E-03	3.1E-03	3.0E-03	3166	2108	1866
H2O2	polysome	CGG	Pro	5.2E-03	5.8E-03	5.7E-03	5644	3996	3501
H2O2	polysome	TGG	Pro	7.2E-03	7.5E-03	7.3E-03	7728	5173	4499
H2O2	polysome	TCA	SeCe	1.5E-04	1.4E-04	3.9E-04	166	96	240
H2O2	polysome	AGA	Ser	3.9E-03	4.1E-03	3.9E-03	4199	2850	2433
H2O2	polysome	CGA	Ser	1.4E-03	1.4E-03	1.6E-03	1483	958	966
H2O2	polysome	GCT	Ser	2.7E-02	2.9E-02	2.8E-02	29569	19847	17483
H2O2	polysome	TGA	Ser	6.4E-03	6.7E-03	6.8E-03	6889	4649	4229
H2O2	polysome	AGT	Thr	2.8E-02	2.4E-02	2.2E-02	30515	16584	13682
H2O2	polysome	CGT	Thr	6.1E-03	6.0E-03	5.2E-03	6603	4145	3208
H2O2	polysome	TGT	Thr	3.7E-03	3.9E-03	3.7E-03	4018	2685	2259
H2O2	polysome	CCA	Trp	5.5E-03	5.5E-03	5.9E-03	5915	3823	3653
H2O2	polysome	GTA	Tyr	6.2E-02	5.4E-02	6.1E-02	67246	37365	37661
H2O2	polysome	AAC	Val	5.5E-03	5.6E-03	5.7E-03	5886	3879	3537
H2O2	polysome	CAC	Val	1.1E-02	1.1E-02	1.0E-02	12069	7494	6483
H2O2	polysome	TAC	Val	4.5E-03	4.6E-03	4.9E-03	4845	3153	3055
heat	polysome	AGC	Ala	4.8E-02	4.4E-02	4.8E-02	32649	24880	26828
heat	polysome	CGC	Ala	2.1E-02	1.7E-02	1.9E-02	14364	9412	10528
heat	polysome	TGC	Ala	3.1E-02	2.6E-02	3.2E-02	21371	14878	17809
heat	polysome	ACG	Arg	1.8E-02	1.6E-02	1.9E-02	12132	9123	10646
heat	polysome	CCG	Arg	2.3E-02	2.0E-02	2.4E-02	15479	11489	13578
heat	polysome	CCT	Arg	1.1E-02	1.2E-02	1.0E-02	7805	6856	5797

Table 4.S3: polysome tRNA abundance (continued)

treatment	sample	anticodon	AA	rpm_1	rpm_2	rpm_3	sum_count_1	sum_count_2	sum_count_3
heat	polysome	TCG	Arg	2.3E-02	1.9E-02	2.1E-02	15471	11083	11796
heat	polysome	TCT	Arg	1.7E-02	1.5E-02	2.2E-02	11532	8553	12307
heat	polysome	GTT	Asn	4.0E-02	6.1E-02	6.4E-02	27416	34430	35415
heat	polysome	GTC	Asp	9.2E-02	1.2E-01	1.2E-01	62407	70403	64493
heat	polysome	GCA	Cys	1.7E-03	1.5E-03	8.2E-04	1132	829	457
heat	polysome	CTG	Gln	1.0E-02	9.9E-03	8.0E-03	7074	5654	4470
heat	polysome	TTG	Gln	3.0E-03	2.6E-03	1.9E-03	2075	1489	1068
heat	polysome	CTC	Glu	6.8E-02	6.2E-02	5.5E-02	46320	35439	30805
heat	polysome	TTC	Glu	1.8E-02	1.7E-02	1.5E-02	11993	9540	8165
heat	polysome	CCC	Gly	1.6E-02	1.4E-02	1.2E-02	11239	8214	6768
heat	polysome	GCC	Gly	4.0E-02	3.5E-02	2.6E-02	27267	20160	14309
heat	polysome	TCC	Gly	2.2E-02	2.0E-02	2.2E-02	14905	11606	12035
heat	polysome	GTG	His	5.9E-03	6.2E-03	4.6E-03	3992	3499	2570
heat	polysome	AAT	Ile	5.4E-02	4.3E-02	5.6E-02	37069	24411	31013
heat	polysome	TAT	Ile	1.9E-02	1.5E-02	1.8E-02	12665	8763	10250
heat	polysome	AAG	Leu	1.2E-02	1.0E-02	1.0E-02	7870	5734	5808
heat	polysome	CAA	Leu	5.6E-03	4.6E-03	4.6E-03	3807	2628	2564
heat	polysome	CAG	Leu	5.2E-03	5.3E-03	5.7E-03	3529	2990	3174
heat	polysome	TAA	Leu	2.8E-03	2.6E-03	2.2E-03	1900	1496	1201
heat	polysome	TAG	Leu	6.0E-03	5.4E-03	5.5E-03	4114	3047	3057
heat	polysome	CTT	Lys	7.8E-02	7.3E-02	8.1E-02	52883	41294	45135
heat	polysome	TTT	Lys	1.9E-02	2.0E-02	1.8E-02	12975	11132	10090
heat	polysome	CAT	Mete	2.6E-02	2.1E-02	2.4E-02	17510	11876	13314
heat	polysome	CAT	Meti	2.4E-02	2.4E-02	1.5E-02	16481	13407	8428
heat	polysome	TGC	mtAla	1.8E-04	2.5E-04	1.9E-04	126	141	106
heat	polysome	TCG	mtArg	5.6E-05	3.7E-05	2.2E-05	38	21	12
heat	polysome	GTT	mtAsn	3.5E-04	3.2E-04	3.3E-04	237	181	182
heat	polysome	GTC	mtAsp	1.9E-05	1.9E-05	2.0E-05	13	11	11
heat	polysome	GCA	mtCys	1.3E-04	8.1E-05	4.5E-05	86	46	25
heat	polysome	TTG	mtGln	6.3E-04	6.2E-04	4.7E-04	427	350	263
heat	polysome	TTC	mtGlu	2.9E-03	2.5E-03	2.0E-03	1959	1437	1100
heat	polysome	TCC	mtGly	7.6E-05	3.9E-05	6.3E-05	52	22	35
heat	polysome	GTG	mtHis	8.5E-05	7.2E-05	7.9E-05	58	41	44
heat	polysome	GAT	mtIle	3.1E-04	2.5E-04	2.0E-04	211	142	109
heat	polysome	TAA	mtLeu	3.1E-04	2.7E-04	2.3E-04	210	155	128
heat	polysome	TAG	mtLeu	1.5E-04	1.2E-04	7.0E-05	99	69	39

Table 4.S3: polysome tRNA abundance (continued)

treatment	sample	anticodon	AA	rpm_1	rpm_2	rpm_3	sum_count_1	sum_count_2	sum_count_3
heat	polysome	TTT	mtLys	9.4E-05	1.0E-04	1.0E-04	64	58	58
heat	polysome	CAT	mtMet	5.4E-04	4.9E-04	2.8E-04	365	281	158
heat	polysome	GAA	mtPhe	6.9E-04	6.6E-04	6.0E-04	473	376	335
heat	polysome	TGG	mtPro	3.0E-04	1.9E-04	1.9E-04	207	108	107
heat	polysome	GCT	mtSer	2.3E-04	2.0E-04	1.5E-04	159	114	86
heat	polysome	TGA	mtSer	9.3E-04	7.7E-04	8.4E-04	637	440	466
heat	polysome	TGT	mtThr	4.0E-05	8.1E-05	4.7E-05	27	46	26
heat	polysome	TCA	mtTrp	2.2E-04	1.8E-04	1.4E-04	151	100	78
heat	polysome	GTA	mtTyr	4.2E-04	3.3E-04	2.8E-04	288	188	157
heat	polysome	TAC	mtVal	2.1E-02	2.5E-02	1.5E-02	14044	14023	8237
heat	polysome	GAA	Phe	3.2E-02	3.4E-02	3.3E-02	21646	19414	18329
heat	polysome	AGG	Pro	3.2E-03	3.0E-03	2.4E-03	2186	1730	1323
heat	polysome	CGG	Pro	5.7E-03	5.6E-03	4.5E-03	3911	3173	2500
heat	polysome	TGG	Pro	7.8E-03	7.6E-03	5.7E-03	5339	4306	3163
heat	polysome	TCA	SeCe	1.4E-04	1.5E-04	8.5E-05	95	88	47
heat	polysome	AGA	Ser	4.7E-03	4.1E-03	4.9E-03	3188	2348	2701
heat	polysome	CGA	Ser	1.5E-03	1.2E-03	1.2E-03	1013	673	670
heat	polysome	GCT	Ser	2.4E-02	3.1E-02	3.1E-02	16621	17501	17486
heat	polysome	TGA	Ser	7.5E-03	6.7E-03	7.9E-03	5091	3825	4414
heat	polysome	AGT	Thr	2.4E-02	2.6E-02	2.4E-02	16259	14521	13496
heat	polysome	CGT	Thr	5.9E-03	6.0E-03	5.9E-03	4048	3398	3269
heat	polysome	TGT	Thr	4.4E-03	3.7E-03	2.8E-03	2976	2083	1532
heat	polysome	CCA	Trp	7.3E-03	5.7E-03	5.2E-03	4958	3231	2897
heat	polysome	GTA	Tyr	5.5E-02	6.3E-02	6.7E-02	37566	35942	36971
heat	polysome	AAC	Val	7.8E-03	6.5E-03	5.2E-03	5297	3712	2894
heat	polysome	CAC	Val	1.5E-02	1.3E-02	9.6E-03	10048	7153	5319
heat	polysome	TAC	Val	6.1E-03	5.3E-03	5.2E-03	4165	3012	2867

Table 4.S4: polysome tRNA charging

sample	source	treatment	AA	anticodon	rep_1_charging	rep_2_charging	rep_3_charging
polysome	cytosolic	AsO2	Ala	AGC	0.416701	0.34369	0.388141
polysome	cytosolic	AsO2	Ala	CGC	0.432639	0.384585	0.440421
polysome	cytosolic	AsO2	Ala	TGC	0.429299	0.37447	0.430493
polysome	cytosolic	AsO2	Arg	ACG	0.60924	0.557096	0.596006
polysome	cytosolic	AsO2	Arg	CCG	0.701953	0.717444	0.717408
polysome	cytosolic	AsO2	Arg	CCT	0.727666	0.709429	0.779586
polysome	cytosolic	AsO2	Arg	TCG	0.678426	0.669537	0.670005
polysome	cytosolic	AsO2	Arg	TCT	0.605072	0.559633	0.618932
polysome	cytosolic	AsO2	Asn	GTT	0.603992	0.525824	0.556005
polysome	cytosolic	AsO2	Asp	GTC	0.687826	0.652516	0.69641
polysome	cytosolic	AsO2	Cys	GCA	0.752809	0.676259	0.747967
polysome	cytosolic	AsO2	Gln	CTG	0.590791	0.588819	0.629053
polysome	cytosolic	AsO2	Gln	TTG	0.585848	0.531599	0.538259
polysome	cytosolic	AsO2	Glu	CTC	0.696532	0.679738	0.695383
polysome	cytosolic	AsO2	Glu	TTC	0.662405	0.578778	0.592203
polysome	cytosolic	AsO2	Gly	CCC	0.55443	0.526758	0.540032
polysome	cytosolic	AsO2	Gly	GCC	0.53907	0.547595	0.548133
polysome	cytosolic	AsO2	Gly	TCC	0.571127	0.550313	0.581465
polysome	cytosolic	AsO2	His	GTG	0.728191	0.705676	0.724302
polysome	cytosolic	AsO2	Ile	AAT	0.38928	0.300908	0.375587
polysome	cytosolic	AsO2	Ile	TAT	0.600579	0.548088	0.616676
polysome	cytosolic	AsO2	Leu	AAG	0.648389	0.621561	0.614424
polysome	cytosolic	AsO2	Leu	CAA	0.669421	0.626122	0.606705
polysome	cytosolic	AsO2	Leu	CAG	0.537234	0.551829	0.576427
polysome	cytosolic	AsO2	Leu	TAA	0.535238	0.530562	0.548463
polysome	cytosolic	AsO2	Leu	TAG	0.611111	0.575847	0.551786
polysome	cytosolic	AsO2	Lys	CTT	0.687247	0.710664	0.693794
polysome	cytosolic	AsO2	Lys	TTT	0.699882	0.712347	0.708906
polysome	cytosolic	AsO2	Mete	CAT	0.687702	0.67663	0.689283
polysome	cytosolic	AsO2	Meti	CAT	0.423983	0.404899	0.405726
polysome	mitochondrial	AsO2	mtAla	TGC	0.486842	0.390805	0.466667
polysome	mitochondrial	AsO2	mtArg	TCG	0.375	0.454545	0.166667
polysome	mitochondrial	AsO2	mtAsn	GTT	0.562044	0.539063	0.618421
polysome	mitochondrial	AsO2	mtAsp	GTC	0.368421	0.352941	0.470588

Table 4.S4: polysome tRNA charging (continued)

sample	source	treatment	AA	anticodon	rep_1_charging	rep_2_charging	rep_3_charging
polysome	mitochondrial	AsO2	mtCys	GCA	0.648649	0.510638	0.666667
polysome	mitochondrial	AsO2	mtGln	TTG	0.708738	0.616162	0.680851
polysome	mitochondrial	AsO2	mtGlu	TTC	0.628107	0.636364	0.645115
polysome	mitochondrial	AsO2	mtGly	TCC	0.636364	0.384615	0.785714
polysome	mitochondrial	AsO2	mtHis	GTG	0.776316	0.684211	0.722222
polysome	mitochondrial	AsO2	mtIle	GAT	0.753425	0.727273	0.811594
polysome	mitochondrial	AsO2	mtLeu	TAA	0.666667	0.685185	0.68
polysome	mitochondrial	AsO2	mtLeu	TAG	0.545455	0.529412	0.588235
polysome	mitochondrial	AsO2	mtLys	TTT	0.675676	0.621212	0.73913
polysome	mitochondrial	AsO2	mtMet	CAT	0.663717	0.621622	0.612403
polysome	mitochondrial	AsO2	mtPhe	GAA	0.554795	0.537954	0.549738
polysome	mitochondrial	AsO2	mtPro	TGG	0.655172	0.622642	0.666667
polysome	mitochondrial	AsO2	mtSer	GCT	0.444444	0.346154	0.8
polysome	mitochondrial	AsO2	mtSer	TGA	0.533088	0.457995	0.533865
polysome	mitochondrial	AsO2	mtThr	TGT	0.764706	0.657895	0.56
polysome	mitochondrial	AsO2	mtTrp	TCA	0.817073	0.835052	0.881818
polysome	mitochondrial	AsO2	mtTyr	GTA	0.527778	0.496815	0.567797
polysome	mitochondrial	AsO2	mtVal	TAC	0.722786	0.705484	0.702624
polysome	cytosolic	AsO2	Phe	GAA	0.610442	0.540016	0.608285
polysome	cytosolic	AsO2	Pro	AGG	0.577154	0.571154	0.548583
polysome	cytosolic	AsO2	Pro	CGG	0.538986	0.564674	0.558304
polysome	cytosolic	AsO2	Pro	TGG	0.553527	0.542906	0.526582
polysome	cytosolic	AsO2	SeCe	TCA	1	0	1
polysome	cytosolic	AsO2	Ser	AGA	0.535211	0.49863	0.539906
polysome	cytosolic	AsO2	Ser	CGA	0.588745	0.601399	0.586667
polysome	cytosolic	AsO2	Ser	GCT	0.686755	0.697124	0.686293
polysome	cytosolic	AsO2	Ser	TGA	0.547475	0.543468	0.531926
polysome	cytosolic	AsO2	Thr	AGT	0.649087	0.575427	0.628614
polysome	cytosolic	AsO2	Thr	CGT	0.669251	0.59284	0.610058
polysome	cytosolic	AsO2	Thr	TGT	0.750478	0.690501	0.679745
polysome	cytosolic	AsO2	Trp	CCA	0.725402	0.691111	0.7315
polysome	cytosolic	AsO2	Tyr	GTA	0.623181	0.564275	0.611669
polysome	cytosolic	AsO2	Val	AAC	0.472614	0.469187	0.467697
polysome	cytosolic	AsO2	Val	CAC	0.496974	0.437606	0.467076
polysome	cytosolic	AsO2	Val	TAC	0.589806	0.570871	0.625296

Table 4.S4: polysome tRNA charging (continued)

sample	source	treatment	AA	anticodon	rep_1_charging	rep_2_charging	rep_3_charging
polysome	cytosolic	control	Ala	AGC	0.312539	0.35537	0.392879
polysome	cytosolic	control	Ala	CGC	0.356614	0.408066	0.45479
polysome	cytosolic	control	Ala	TGC	0.333536	0.411834	0.400345
polysome	cytosolic	control	Arg	ACG	0.550245	0.657574	0.61854
polysome	cytosolic	control	Arg	CCG	0.621486	0.709521	0.699115
polysome	cytosolic	control	Arg	CCT	0.591367	0.660027	0.628959
polysome	cytosolic	control	Arg	TCG	0.590549	0.70962	0.664375
polysome	cytosolic	control	Arg	TCT	0.436865	0.584559	0.578125
polysome	cytosolic	control	Asn	GTT	0.490342	0.492533	0.505487
polysome	cytosolic	control	Asp	GTC	0.526577	0.600045	0.562807
polysome	cytosolic	control	Cys	GCA	0.575419	0.804688	0.650307
polysome	cytosolic	control	Gln	CTG	0.473361	0.552736	0.509009
polysome	cytosolic	control	Gln	TTG	0.458256	0.519824	0.419355
polysome	cytosolic	control	Glu	CTC	0.611939	0.685526	0.646439
polysome	cytosolic	control	Glu	TTC	0.530869	0.617949	0.583808
polysome	cytosolic	control	Gly	CCC	0.443127	0.505005	0.522887
polysome	cytosolic	control	Gly	GCC	0.481802	0.544226	0.565902
polysome	cytosolic	control	Gly	TCC	0.480684	0.541786	0.562905
polysome	cytosolic	control	His	GTG	0.59207	0.629176	0.627005
polysome	cytosolic	control	Ile	AAT	0.258741	0.307968	0.291629
polysome	cytosolic	control	Ile	TAT	0.437434	0.51087	0.458647
polysome	cytosolic	control	Leu	AAG	0.551935	0.58483	0.617128
polysome	cytosolic	control	Leu	CAA	0.561424	0.587863	0.620939
polysome	cytosolic	control	Leu	CAG	0.494505	0.528525	0.595712
polysome	cytosolic	control	Leu	TAA	0.431235	0.496	0.523973
polysome	cytosolic	control	Leu	TAG	0.468869	0.52496	0.55
polysome	cytosolic	control	Lys	CTT	0.563727	0.681122	0.651159
polysome	cytosolic	control	Lys	TTT	0.503218	0.575269	0.586912
polysome	cytosolic	control	Mete	CAT	0.536717	0.629963	0.582781
polysome	cytosolic	control	Meti	CAT	0.496324	0.528852	0.661504
polysome	mitochondrial	control	mtAla	TGC	0.592593	0.666667	0.756098
polysome	mitochondrial	control	mtArg	TCG	0.714286	0.75	0.75
polysome	mitochondrial	control	mtAsn	GTT	0.478723	0.674419	0.666667
polysome	mitochondrial	control	mtAsp	GTC	0.666667	0.75	1
polysome	mitochondrial	control	mtCys	GCA	0.62069	0.590909	0.923077
polysome	mitochondrial	control	mtGln	TTG	0.644628	0.738318	0.709302

Table 4.S4: polysome tRNA charging (continued)

sample	source	treatment	AA	anticodon	rep_1_charging	rep_2_charging	rep_3_charging
polysome	mitochondrial	control	mtGlu	TTC	0.716783	0.757716	0.803571
polysome	mitochondrial	control	mtGly	TCC	0.8	0.333333	0.785714
polysome	mitochondrial	control	mtHis	GTG	0.789474	1	0.684211
polysome	mitochondrial	control	mtIle	GAT	0.728571	0.745763	0.901408
polysome	mitochondrial	control	mtLeu	TAA	0.511111	0.511628	0.518519
polysome	mitochondrial	control	mtLeu	TAG	0.785714	0.823529	1
polysome	mitochondrial	control	mtLys	TTT	0.7	0.851852	0.909091
polysome	mitochondrial	control	mtMet	CAT	0.672897	0.590361	0.961877
polysome	mitochondrial	control	mtPhe	GAA	0.570175	0.618705	0.627273
polysome	mitochondrial	control	mtPro	TGG	0.5	0.8	0.678571
polysome	mitochondrial	control	mtSer	GCT	0.714286	0.25	0.5
polysome	mitochondrial	control	mtSer	TGA	0.483871	0.59542	0.433735
polysome	mitochondrial	control	mtThr	TGT	0.785714	0.727273	0.583333
polysome	mitochondrial	control	mtTrp	TCA	0.851064	0.813953	0.879121
polysome	mitochondrial	control	mtTyr	GTA	0.595238	0.767442	0.740741
polysome	mitochondrial	control	mtVal	TAC	0.664168	0.73436	0.737582
polysome	cytosolic	control	Phe	GAA	0.436433	0.470939	0.48416
polysome	cytosolic	control	Pro	AGG	0.507143	0.591518	0.582192
polysome	cytosolic	control	Pro	CGG	0.545082	0.610209	0.600567
polysome	cytosolic	control	Pro	TGG	0.486023	0.583062	0.611276
polysome	cytosolic	control	SeCe	TCA	NA	1	NA
polysome	cytosolic	control	Ser	AGA	0.504305	0.520635	0.542117
polysome	cytosolic	control	Ser	CGA	0.504202	0.552511	0.584158
polysome	cytosolic	control	Ser	GCT	0.646854	0.702312	0.683942
polysome	cytosolic	control	Ser	TGA	0.498134	0.551412	0.558502
polysome	cytosolic	control	Thr	AGT	0.521488	0.652186	0.523216
polysome	cytosolic	control	Thr	CGT	0.582951	0.635009	0.602244
polysome	cytosolic	control	Thr	TGT	0.559043	0.737132	0.59867
polysome	cytosolic	control	Trp	CCA	0.589103	0.721925	0.674377
polysome	cytosolic	control	Tyr	GTA	0.475698	0.568946	0.519687
polysome	cytosolic	control	Val	AAC	0.396921	0.45702	0.49604
polysome	cytosolic	control	Val	CAC	0.385732	0.439747	0.435657
polysome	cytosolic	control	Val	TAC	0.458199	0.56338	0.565012
polysome	cytosolic	H2O2	Ala	AGC	0.395581	0.340091	0.432339
polysome	cytosolic	H2O2	Ala	CGC	0.457376	0.440957	0.456998
polysome	cytosolic	H2O2	Ala	TGC	0.427859	0.362346	0.444391

Table 4.S4: polysome tRNA charging (continued)

sample	source	treatment	AA	anticodon	rep_1_charging	rep_2_charging	rep_3_charging
polysome	cytosolic	H2O2	Arg	ACG	0.615653	0.563582	0.645311
polysome	cytosolic	H2O2	Arg	CCG	0.683846	0.659711	0.708021
polysome	cytosolic	H2O2	Arg	CCT	0.688808	0.697329	0.671275
polysome	cytosolic	H2O2	Arg	TCG	0.670096	0.624685	0.683138
polysome	cytosolic	H2O2	Arg	TCT	0.573118	0.49501	0.548323
polysome	cytosolic	H2O2	Asn	GTT	0.518771	0.464416	0.565764
polysome	cytosolic	H2O2	Asp	GTC	0.557047	0.534079	0.58226
polysome	cytosolic	H2O2	Cys	GCA	0.630332	0.647727	0.620482
polysome	cytosolic	H2O2	Gln	CTG	0.573446	0.504112	0.529858
polysome	cytosolic	H2O2	Gln	TTG	0.507565	0.481982	0.492347
polysome	cytosolic	H2O2	Glu	CTC	0.636407	0.646027	0.701771
polysome	cytosolic	H2O2	Glu	TTC	0.559406	0.510411	0.626486
polysome	cytosolic	H2O2	Gly	CCC	0.525037	0.477143	0.539332
polysome	cytosolic	H2O2	Gly	GCC	0.564135	0.53881	0.611901
polysome	cytosolic	H2O2	Gly	TCC	0.549893	0.516896	0.562432
polysome	cytosolic	H2O2	His	GTG	0.647235	0.615464	0.669689
polysome	cytosolic	H2O2	Ile	AAT	0.305455	0.282815	0.346188
polysome	cytosolic	H2O2	Ile	TAT	0.552632	0.499461	0.452962
polysome	cytosolic	H2O2	Leu	AAG	0.574597	0.579288	0.647247
polysome	cytosolic	H2O2	Leu	CAA	0.596211	0.578295	0.669034
polysome	cytosolic	H2O2	Leu	CAG	0.534211	0.537167	0.573006
polysome	cytosolic	H2O2	Leu	TAA	0.456808	0.50165	0.52861
polysome	cytosolic	H2O2	Leu	TAG	0.568944	0.505308	0.610442
polysome	cytosolic	H2O2	Lys	CTT	0.650564	0.624711	0.673441
polysome	cytosolic	H2O2	Lys	TTT	0.530043	0.581986	0.646817
polysome	cytosolic	H2O2	Mete	CAT	0.623718	0.563354	0.617151
polysome	cytosolic	H2O2	Meti	CAT	0.582161	0.500759	0.536973
polysome	mitochondrial	H2O2	mtAla	TGC	0.5	0.447368	0.710526
polysome	mitochondrial	H2O2	mtArg	TCG	0.444444	0.75	0.75
polysome	mitochondrial	H2O2	mtAsn	GTT	0.563452	0.646552	0.631579
polysome	mitochondrial	H2O2	mtAsp	GTC	0.75	1	NA
polysome	mitochondrial	H2O2	mtCys	GCA	0.702703	0.636364	0.684211
polysome	mitochondrial	H2O2	mtGln	TTG	0.602941	0.742424	0.663265
polysome	mitochondrial	H2O2	mtGlu	TTC	0.672101	0.649171	0.671378
polysome	mitochondrial	H2O2	mtGly	TCC	0.6875	0.666667	0.75
polysome	mitochondrial	H2O2	mtHis	GTG	0.884615	0.333333	0.857143

Table 4.S4: polysome tRNA charging (continued)

sample	source	treatment	AA	anticodon	rep_1_charging	rep_2_charging	rep_3_charging
polysome	mitochondrial	H2O2	mtIle	GAT	0.805085	0.740741	0.632653
polysome	mitochondrial	H2O2	mtLeu	TAA	0.552632	0.435897	0.666667
polysome	mitochondrial	H2O2	mtLeu	TAG	0.576923	0.888889	0.933333
polysome	mitochondrial	H2O2	mtLys	TTT	0.8	0.5	0.818182
polysome	mitochondrial	H2O2	mtMet	CAT	0.736364	0.72	0.74359
polysome	mitochondrial	H2O2	mtPhe	GAA	0.52093	0.541667	0.519685
polysome	mitochondrial	H2O2	mtPro	TGG	0.666667	0.421053	0.571429
polysome	mitochondrial	H2O2	mtSer	GCT	0.653846	0.857143	0.625
polysome	mitochondrial	H2O2	mtSer	TGA	0.577061	0.517766	0.576419
polysome	mitochondrial	H2O2	mtThr	TGT	0.461538	0.533333	0.5
polysome	mitochondrial	H2O2	mtTrp	TCA	0.672727	0.846154	0.851852
polysome	mitochondrial	H2O2	mtTyr	GTA	0.666667	0.675	0.686275
polysome	mitochondrial	H2O2	mtVal	TAC	0.714212	0.660232	0.692364
polysome	cytosolic	H2O2	Phe	GAA	0.496937	0.476471	0.534038
polysome	cytosolic	H2O2	Pro	AGG	0.571429	0.525526	0.60443
polysome	cytosolic	H2O2	Pro	CGG	0.575465	0.525403	0.627728
polysome	cytosolic	H2O2	Pro	TGG	0.52033	0.505747	0.579156
polysome	cytosolic	H2O2	SeCe	TCA	1	NA	0.4
polysome	cytosolic	H2O2	Ser	AGA	0.536996	0.493311	0.493384
polysome	cytosolic	H2O2	Ser	CGA	0.513889	0.567073	0.591623
polysome	cytosolic	H2O2	Ser	GCT	0.663351	0.642929	0.685745
polysome	cytosolic	H2O2	Ser	TGA	0.52314	0.486989	0.580263
polysome	cytosolic	H2O2	Thr	AGT	0.641603	0.539908	0.597592
polysome	cytosolic	H2O2	Thr	CGT	0.645258	0.57641	0.62202
polysome	cytosolic	H2O2	Thr	TGT	0.706228	0.637295	0.655629
polysome	cytosolic	H2O2	Trp	CCA	0.717449	0.641509	0.674138
polysome	cytosolic	H2O2	Tyr	GTA	0.545174	0.491247	0.514366
polysome	cytosolic	H2O2	Val	AAC	0.451883	0.423745	0.472138
polysome	cytosolic	H2O2	Val	CAC	0.460587	0.431716	0.435765
polysome	cytosolic	H2O2	Val	TAC	0.566122	0.497642	0.543478
polysome	cytosolic	heat	Ala	AGC	0.372414	0.357462	0.263158
polysome	cytosolic	heat	Ala	CGC	0.381242	0.381569	0.278226
polysome	cytosolic	heat	Ala	TGC	0.400941	0.344444	0.26299
polysome	cytosolic	heat	Arg	ACG	0.614102	0.577143	0.488861
polysome	cytosolic	heat	Arg	CCG	0.634806	0.675536	0.587595
polysome	cytosolic	heat	Arg	CCT	0.660112	0.632296	0.45614

Table 4.S4: polysome tRNA charging (continued)

sample	source	treatment	AA	anticodon	rep_1_charging	rep_2_charging	rep_3_charging
polysome	cytosolic	heat	Arg	TCG	0.616421	0.599577	0.529595
polysome	cytosolic	heat	Arg	TCT	0.514096	0.503916	0.378251
polysome	cytosolic	heat	Asn	GTT	0.525286	0.482923	0.361334
polysome	cytosolic	heat	Asp	GTC	0.56723	0.547897	0.49481
polysome	cytosolic	heat	Cys	GCA	0.588235	0.571429	0.47191
polysome	cytosolic	heat	Gln	CTG	0.490934	0.466019	0.386364
polysome	cytosolic	heat	Gln	TTG	0.450102	0.456647	0.350254
polysome	cytosolic	heat	Glu	CTC	0.62311	0.624139	0.594293
polysome	cytosolic	heat	Glu	TTC	0.561518	0.508427	0.512077
polysome	cytosolic	heat	Gly	CCC	0.459335	0.469644	0.34264
polysome	cytosolic	heat	Gly	GCC	0.493286	0.517158	0.465644
polysome	cytosolic	heat	Gly	TCC	0.501924	0.505674	0.417131
polysome	cytosolic	heat	His	GTG	0.608016	0.581649	0.584989
polysome	cytosolic	heat	Ile	AAT	0.309258	0.297248	0.205172
polysome	cytosolic	heat	Ile	TAT	0.462578	0.45102	0.304609
polysome	cytosolic	heat	Leu	AAG	0.556677	0.557039	0.498588
polysome	cytosolic	heat	Leu	CAA	0.565337	0.552567	0.513274
polysome	cytosolic	heat	Leu	CAG	0.514888	0.524671	0.440529
polysome	cytosolic	heat	Leu	TAA	0.412844	0.407895	0.392045
polysome	cytosolic	heat	Leu	TAG	0.564516	0.454545	0.341379
polysome	cytosolic	heat	Lys	CTT	0.605687	0.622231	0.577284
polysome	cytosolic	heat	Lys	TTT	0.57187	0.547945	0.493197
polysome	cytosolic	heat	Mete	CAT	0.558463	0.550907	0.440812
polysome	cytosolic	heat	Meti	CAT	0.540679	0.523151	0.46184
polysome	mitochondrial	heat	mtAla	TGC	0.62069	0.5	0.4
polysome	mitochondrial	heat	mtArg	TCG	0.833333	0.5	NA
polysome	mitochondrial	heat	mtAsn	GTT	0.573034	0.52381	0.568966
polysome	mitochondrial	heat	mtAsp	GTC	0	0.75	1
polysome	mitochondrial	heat	mtCys	GCA	0.375	0.764706	0.625
polysome	mitochondrial	heat	mtGln	TTG	0.642857	0.705357	0.486111
polysome	mitochondrial	heat	mtGlu	TTC	0.684736	0.654206	0.690632
polysome	mitochondrial	heat	mtGly	TCC	0.571429	0	0.75
polysome	mitochondrial	heat	mtHis	GTG	0.571429	0.916667	0.52381
polysome	mitochondrial	heat	mtIle	GAT	0.705882	0.779661	0.904762
polysome	mitochondrial	heat	mtLeu	TAA	0.392157	0.314286	0.432432
polysome	mitochondrial	heat	mtLeu	TAG	0.75	0.6	0.166667

Table 4.S4: polysome tRNA charging (continued)

sample	source	treatment	AA	anticodon	rep_1_charging	rep_2_charging	rep_3_charging
polysome	mitochondrial	heat	mtLys	TTT	0.962963	0.642857	0.444444
polysome	mitochondrial	heat	mtMet	CAT	0.730337	0.679487	0.575758
polysome	mitochondrial	heat	mtPhe	GAA	0.62069	0.601351	0.489583
polysome	mitochondrial	heat	mtPro	TGG	0.764706	0.454545	0.538462
polysome	mitochondrial	heat	mtSer	GCT	0.416667	0.666667	0.222222
polysome	mitochondrial	heat	mtSer	TGA	0.560811	0.563218	0.482353
polysome	mitochondrial	heat	mtThr	TGT	0.7	0.904762	0.8
polysome	mitochondrial	heat	mtTrp	TCA	0.792683	0.78125	0.923077
polysome	mitochondrial	heat	mtTyr	GTA	0.526316	0.651163	0.45
polysome	mitochondrial	heat	mtVal	TAC	0.693434	0.706128	0.667232
polysome	cytosolic	heat	Phe	GAA	0.509465	0.468526	0.28608
polysome	cytosolic	heat	Pro	AGG	0.497354	0.509579	0.467662
polysome	cytosolic	heat	Pro	CGG	0.517618	0.536013	0.506667
polysome	cytosolic	heat	Pro	TGG	0.468108	0.4757	0.507614
polysome	cytosolic	heat	SeCe	TCA	NA	1	NA
polysome	cytosolic	heat	Ser	AGA	0.500766	0.495146	0.393229
polysome	cytosolic	heat	Ser	CGA	0.597884	0.673077	0.494118
polysome	cytosolic	heat	Ser	GCT	0.646047	0.612392	0.567949
polysome	cytosolic	heat	Ser	TGA	0.503759	0.479062	0.416481
polysome	cytosolic	heat	Thr	AGT	0.557692	0.538913	0.466667
polysome	cytosolic	heat	Thr	CGT	0.547208	0.602225	0.506515
polysome	cytosolic	heat	Thr	TGT	0.593692	0.589674	0.628571
polysome	cytosolic	heat	Trp	CCA	0.660249	0.564054	0.589404
polysome	cytosolic	heat	Tyr	GTA	0.539482	0.479029	0.360232
polysome	cytosolic	heat	Val	AAC	0.409772	0.435502	0.329806
polysome	cytosolic	heat	Val	CAC	0.403482	0.444732	0.333678
polysome	cytosolic	heat	Val	TAC	0.493204	0.522034	0.411321

Table 4.S5: Index primers and barcode oligos

Table 4.S5.1 Index PCR Primers

Index number	**Illumina small rna number**	**Index from Illumina**	**Full sequence (DIFFERENT FROM ILLUMINA RPL1, RPL2, etc.)**
PCR Illumina multiplex	Illumina multiplex		AATGATACGGCGACCACCGAGATCTACACGTTCAGAGT TCTACAGTCCGACGATC
1	RPI1	CGTGAT	CAAGCAGAAGACGGCATACGAGATCGTGATGTGACTGG AGTTCAGACGTGTGCTCTTCCGATCT
2	RPI2	ACATCG	CAAGCAGAAGACGGCATACGAGATACATCGGTGACTGG AGTTCAGACGTGTGCTCTTCCGATCT
3	RPI3	GCCTAA	CAAGCAGAAGACGGCATACGAGATGCCTAAGTGACTGG AGTTCAGACGTGTGCTCTTCCGATCT
4	RPI4	TGGTCA	CAAGCAGAAGACGGCATACGAGATTGGTCAGTGACTGG AGTTCAGACGTGTGCTCTTCCGATCT
5	RPI5	CACTGT	CAAGCAGAAGACGGCATACGAGATCACTGTGTGACTGG AGTTCAGACGTGTGCTCTTCCGATCT
6	RPI6	ATTGGC	CAAGCAGAAGACGGCATACGAGATATTGGCGTGACTGG AGTTCAGACGTGTGCTCTTCCGATCT
7	RPI7	GATCTG	CAAGCAGAAGACGGCATACGAGATGATCTGGTGACTGG AGTTCAGACGTGTGCTCTTCCGATCT
8	RPI8	TCAAGT	CAAGCAGAAGACGGCATACGAGATTCAAGTGTGACTGG AGTTCAGACGTGTGCTCTTCCGATCT
9	RPI9	CTGATC	CAAGCAGAAGACGGCATACGAGATCTGATCGTGACTGG AGTTCAGACGTGTGCTCTTCCGATCT
10	RPI10	AAGCTA	CAAGCAGAAGACGGCATACGAGATAAGCTAGTGACTGG AGTTCAGACGTGTGCTCTTCCGATCT
11	RPI11	GTAGCC	CAAGCAGAAGACGGCATACGAGATGTAGCCGTGACTGG AGTTCAGACGTGTGCTCTTCCGATCT
12	RPI12	TACAAG	CAAGCAGAAGACGGCATACGAGATTACAAGGTGACTG GAGTTCAGACGTGTGCTCTTCCGATCT
13	RPI13	TTGACT	CAAGCAGAAGACGGCATACGAGATTTGACTGTGACTGG AGTTCAGACGTGTGCTCTTCCGATCT
14	RPI14	GGAACT	CAAGCAGAAGACGGCATACGAGATGGAACTGTGACTG GAGTTCAGACGTGTGCTCTTCCGATCT
15	RPI15	TGACAT	CAAGCAGAAGACGGCATACGAGATTGACATGTGACTGG AGTTCAGACGTGTGCTCTTCCGATCT

Table 4.S5.1 Index PCR Primers (continued)

Index number	**Illumina small rna number**	**Index from Illumina**	**Full sequence (DIFFERENT FROM ILLUMINA RPL1, RPL2, etc.)**
16	RPI16	GGACGG	CAAGCAGAAGACGGCATACGAGATGGACGGGTGACTG GAGTTCAGACGTGTGCTCTTCCGATCT
17	RPI17	CTCTAC	CAAGCAGAAGACGGCATACGAGATCTCTACGTGACTGG AGTTCAGACGTGTGCTCTTCCGATCT
18	RPI18	GCGGAC	CAAGCAGAAGACGGCATACGAGATGCGGACGTGACTG GAGTTCAGACGTGTGCTCTTCCGATCT
19	RPI19	TTTCAC	CAAGCAGAAGACGGCATACGAGATTTTCACGTGACTGG AGTTCAGACGTGTGCTCTTCCGATCT
20	RPI20	GGCCAC	CAAGCAGAAGACGGCATACGAGATGGCCACGTGACTG GAGTTCAGACGTGTGCTCTTCCGATCT
21	RPI21	CGAAAC	CAAGCAGAAGACGGCATACGAGATCGAAACGTGACTG GAGTTCAGACGTGTGCTCTTCCGATCT
22	RPI22	CGTACG	CAAGCAGAAGACGGCATACGAGATCGTACGGTGACTGG AGTTCAGACGTGTGCTCTTCCGATCT
23	RPI23	CCACTC	CAAGCAGAAGACGGCATACGAGATCCACTCGTGACTGG AGTTCAGACGTGTGCTCTTCCGATCT
24	RPI24	GCTACC	CAAGCAGAAGACGGCATACGAGATGCTACCGTGACTGG AGTTCAGACGTGTGCTCTTCCGATCT

Table 4.S5.2 Read 1 4nt Barcode primers

Name	Alt. Name	IDT ordering sequence	Barcode sequence (read 1)
L1_bc1	read1_bc1	/5Phos/rACT **GGAA** GAT CGT CGG ACT GTA GAA CAT /iBiodT/AG AGT TCT ACA GTC CGA CGA TC **TTCC** AG rU/3Phos/	TTCC
L1_bc2	read1_bc2	/5Phos/rACT **CAGA** GAT CGT CGG ACT GTA GAA CAT /iBiodT/AG AGT TCT ACA GTC CGA CGA TC **TCTG** AG rU/3Phos/	TCTG
L1_bc3	read1_bc3	/5Phos/rACT **ACCA** GAT CGT CGG ACT GTA GAA CAT /iBiodT/AG AGT TCT ACA GTC CGA CGA TC **TGGT** AG rU/3Phos/	TGGT

Table 4.S5.2 Read 1 4nt Barcode primers (continued)

Name	Alt. Name	IDT ordering sequence	Barcode sequence (read 1)
L1_bc4	read1_bc4	/5Phos/rACT **TCAG** GAT CGT CGG ACT GTA GAA CAT /iBiodT/AG AGT TCT ACA GTC CGA CGA TC **CTGA** AG rU/3Phos/	CTGA
L1_bc5	read1_bc5	/5Phos/rACT **ATGG** GAT CGT CGG ACT GTA GAA CAT /iBiodT/AG AGT TCT ACA GTC CGA CGA TC **CCAT** AG rU/3Phos/	CCAT
L1_bc6	read1_bc6	/5Phos/rACT **GATG** GAT CGT CGG ACT GTA GAA CAT /iBiodT/AG AGT TCT ACA GTC CGA CGA TC **CATC** AG rU/3Phos/	CATC
L1_bc7	read1_bc7	/5Phos/rACT **CTAC** GAT CGT CGG ACT GTA GAA CAT /iBiodT/AG AGT TCT ACA GTC CGA CGA TC **GTAG** AG rU/3Phos/	GTAG
L1_bc8	read1_bc8	/5Phos/rACT **TACC** GAT CGT CGG ACT GTA GAA CAT /iBiodT/AG AGT TCT ACA GTC CGA CGA TC **GGTA** AG rU/3Phos/	GGTA
L1_bc9	read1_bc9	/5Phos/rACT **AGTC** GAT CGT CGG ACT GTA GAA CAT /iBiodT/AG AGT TCT ACA GTC CGA CGA TC **GACT** AG rU/3Phos/	GACT
L1_bc10	read1_bc10	/5Phos/rACT **TGGT** GAT CGT CGG ACT GTA GAA CAT /iBiodT/AG AGT TCT ACA GTC CGA CGA TC **ACCA** AG rU/3Phos/	ACCA
L1_bc11	read1_bc11	/5Phos/rACT **GTCT** GAT CGT CGG ACT GTA GAA CAT /iBiodT/AG AGT TCT ACA GTC CGA CGA TC **AGAC** AG rU/3Phos/	AGAC
L1_bc12	read1_bc12	/5Phos/rACT **CCTT** GAT CGT CGG ACT GTA GAA CAT /iBiodT/AG AGT TCT ACA GTC CGA CGA TC **AAGG** AG rU/3Phos/	AAGG
Read2 L2 oligo		/5Phos/NNN NNN AGA TCG GAA GAG CAC ACG /3ddC/	

Table 4.S5.3 Read 1 4nt Barcode primers

Name	IDT ordering sequence	Barcode (read 2)
read2_bc1	/5Phos/rACT **GGAA** AGA TCG Gaa gag cac acg at /iBiodT/agaCGT GTG CTC TTC CGA TCT **TTCC** AG rU/3Phos/	TTCC
read2_bc2	/5Phos/rACT **CAGA** AGA TCG Gaa gag cac acg at /iBiodT/agaCGT GTG CTC TTC CGA TCT **TCTG** AG rU/3Phos/	TCTG

Table 4.S5.3 Read 1 4nt Barcode primers (continued)

Name	IDT ordering sequence	Barcode (read 2)
read2_bc3	/5Phos/rACT **ACCA** AGA TCG Gaa gag cac acg at /iBiodT/agaCGT GTG CTC TTC CGA TCT **TGGT** AG rU/3Phos/	TGGT
read2_bc4	/5Phos/rACT **TCAG** AGA TCG Gaa gag cac acg at /iBiodT/agaCGT GTG CTC TTC CGA TCT **CTGA** AG rU/3Phos/	CTGA
read2_bc5	/5Phos/rACT **ATGG** AGA TCG Gaa gag cac acg at /iBiodT/agaCGT GTG CTC TTC CGA TCT **CCAT** AG rU/3Phos/	CCAT
read2_bc6	/5Phos/rACT **GATG** AGA TCG Gaa gag cac acg at /iBiodT/agaCGT GTG CTC TTC CGA TCT **CATC** AG rU/3Phos/	CATC
read2_bc7	/5Phos/rACT **CTAC** AGA TCG Gaa gag cac acg at /iBiodT/agaCGT GTG CTC TTC CGA TCT **GTAG** AG rU/3Phos/	GTAG
read2_bc8	/5Phos/rACT **TACC** AGA TCG Gaa gag cac acg at /iBiodT/agaCGT GTG CTC TTC CGA TCT **GGTA** AG rU/3Phos/	GGTA
read2_bc9	/5Phos/rACT **AGTC** AGA TCG Gaa gag cac acg at /iBiodT/agaCGT GTG CTC TTC CGA TCT **GACT** AG rU/3Phos/	GACT
read2_bc10	/5Phos/rACT **TGGT** AGA TCG Gaa gag cac acg at /iBiodT/agaCGT GTG CTC TTC CGA TCT **ACCA** AG rU/3Phos/	ACCA
read2_bc11	/5Phos/rACT **GTCT** AGA TCG Gaa gag cac acg at /iBiodT/agaCGT GTG CTC TTC CGA TCT **AGAC** AG rU/3Phos/	AGAC
read2_bc12	/5Phos/rACT **CCTT** AGA TCG Gaa gag cac acg at /iBiodT/agaCGT GTG CTC TTC CGA TCT **AAGG** AG rU/3Phos/	AAGG
Read1 L2 oligo	/5Phos/NN NNN NGA TCG TCG GAC TGT AGA A/3ddC/	

Table 4.S5.4 Read 2 3nt Barcode primers

Name	Sequence: PO4=5' or 3' phosphate, r=ribo; T*=internal biotin	Barcode (sense)
L1 - bc1	PO4 rACTT GAA AGATCGGAAGAGCACACG AT (T*) AGA CGTGTGCTCTTCCGATCT TTC AAGrU PO4	TTC
L1 - bc2	PO4 rACTT AGG AGATCGGAAGAGCACACG AT (T*) AGA CGTGTGCTCTTCCGATCT CCT AAGrU PO4	CCT
L1 - bc3	PO4 rACTT GTT AGATCGGAAGAGCACACG AT (T*) AGA CGTGTGCTCTTCCGATCT AAC AAGrU PO4	AAC
L1 - bc4	PO4 rACTT ACC AGATCGGAAGAGCACACG AT (T*) AGA CGTGTGCTCTTCCGATCT GGT AAGrU PO4	GGT

Table 4.S5.4 Read 2 3nt Barcode primers (continued)

Name	Sequence: PO4=5' or 3' phosphate, r=ribo; T*=internal biotin	Barcode (sense)
L1 - bc5	PO4 rACTT CCA AGATCGGAAGAGCACACG AT (T*) AGA CGTGTGCTCTTCCGATCT TGG AAGrU PO4	TGG
L1 - bc6	PO4 rACTT TTG AGATCGGAAGAGCACACG AT (T*) AGA CGTGTGCTCTTCCGATCT CAA AAGrU PO4	CAA
L1 - bc7	PO4 rACTT TGT AGATCGGAAGAGCACACG AT (T*) AGA CGTGTGCTCTTCCGATCT ACA AAGrU PO4	ACA
L1 - bc8	PO4 rACTT CAC AGATCGGAAGAGCACACG AT (T*) AGA CGTGTGCTCTTCCGATCT GTG AAGrU PO4	GTG
L1-bc9	PO4 rACTT GCG AGATCGGAAGAGCACACG AT (T*) AGA CGTGTGCTCTTCCGATCT CGC AAGrU PO4	CGC
L1-bc10	PO4 rACTT CTA AGATCGGAAGAGCACACG AT (T*) AGA CGTGTGCTCTTCCGATCT TAG AAGrU PO4	TAG
L1-bc11	PO4 rACTT ATT AGATCGGAAGAGCACACG AT (T*) AGA CGTGTGCTCTTCCGATCT AAT AAGrU PO4	AAT
L1-bc12	PO4 rACTT GGC AGATCGGAAGAGCACACG AT (T*) AGA CGTGTGCTCTTCCGATCT GCC AAGrU PO4	GCC